Spring 2022

Evaluating the Role of the Alzheimer's Disease Risk Factor Pyk2 in Tau Phosphorylation, Pathology and Related Dysfunction

Alex Harrison Brody
Yale University Graduate School of Arts and Sciences, alhabrody@gmail.com

Abstract

Evaluating the Role of the Alzheimer's Disease Risk Factor Pyk2 in Tau Phosphorylation, Pathology and Related Dysfunction

Alex Harrison Brody

2022

Alzheimer's disease (AD), the most common cause of dementia, is the 6th leading cause of death in the US and the 5th leading cause of death in individuals 65 and older. As the global population ages, current projections suggest that AD may overwhelm existing healthcare infrastructure in the 21st century, with cases in the US expected to surpass 13.8 million by 2060. The need for additional disease modifying therapies is paramount, though the development of novel therapeutic strategies for the treatment of AD is limited by our current understanding of AD pathophysiology. The vast majority of AD cases are sporadic in nature, with age being the single greatest risk factor, however a growing list of genetic risk factors identified through recent genome wide association studies (GWAS) has the potential to reveal key insights into the molecular mechanisms that govern AD susceptibility and mediate disease progression.

Given that AD is defined by the pathological processing of both Aβ and Tau, any evaluation of a specific AD risk factor must consider the role that gene-product plays with respect to both proteins. Our group has previously reported that the AD risk factor Pyk2 is required for Aβ synaptotoxicity as well as the presentation of Aβ-associated

phenotypes in AD animal models. Although Pyk2 has been previously shown to regulate kinases known to phosphorylate Tau at pathophysiologically-relevant residues (e.g. GSK3β and Fyn), and while at least one group has reported direct phosphorylation of Tau by Pyk2 through over-expression experiments, direct evidence demonstrating Pyk2-dependent modulation of Tau phosphorylation through the manipulation of endogenous Pyk2 is lacking.

Experiments described here show that both genetic deletion and pharmacological inhibition of Pyk2 increases the phosphorylation of Tau at a number of pathophysiologically-relevant residues. Furthermore, genetic deletion of Pyk2 in PS19 animals that over-express a mutant form of human Tau associated with frontotemporal dementia significantly reduces animal survivorship, impairs memory and augments synaptic C1q deposition. These results suggest that, while Pyk2 contributes to toxic Aβ signaling, Pyk2 conversely suppresses Tau phosphorylation and Tau-associated phenotypes. To explore the mechanism by which Pyk2 suppresses Tau phosphorylation, we conducted phospho-proteomics on hippocampal synaptosomes from WT and $Pyk2^{-/-}$ animals, revealing a number of proximate regulators of Tau modulated by Pyk2 expression. From this list of six kinases, we confirm that the activity of at least one hit, LKB1, is suppressed by basal levels of Pyk2 activity. We also show that the activity of a direct substrate of LKB1 and a known kinase of Tau, p38 MAPK, is also inhibited by Pyk2. Revealingly, the activities of LKB1 and p38 MAPK are highest in $PS19^{0/+}$;$Pyk2^{-/-}$ mice, suggesting that the activities of these two kinases may at least partially explain the increased Tau phosphorylation and exacerbated Tau-associated

phenotypes observed in these animals. While the implications of these data preclude Pyk2 as a promising pharmacological target using conventional therapeutic approaches, these results, in conjunction with previous results from our group, uncover a complex role for Pyk2 at the intersection of Aβ and Tau.

Evaluating the Role of the Alzheimer's Disease Risk Factor Pyk2 in Tau Phosphorylation, Pathology and Related Dysfunction

A Dissertation
Presented to the Faculty of the Graduate School
of
Yale University
in Candidacy for the Degree of
Doctor of Philosophy

by
Alex Harrison Brody

Dissertation Director: Stephen M. Strittmatter

May, 2022

Table of Contents

CHAPTER 1

Synaptotoxic Signaling by Amyloid Beta Oligomers in Alzheimer's Disease through Prion Protein and mGluR5

Abstract

Alzheimer's disease (AD) represents an impending global health crisis, yet the complexity of AD pathophysiology has so far precluded the development of any interventions to successfully slow or halt AD progression. It is clear that accumulation of Amyloid-beta (Aβ) peptide triggers progressive synapse loss to cause AD symptoms. Once initiated by Aβ, disease progression is complicated and accelerated by inflammation and by Tau pathology. The recognition that Aβ peptide assumes multiple distinct states and that soluble oligomeric species (Aβo) are critical for synaptic damage is central to molecular understanding of AD. This knowledge has led to the identification of specific Aβo receptors, such as cellular prion protein (PrP^C), mediating synaptic toxicity and neuronal dysfunction. The identification of PrP^C as an Aβo receptor has illuminated an Aβo-induced signaling cascade involving mGluR5, Fyn and Pyk2 that links Aβ and Tau pathologies. This pathway provides novel potential therapeutic targets for disease-modifying AD therapy. Here, we discuss the methods by which several putative Aβo receptors were identified. We also offer and in-depth examination of the known molecular mechanisms believed to mediate Aβo-induced synaptic dysfunction, toxicity and memory dysfunction.

Introduction

Alzheimer's disease (AD) is the most common cause of dementia and the sixth leading cause of death in the United States, where there are an estimated 5.5 million individuals

currently living with the disease. While AD is now the fifth leading cause of death in Americans 65 and older, the number of individuals who will succumb to AD or AD-related complications is expected to rise as deaths from heart disease and prostate cancer continue to fall [1]. While no dollar amount can accurately represent the pain and suffering AD inflicts on patients and their families, an estimated 236 billion US dollars were spent on health care and long-term care services for patients with AD in 2016, while an additional 230 billion US dollars were lost due to unearned wages and opportunity costs [2, 3], a total figure representing approximately 2.5% of US gross domestic product in 2016*. AD's rapidly increasing prevalence along with the current lack of therapeutic interventions to successfully slow or halt disease progression makes AD an impending global health crisis.

AD is classically characterized by both the extracellular accumulation of senile plaques composed of amyloid beta (Aβ) and the intracellular deposition of neurofibrillary tangles (NFTs) composed of hyperphosphorylated Tau [4]. While Alois Alzheimer first described these senile plaques and NFTs in the brains patients who had suffered from dementia over a century ago [5], it would take more than three-quarters of a century for the protein constituents of senile plaques and NFTs to finally be purified and identified (reviewed by [6]). In addition to the hallmark appearance of these two lesion types, AD is also characterized by the appearance of neuropil threads, dystrophic neurites and cerebral amyloid angiopathy as well as neuro-inflammation, synapse loss, neuronal cell death and cortical atrophy [7, 8]. As the disease progresses, characteristic symptoms such as impairments in episodic memory and olfactory deficits eventually transition into severe dementia and ultimately death [9]. The molecular mechanisms that mediate the progression of AD pathophysiology and associated symptomatology are the focus of this chapter.

*Updated AD epidemiological statistics are provided in Chapter 3.

The Amyloid Hypothesis and its Critiques

Despite the prerequisite coincidence of both Aβ and hyperphosphorylated Tau aggregation in AD pathology, a number of observations led to the development and widespread focus on the "amyloid cascade hypothesis," which highlights Aβ accumulation as the primary causative factor of AD [10]. The first line of evidence to support the amyloid cascade hypothesis comes from genomic data of patients with rare forms of familial, early-onset AD. Apart from their early onset and dominant inheritance, the pathology and symptoms of these cases are indistinguishable from common late-onset AD. Most of the identified genetic mutations known to be associated with familial AD involve mechanisms that result in the pathogenic processing and increased aggregation of Aβ itself [11]. In fact, the first early-onset AD-associated mutations identified were found in the gene that encodes amyloid-precursor protein (APP), a single-transmembrane protein that when cleaved by the protease γ-secretase liberates Aβ peptide extracellularly [12]. Every known familial mutation of APP associated with AD either occurs in or immediately flanks the Aβ domain of APP (reviewed by [6]).

Additional early-onset AD-associated mutations have been identified in the genes of both presinilin 1 (PS1) and presinilin 2 (PS2), either of which can form a catalytic subunit of γ-secretase [11]. It is widely believed that these autosomal dominant mutations lead to an amyloidogenic shift in the cleavage of APP resulting in the favored generation of the $A\beta_{42}$ isoform over the smaller, less hydrophobic $A\beta_{40}$ isoform (reviewed by [6]).

Secondly, changes in CSF concentrations of $A\beta_{42}$, the suspected pathological isoform of Aβ that most readily oligomerizes to form protein aggregates [13], precede changes in CSF concentrations of Tau [14]. A characteristic biomarker of AD is a reduction in CSF $A\beta_{42}$

levels [15]. In fact, an analysis of data collected from the Alzheimer's Disease Neuroimaging Initiative (ADNI) revealed CSF $A\beta_{42}$ concentration to be the most sensitive biomarker for the detection of AD [16]. Coincident with decreased CSF $A\beta_{42}$, the peptide is deposited in Aβ plaques. The presence of plaque can be detected by positron emission tomography (PET) imaging with ligands such as Pittsburgh compound B (PiB), a radioactive label which binds selectively to Aβ plaque. The detection of Aβ plaque by PET and decreased CSF Aβ levels are contemporaneous and observed well before the emergence of AD symptomology [17-19], reviewed by [20]. Thus, the earliest signs of clinical AD validate Aβ as a trigger for the ensuing decades-long disease process that ends in severe dementia and death.

Experimental validation of the amyloid hypothesis derives from the repeated demonstration that transgenic mice overexpressing human mutant APP with or without mutated forms of presenilin (corresponding to mutations seen in familial AD) develop both senile plaques and age-dependent AD-like phenotypes including synapse loss and impaired memory and cognition [21-26].

Despite these multiple findings, there have been substantial challenges to the amyloid cascade hypothesis, prompting continued reevaluation. First, the degree of plaque burden observed in AD brains correlates with neither the degree of patient cognitive impairment nor the duration of patient illness [27]. This may be related to Aβ functioning as a trigger of a process which becomes much more complicated over time, involving the immune system, metabolism and Tau. Thus, one hypothesis does not explain all phenomena in AD. Second, there exist a considerable number of documented cases in which appreciable senile plaque burden is observed in brains collected from healthy individuals with no presentation of dementia [28, 29]. This may suggest that these individuals died during the presymptomatic

stage of AD, and were destined to develop AD if they had survived, though this must remain unproven. Finally, while immunotherapy with antibodies raised against Aβ have been shown to reduce plaque burden in AD patients, such interventions have failed to improve patient outcome [30-33], reviewed by [34]. Caveats have been provided that anti-Aβ interventions were too late or at too low dose in these instances, and ongoing trials explore these possibilities.

Soluble, Oligomeric Aβ Toxicity as Key to Amyloid Cascade Hypothesis

A key shift for the AD field came after observations that transgenic mice overexpressing a disease-causing mutant form of human APP showed a reduced density of presynaptic terminals paired with severe impairments in synaptic transmission in the hippocampus months before the appearance of amyloid plaques [35]. These results strongly suggest that some component of mutated APP could be leading to synapse loss in early stages of the disease through a mechanism independent of senile plaque accumulation. Around the same time Lambert and colleagues demonstrated that soluble Aβo could inhibit LTP in mouse hippocampal slices, suggesting that a soluble, oligomerized form of Aβ might represent the species that triggers synapse loss and memory impairment in AD [36]. Immunological studies, in particular those of Glabe and colleagues, provided clear evidence for antigenically distinct conformations of Aβ peptide as monomer, oligomer and fibril [37]. Soon after, Gong and colleagues discovered that patient-derived soluble Aβo bound to dendrites in cultured mouse hippocampal neurons with high, “ligand-like” specificity [38].

Further support for the Aβ oligomer hypothesis came from experiments conducted by Selkoe and colleagues demonstrating that acute administration of soluble Aβo (but not Aβ

monomers or insoluble amyloid plaque cores) derived from AD brains could inhibit long-term potentiation (LTP, an electrophysiological enhancement mechanism believed to contribute to memory formation) and enhance long-term depression (LTD, a mechanism that mediates a stable reduction in post-synaptic response) in hippocampal slices. The authors additionally showed that 10-day incubation with patient-derived Aβo significantly reduced spine density in cultured rat pyramidal cells [28].

Although amyloid plaque burden does not correlate with memory loss, astrocyte inflammatory response or neuronal loss in transgenic AD animals, the level of oligomeric Aβ in the brain does [39-42]. Similarly, while increases in the amount of Aβ monomers and Aβ plaque burden are indeed pathological hallmarks of AD, Aβo represents the species of Aβ that correlates most strongly with the severity of dementia in humans [6, 43-47]. Taken together, these results suggest that soluble Aβo likely represents the most synaptotoxic and pathophysiologically relevant form of Aβ to AD. A caveat remains that Aβo is a generic term for a collection of heterogeneous Aβ oligomer states, and the relative role of different oligomer species is ill defined [42, 48].

Mechanisms of Aβ Oligomer Toxicity at the Synapse

Synapse loss is the strongest pathological correlate of cognitive deficits in AD [49] and can be observed in the earliest stage of AD progression [50]. Further physiological evidence of Aβ-induced synapse loss comes from the observation that the degree of synapse loss is greatest surrounding amyloid plaques [51]. In AD transgenic animals, Aβo has been found to colocalize with synaptic puncta, and this degree of colocalization correlates positively with the loss of excitatory synapses [44].

The mechanisms of Aβo-induced disruption of synaptic transmission and subsequent synapse loss are obviously key to explaining AD, but have only recently begun to be elucidated [52] (**Fig. 1**). Considering the importance of glutamatergic signaling in synaptic transmission and plasticity, it is unsurprising that Aβo treatment reduces the expression of both AMPA and NDMA receptors as well as PSD-95, a membrane associated scaffolding protein and a common marker of post synaptic densities, in glutamatergic synapses [53, 54], reviewed by [55]. However, the mechanism by which extracellular Aβo signals to affect synaptic plasticity was absent of molecular understanding prior to the last ten years.

Neuronal Receptor as Central Mediator of Aβo Synapse Damage

The evidence that Aβo action to impair synapses is central to AD pathophysiology focuses attention on the initial molecular mechanisms that trigger these toxicities. One hypothesis is that Aβo interacts with phospholipid bilayers directly to alter conductance non-specifically. While there is evidence for such membrane-disrupting activity at high Aβ concentration, it is unclear how this might explain the selectivity in AD for the CNS and for specific pathways within the brain, or for synapses. Instead, the potent, selective and rapid effects of Aβo on synaptic function suggest that specific polypeptide cell surface receptors for their action exist. Certain effects on synaptic function may be non-cell autonomous. For example, Aβo may trigger microglial- and/or compliment-mediated attack on the synapse [56]. Especially, in late stages of disease as inflammation and cellular reaction becomes prominent, the cellular environment around neuronal synapses and non-cell-autonomous synapse damage may be key. However, at the first triggering stages of AD, direct interaction of Aβo with neuronal synaptic receptors to mediate dysregulation and synapse loss appear most consistent with the phenomena described above.

What characteristics might be expected of a neuronal receptor mediating Aβo synaptic dysfunction and loss? The relevant binding site is expected to be oligomer-specific, of high affinity and present at adult synapses. Evidence for a role requires demonstration not only of binding but also protection from the deleterious effects of Aβo in cells and slices, as well as AD transgenes in experimental animal models. While assessment of human genetic risk for AD might bolster the case for specific receptor function, none of the currently identified human genetic risk genes can be classified as a synaptic receptor protein, implying that the relevant proteins may not exhibit substantial polymorphisms. The biochemical basis for discovery of a potential Aβo receptor is strongest when unbiased genome-wide methods are utilized, and receptor expression cloning has been applied to a number of systems. In our studies of neuronal receptors for Semaphorins [57-60], Nogo [61], MAG [62], LGI1 [63], RGM [64] and PGRN [65], we utilized tagged recombinant protein ligands to screen brain cDNA libraries expressed in non-neuronal cell lines. In each case, receptors relevant to physiological and pathological functions were discovered. Therefore, the expression cloning method is predicted to be of utility for identification of Aβo receptors.

Identification of PrP^C as a Receptor for Aβo

Using an adult mouse brain library of 225,000 cDNA clones expressed in Cos-7 cells, cellular prion protein (PrP^C), a membrane-anchored glycoprotein, was identified in a screen for Aβo-binding [66]. Cos-7 cells expressing PrP^C were found to have a substantially higher affinity for Aβo compared to low-molecular-weight Aβ and a dissociation constant identical to that of Aβo for cultured hippocampal neurons, observations that respectively reveal both PrP^C's oligomeric-specificity and high affinity for Aβo [66-70]. While LTP is inhibited in wildtype mouse hippocampal slices treated with Aβo, no such Aβo-induced LTP inhibition is

detected in hippocampal slices from mice in which PrP^C was genetically deleted, thereby supporting PrP^C's role as a pathophysiologically-relevant Aβo receptor [66]. Similarly, Aβo-induced LTP inhibition in wildtype hippocampal slices could be rescued through pretreatment with an anti-PrP^C antibody. While one study did not observe a requirement for PrP^C in Aβo inhibition [71], this key observation has been confirmed now in multiple studies [72-77].

Subsequent work has corroborated PrP^C's role as a pathophysiologically-relevant receptor for Aβo. PrP^C has been shown to be required for Aβo-induced loss of synapses [78-80], memory impairment and cognitive deficits [81, 82], dendritic spine turnover in vivo [52] and the early mortality phenotype of APP/PS1 transgenic mice [77, 82]. The role of PrP^C as a human disease relevant receptor for $Aβ_{42}$ has also been confirmed; $Aβ_{42}$ has been shown to bind specifically to immobilized PrP^C in brain homogenates from AD patients but not in homogenates derived from healthy controls, an effect that is dependent on the significantly higher concentration of $Aβ_{42}$ present in AD brains [42, 83, 84].

Thus, a preponderance of evidence suggests that for Aβo, PrP^C meets typical requirements for a putative receptor: high affinity, specificity, saturability, reversibility and the ability to mediate biologically relevant, downstream, intracellular signaling events [85]. However, it is important to note that while PrP^C was the only positive hit identified in the unbiased genome-wide screen, the genetic deletion of PrP^C in cultured mouse neurons only reduced Aβo-binding by 50%, suggesting the contribution of other Aβo-binding cell-surface molecules in addition to PrP^C [66].

While the necessity of PrP^C to mediate Aβo-induced reduction in synaptic density, LTP inhibition and synaptotoxicity has been well documented [42, 66, 76, 78, 81, 82, 86-88], certain Aβ-induced phenotypes, including neural network dysfunction and in vitro dendritic spine loss after longer periods of high-concentration Aβo incubation, appear to be independent of PrP^C, suggesting that these phenotypes may be mediated by alternative Aβo receptors or possibly distinct species of oligomeric Aβ [68, 69, 71, 89]. However, since PrP^C is the only putative Aβ receptor shown to bind specifically to Aβo, the identity of additional Aβo receptors requires further investigation (reviewed by [90]).

Identification of mGluR5 as an Aβo Coreceptor

The activation of intracellular Fyn kinase and its subsequent phosphorylation of NMDARs has been shown to be triggered by the Aβo-PrP^C complex [70, 84, 91]. A requirement for this signaling pathway was employed to identify a transmembrane co-receptor that might link the GPI-anchored PrP^C to the cytoplasmic Fyn kinase, both of which are enriched in the post synaptic density (PSD) [84, 92, 93]. A screen of 61 transmembrane PSD-enriched proteins expressed in HEK293T cells identified mGluR5 as the only candidate to mediate Aβo-induced Fyn phosphorylation in a PrP^C-dependent manner [93] (**Fig. 2**). In cultured cortical neurons, Aβo-induced Fyn activation is eliminated with the application of mGluR5 antagonists MPEP and MTEP (but not the mGluR1 antagonist MPMQ) and through the genetic deletion of mGluR5. Notably, while mGluR5 associates with both PrP^C and Fyn, mGluR5 does not bind directly to Aβo. Additionally, the interaction between Aβo-PrP^C is independent of mGluR5 expression, suggesting the existence of direct, pairwise associations between Aβo and PrP^C, PrP^C and mGluR5 and mGluR5 and Fyn.

In high-density cortical cultures, Aβo administration (but not Aβ monomers) increased levels of intracellular calcium through a mechanism dependent on the expression of both mGluR5 and PrP^C [93]. Although Fyn is also activated through Aβo-PrP^C-mGluR5 signaling, the administration of saracatinib to inhibit Fyn failed to eliminate Aβo-induced increases in intracellular calcium in high-density cortical cultures. Conversely, such increases were abolished through the application of thapsigargin, which inhibits the release of calcium from endoplasmic reticulum stores. Since the pharmacological inhibition of Fyn has been shown to rescue memory deficits and spine loss in APPswe/PS1ΔE9 transgenic mice, these results suggest the existence of at least two pharmacologically divergent Aβo-PrP^C-mGluR5 signaling pathways [94].

Aβo-Induced Disruption of the mGluR5-Homer1b/c-Pyk2-CamKII Complex

In lysates extracted from acute mouse brain slices, anti-PrP^C co-immunoprecipitation reveals that the PrP^C-mGluR5 complex associates with Homer1b/c, Pyk2 and CamKII [77, 95, 96] (**Fig. 2**). Moreover, the mGluR5-Homer1b/c-Pyk2-CamKII complex is modulated by Aβo. While acute DHPG administration enhances the indirect association between PrP^C and Homer1b/c and reduces PrP^C's association with Pyk2 and CamKII, acute Aβo administration enhances not only the association between PrP^C and mGluR5, but the association between PrP^C and CamKII. Conversely, through mGluR5, acute Aβo administration reduces PrP^C's indirect association with Homer1b/c and Pyk2, suggesting that normal glutamatergic signaling mediated by mGluR5 is aberrantly disrupted by Aβo. Furthermore, pretreatment of brain slices with Aβo blocks DHPG's normal ability to modulate mGluR5's interactions with Homer1b/c and CamKII.

Since Aβo levels are chronically elevated in the AD brain and correlate with disease severity, the disruption of normal mGluR5 signaling would be persistent, and worsening as the disease progresses. In brain slices from APPswe/PS1ΔE9 transgenic mice, DHPG-induced changes in the behavior of the mGluR5-Homer1b/c-Pyk2-CamKII complex are completely abolished [95]. Additionally, DHPG-induced activation of Pyk2 and CamKII is absent in brain slices from APPswe/PS1ΔE9 animals, suggesting that chronic exposure to pathologically high levels of Aβo disrupts glutamate's ability to regulate Pyk2 and CamKII signaling through mGluR5. Interestingly, DHPG and Aβo's ability to activate Pyk2 activity is dependent on Fyn, since pharmacological inhibition of Fyn abolishes DHPG and Aβo-induced Pyk2 phosphorylation at Tyr402.

It has been previously demonstrated that mGluR-dependent synaptic plasticity is dependent on the interaction between Homer and mGluR proteins [97] and that CamKII's dissociation from mGluR is associated with LTP [98], it is quite possible that Aβo's ability to disrupt synaptic plasticity is at least partially explained by the Aβo-induced disruption of these two synaptic proteins. Whatever role Pyk2 may have in mediating Aβo-induced disruption of synaptic plasticity has yet to be fully elucidated, but Fyn signaling is likely to be implicated in such a mechanism.

Targeting the Aβo-PrP^{C}-mGluR5 Complex

The role of mGluR5 in mediating Aβo-induced synaptic dysfunction and memory impairment has been repeatedly demonstrated [74, 93, 99-105]. However, since the inhibition of glutamatergic signaling via mGluR5 disrupts normal learning and memory, any therapeutic

intervention designed to disrupt Aβo-PrP^{C} signaling through mGluR5 would ideally leave physiological glutamatergic signaling intact [93, 106-111].

Our group recently demonstrated that the silent allosteric modulator (SAM) of mGluR5 BMS-984923 selectively inhibits Aβo-induced inhibition of LTP in mouse hippocampal slices, memory deficits and synaptic loss in APP/PS1 transgenic mice, and Tau pathology in triple transgenic (3xTg) mice expressing APP, PS1 and human mutant Tau while preserving normal mGluR5-mediated glutamatergic signaling [96]. Thus, BMS-984923 may represent a potentially effective disease-modifying therapy for AD.

Additional Receptors for Aβ: LilRB2, α7nAChR and Others

While PrP^{C}'s interaction with Aβo was discovered via a genome-wide unbiased screen, a number of other receptors for Aβo have been proposed from selected candidate studies, and we have reviewed these in detail (reviewed by [90]). The relative roles of these different receptor mechanisms require further investigation. Here, we briefly describe a few of these pathways.

Shatz and colleagues started with physiological studies showing that LilRB2 is a receptor for both MHC proteins and myelin inhibitor proteins, which titrates synaptic plasticity [112-114]. Based on this background, they considered whether it might also bind Aβo and modify synapse function and stability. Their studies demonstrated a role for LilRB2 in mediating Aβo action to inhibit LTP in slices and to mediate impairments in AD transgenic mice [115]. The interplay of Aβo with endogenous ligands at different development stages has not yet been clarified.

In 2000, Wang and colleagues proposed α7nAChR, a homomeric, ionotropic acetylcholine receptor with high Ca^{2+} permeability as a receptor for monomeric $A\beta_{42}$, a proposal that was in part informed by the loss of cholinergic neurons commonly observed in AD [116, 117]. Subsequent work by Dineley and colleagues demonstrated that in brain slices both nicotine and $A\beta_{42}$ administration could stimulate the activation of extracellular signal-regulated kinase 2 (ERK2), an effect that could be reversed with the application of MLA, an α7nAChR antagonist [118]. Conversely, pretreatment of slices with $A\beta_{42}$ prevented nicotine-induced activation of ERK2 in a manner that reflects Aβo's ability to impair DHPG-induced regulation of the mGluR5-Homer1b/c-Pyk2-CamKII Complex. Furthermore, the authors showed that the degree of α7nAChR brain expression in mice correlated positively with memory deficits in a Morris water maze task.

Additional research conducted by Greengard's team in the mid 2000s demonstrated that soluble Aβ treatment induced the endocytosis of NDMA receptors in cultured cortical neurons through a mechanism involving the binding of Aβ to α7nAChR and the subsequent activation of the striatally-enriched phosphatase (STEP) via dephosphorylation by the Ca^{2+}-sensitive phosphatase PP2B, also known as calcineurin [119]. The authors hypothesized that the activation of α7nAChR by soluble Aβ could promote calcium influx and the activation of calcineurin (mirroring Aβo's previously discussed ability to stimulate the release of calcium from intracellular stores, a mechanism dependent on the formation of the Aβo-PrP^C-mGluR5 complex). Once activated, calcineurin could then dephosphorylate and thus activate STEP. Activated STEP would then promote the dephosphorylation of the NDMA receptor subunit NR2B at Tyr1472, a residue whose phosphorylation-state regulates the activity and endocytosis of NDMA receptors.

Other experiments have confirmed that Aβo treatment reduces NMDA receptor Ca^{2+}-conductance, which consequently leads to a reduction in the activity of CamKII, the inhibition of LTP and the promotion of LTD [120]; reviewed by [121]. Aβo-induced calcineurin activation has also been shown to be mediated by the activation of mGluRs, initiating a cascade that ultimately leads to the endocytosis of AMPA receptors [120, 122].

Tau and Aβ in Concert: The Role of Fyn and Pyk2

A possible link between Aβ and Tau pathology is elucidated by considering Aβo's ability to activate Fyn, since Fyn has previously been shown to both physically associate with Tau and to phosphorylate tyrosine residues of Tau [123, 124]. The phosphorylation of Tau by Fyn depends on the upstream formation of the Aβo-PrP^C complex [91], and the endogenous expression of PrP^C correlates positively with the expression of Tau in a transgenic APP/PS1 mice [125]. Notably, extracts from human AD brains have been shown to activate Fyn in cultured mouse cortical neurons [84].

While the role of hyperphosphorylated Tau in neuronal cell death has traditionally been thought to occur through the physical impedance of axonal trafficking, more recent work suggests a mechanistic relationship between Aβ and Tau that mediates synaptic dysfunction and neuronal toxicity. Hyperphosphorylated Tau has been shown to abnormally localize to dendrites [126]. Aβo also promotes downstream phosphorylation of Tau [98]. Conversely, it has also been demonstrated that Aβ-induced memory impairment and neuronal hyperexcitability in transgenic mice overexpressing mutant human APP depends on the expression of endogenous Tau [127]. Additionally, the pathological localization of Fyn

to the postsynaptic site and its subsequent binding to NMDA receptors intracellularly is also dependent on the expression of Tau [128].

The pathological relationship between Tau and Fyn is bidirectional; while activated Fyn can phosphorylate Tau, phosphorylated Tau has a higher propensity to bind with Fyn, increasing the likelihood of Fyn's inappropriate localization into dendrites [129]. Specifically, Tau delivers Fyn preferentially to NMDA receptors, where Fyn readily promotes the phosphorylation of the NMDA receptor subunit NR2B at Tyr1472 [130]. The phosphorylation of NR2B at Tyr1472 has been shown to both inhibit NMDA receptor endocytosis and increase NMDA receptor current [119, 130].

The role of Fyn in linking Aβ and Tau pathologies implicates it as a potential therapeutic target for AD treatment. As mentioned previously, inhibiting Fyn pharmacologically with the Src family kinase inhibitor AZD0530 rescues both memory impairment and synapse loss in APP/PS1 mice [94]. As such, AZD0530 is currently being evaluated as a candidate for disease-modifying therapy in a multi-center NIH-funded Phase 2a clinical trial (ClinicalTrials.gov NCT02167256) [131]*. Evidence suggest that Fyn and Pyk2 may function together to mediate pathological Aβo signaling. Pyk2 was identified as a late-onset AD (LOAD) risk gene in the largest Genome Wide Association Study yet conducted to assess AD risk, and Pyk2 was separately identified as a non-ApoE4 genetic risk loci for AD [132, 133]. Additionally, Pyk2 has been identified as a node for differential gene expression in both ApoE4 allele carriers and in patients with early-onset AD [135].

*Clinical trial NCT02167256 was discontinued in 2018 after failing to meet primary endpoints [134] .

Pyk2, like Fyn, is enriched in PSDs and has been shown to play a mechanistic role in regulating synaptic plasticity [136-140]. Bartos and colleagues showed that NMDAR-mediated Ca^{2+} influx induced Pyk2 autophosphorylation and binding to PSD-95, a process that is necessary for LTP induction in hippocampal slices. More recently Giralt and colleagues showed that genetic deletion of Pyk2 in mice impaired performance on hippocampal-dependent behavioral tasks as well as the induction of LTP in hippocampal slices [141]. Conversely, Hsin and colleagues demonstrated that Pyk2 was required for LTD induction, and that Pyk2 overexpression also blocked LTP [142].

As mentioned previously, Pyk2's association with mGluR5 is disrupted in the presence of Aβo [77]. Pyk2 has also been shown to interact directly with Fyn, which phosphorylates and thus fully activates Pyk2 [139, 143, 144]. While Fyn has been shown to phosphorylate residues of Tau, Pyk2 has been shown to interact with and phosphorylate GSK3β [145, 146], a kinase thought to be involved in the hyperphosphorylation of Tau (reviewed by [147]). Taken together, these results suggest that Pyk2 may play a critical role in mediating Aβ-induced synaptic dysregulation through a process involving Fyn. However, the specifics of this mechanism have yet to be elucidated.

Aβ and Disrupted Homeostatic Equilibrium

It may appear as if different studies of Aβo on NMDA receptor activity were contradictory with one another. On the one hand, the phosphorylation of NR2B at Tyr1472 via Fyn increases NMDA receptor net activity [84]. On the other hand, NR2B dephosphorylation by STEP promotes the endocytosis of NMDA receptors, which would reasonably lead to a net reduction in NMDA receptor-mediated currents [119]. However, it would also appear that

this pathological system includes redundancies that promote NR2B dephosphorylation; while STEP dephosphorylates NR2B directly, it also dephosphorylates and inactivates Fyn [148]. Because mGluR5 activation triggers the localization of STEP into dendrites [122] and because Aβo has been shown to activate mGluR5, Aβo would also have the dual effect of both activating Fyn and promoting its inactivation through recruitment of STEP at different time points [84]. The system is further complicated by the previously discussed observation that Aβo also leads to Tau phosphorylation and thus the activation and recruitment of Fyn to the postsynaptic density.

Nevertheless, it is highly probable that this system would result in an overall shift towards NMDA receptor dysregulation in such a way that contributes to neuronal toxicity. Given the necessity of stable NMDA receptor expression for the maintenance of LTP, which would be precluded by chronic STEP activation, the net result of NR2B phosphorylation by Fyn might solely be to disrupt calcium homeostasis within the cell. Indeed, Aβo administration has been shown to disrupt Ca^{2+}-homeostasis through a mechanism dependent on NR2B activation [149]. Promisingly, and in support of this theory, an uncompetitive NMDA receptor channel blocker memantine has shown modest effectiveness in symptomatically improving memory in AD patients [150]; reviewed by [151].

Future Directions

There remain many unanswered questions regarding the mechanisms of oligomeric Aβ-induced neurotoxicity and its contribution to the pathophysiology of AD. For example, the precise Aβo species that are the most pathologically relevant forms require better definition. While Shankar and colleagues initially determined Aβ dimers to be the neurotoxic species,

other groups have subsequently reached conflicting conclusions [28, 42]; reviewed by [6]. Considering the existence of Aβo-induced phenotypes that appear to be independent of PrP^C, it is likely that a number of additional receptors are mediating these phenotypes. Indeed, a number of other teams have identified Aβ receptors in addition to PrP^C, LilRB2 and α7nAChR including RAGE [152], $p75^{NTR}$ [153, 154], NgR1 [155], EphB2 [89] and EphA4 [156], FcγRIIB [157], Sortilin [158], IR [159], EGFR [160] and σ_2R/PGRMC1 [161, 162] (reviewed by [90]). It is possible that these additional Aβ receptors may demonstrate distinct specificities for monomeric or particular oligomeric Aβ species, each potentially signaling through distinct molecular pathways. Further studies are required to elucidate the specificity of these receptors and the downstream signaling pathways that are subsequently disrupted by Aβ. In addition, the connections between Aβo neuronal receptor-signaling, glial and immune response, and the progression to Tau pathology remain to be elucidated.

Conclusions

A collection of evidence supports the hypothesis that accumulation of misfolded forms of Aβ peptide trigger the Alzheimer's disease cascade. Synapse damage is an early and critical phenomenon in the progression of the disease with increasing complexity involving cellular inflammation, Tau accumulation and cell death. Receptors for Aβo at the synapse initiate this toxic cascade. Here, we have reviewed a collection of data showing that Aβo interact with PrP^C to trigger mGluR5 signaling at the synapse, a mechanism that involves Fyn and Pyk2 kinases. For experimental AD transgenic mouse models, this pathway is required for synapse loss and memory dysfunction. Clinical tests of the role of this pathway are underway now.

FIGURES

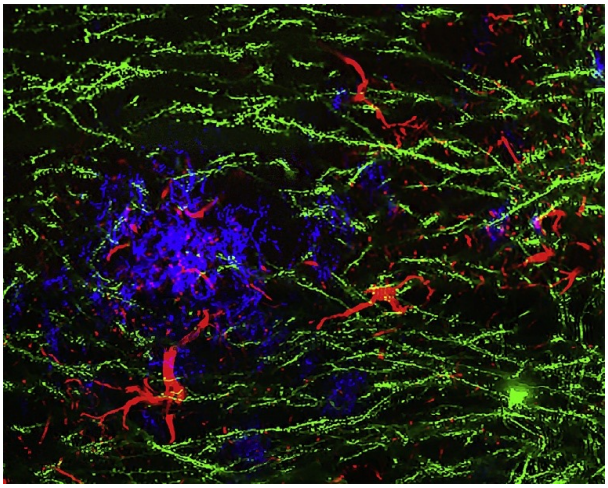

Figure 1. Synaptic Structures and Amyloid Plaques in Alzheimer Model Mice.

Image of cerebral cortical tissue from a transgenic Alzheimer model mouse, expressing human mutant APP and PS1. This mouse also carries a Thy1-EGFP transgene to sparsely fill individual neurons in the cerebral cortex (green). The amyloid plaque is stain is blue, and reactive astrocytes are revealed by anti-GFAP staining in red. Derived from experimental system described previously [52].

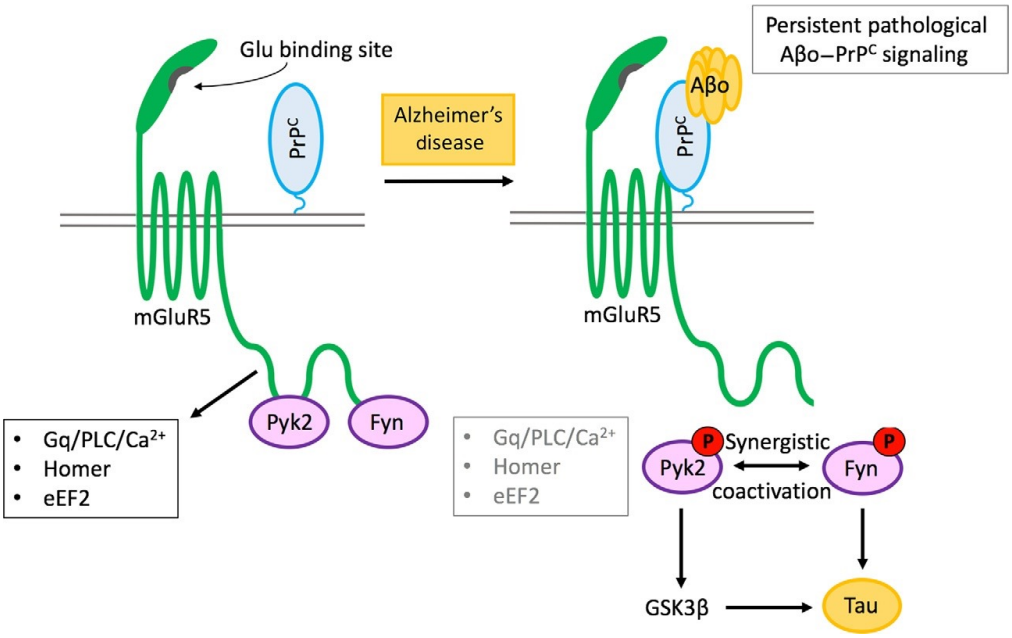

Figure 2. Receptor signaling cascade mediating Alzheimer's disease synapse damage by Aβ oligomers. Schematic illustrates the role of mGluR5 in linking cell surface Aβo–PrP^C complexes to intracellular Fyn/Pyk2 and synaptic loss. Proteins are clustered in the PSD and alter NMDARs, calcium, and protein translation. Pyk2(PTK2B) variation is a verified genetic risk for late-onset AD. Tau plays a role in localizing Fyn. Aberrant PrP^C–mGluR5–Fyn–Tau signaling leads to synaptic malfunction and loss.

ABBREVIATIONS

3×Tg - triple transgenic

Aβ - amyloid beta

AD - Alzheimer's disease

ADNI - Alzheimer's Disease Neuroimaging Initiative

AMPA - α-amino-3-hydroxy-5-methyl-4-isoxazolepropionic acid AMPAR α-amino-3-hydroxy-5-methyl-4-isoxazolepropionic acid receptor APP amyloid precursor protein

CamKII - Ca^{2+}/calmodulin-dependent protein kinase II CNS central nervous system

CSF - cerebrospinal fluid

DHPG - (S)-3,5-dihydroxyphenylglycine

EGFR - epidermal growth factor receptor

ERK2 - extracellular signal-regulated kinase 2

FcγRIIB - Fc gamma receptor IIB

GPI - glycosylphosphatidylinositol

HEK293T - human embryonic kidney cells 293 with SV40 large T antigen IR insulin receptor

LGI1 - leucine-rich, glioma-inactivated 1

LilRB2 - leukocyte immunoglobulin-like receptor B2

LOAD - late-onset Alzheimer's disease

LTD - long-term depression

LTP - long-term potentiation

MAG - myelin-associated glycoprotein

mGluR5 - metabotropic glutamate receptor 5

MHC - major histocompatibility complex

*eEF2 – eukaryotic elongation factor 2

MLA - recombinant histone H3K79me3

MPEP - 2-methyl-6-(phenylethynyl)pyridine

MPMQ - 6-methoxy-N-(4-methoxyphenyl)-4-quinazolinamine

MTEP - 3-((2-methyl-4-thiazolyl)ethynyl)pyridine

NFT - neurofibrillary tangle

NgR1 - Nogo receptor 1

NMDA - N-methyl-D-aspartate

NMDAR - N-methyl-D-aspartate receptor

NR2B - N-methyl D-aspartate receptor subtype 2B

PET - positron emission tomography

PGRN - progranulin

PP2B - protein phosphatase 2B

PrP^C - cellular prion protein

PS1 - presenilin 1

PS2 - presenilin 2

PSD - postsynaptic density

PSD-95 - postsynaptic density protein 95

Pyk2 - protein tyrosine kinase 2

RAGE - receptor for advanced glycation end products

RGM - repulsive guidance molecule A

SAM - silent allosteric modulator

STEP - striatally enriched tyrosine phosphatase

α7nAChR α7 - nicotinic acetylcholine receptor

σ2R/PGRMC1 - sigma 2 receptor/progesterone receptor membrane component 1

DECLARATIONS

Acknowledgments

This work was supported by grants from NIH and the Falk Medical Research Trust to S.M.S.

Conflict of Interest

None.

DISCLOSURE

Chapter 1 was published in *Advances in Pharmacology*.

Brody and Strittmatter, 2018. Synaptotoxic Signaling by Amyloid Beta Oligomers in Alzheimer's Disease through Prion Protein and mGluR5. *Adv Pharmacol.* **82:** 293-323. doi:10.1016/bs.apha.2017.09.007.

License Number 1: 5262000789281

License Number 2: 5264901186638

AUTHORS

A. Harrison Brody[1,2] and Stephen M. Strittmatter[1,2,3,*]

[1]Program in Cellular Neuroscience, Neurodegeneration & Repair, Yale University School of Medicine, New Haven, CT

[2]Department of Neuroscience, Yale University, New Haven, CT

[3]Department of Neurology, Yale University, New Haven, CT

*Correspondence: Stephen.Strittmatter@yale.edu

CHAPTER 2

Validation of iPSC-Derived Human Neurons for AD Modeling

INTRODUCTION

Since Yamanaka and colleagues first succeeded in reprograming adult mouse fibroblasts into induced pluripotent stem cells (iPSCs) through the identification of four minimally sufficient transcription factors (Oct3/4, Sox2, Klf4 and c-myc; now collectively referred to as "Yamanaka factors"), iPSCs and their application have radically transformed the fields of disease modeling, developmental biology and personalized medicine [163]. Once reprogrammed into an embryonic-like state, human iPSCs can be differentiated into a host of distinct cell types, allowing for the rapid, reliable and scalable generation of adult human cells, including neurons, for experimental use [164]. Once differentiated, mature neurons can then be used to model neurodegenerative diseases such as Alzheimer's disease (AD) - either through the application or genetic expression of amyloid β (Aβ) or Tau or through the genetic or pharmacological manipulation of AD risk factors such as Pyk2 [165].

While some methods of differentiating iPSCs into adult cortical neurons rely on the induced over-expression of transgenic transcription factors such as NgN2 (which, while given the benefit of differentiating iPSC-derived neurons more rapidly, has been shown to unexpectedly generate undesired, non-neuronal cell-types), dual SMAD inhibition provides the benefit of generating mature, footprint-free neurons in a way that more closely recapitulates human neural development [166, 167]. Neurons generated from this well-described and highly validated method of neuronal differentiation, which involves the pharmacological inhibition of bone morphogenic protein (BMP) and Activin/TGF-β signaling,

can be further patterned into forebrain cortical neurons through the pharmacological inhibition of Wnt signaling [168-171].

Given the outsized benefits of using cultured human cortical neurons to study human neurodegenerative diseases, the application of iPSC-derived neurons to model AD is quickly growing in popularity. However, considering the potential variability associated with differentiating mature human neurons from iPSCs, validating the methodology applied to any iPSC-to-neuron pipeline is crucial. Here we show that iPSC-derived neurons differentiated using a well-described dual SMAD inhibition protocol express critical Aβ-signaling factors, show evidence of astrocytic cell expression, demonstrate morphological synapses and display canonical Aβ-induced signaling events including the aberrant phosphorylation of eEF2 and Tau.

RESULTS

Mature iPSC-derived human neurons express Aβ-signaling proteins and demonstrate morphological synapses

For our purposes, the utility of iPSC-derived neurons as a model system to study Aβo toxicity and Tau dysfunction depends on the expression of a critical set of proteins. In order to confirm the expression of these proteins, lysates obtained from mature iPSC-derived neurons 50 days post terminal differentiation were blotted for mGluR5, MAP2, NR2B, Pyk2, SV2A, Fyn, CamKII, GSK3β, β-Actin, Tau and PrP^C (**Fig. 1**). Expression of these proteins were compared to those in lysates collected from mouse cortex and hippocampus. While assessing relative levels of protein expression between mouse and iPSC-derived human neurons is complicated by potential differences in species-specific reactivity of each

antibody, we saw appreciable expression of each of the aforementioned proteins across multiple replicates of iPSC-derived neuronal samples. We noticed considerable species-specific reactivity with an antibody used to detect PSD-95 (7E5, CST 36223), which succeeded in detecting PSD-95 expression in mouse brain lysates, but failed to detect PSD-95 expression in lysates from iPSC-derived neurons (**Fig. 2**). An alternative anti-PSD-95 antibody (ab18258), however, was able to detect PSD-95 expression in both mouse brain and in iPSC-derived neurons, emphasizing the importance of considering the specific-specific reactivity of antibodies when comparing expression across species.

Immunoblotting also revealed persistent expression of two transcription factors critical for cortical development in iPSC-derived neurons 65 and 90 days post terminal differentiation, Pax6 and TBR1 (**Fig. 2**). Though the expression of both proteins peak during neural development, Pax6 expression persists in adult cortical interneurons while TBR1 expression is also maintained in the adult forebrain [172, 173]. Persistence of TBR1 expression has previously been confirmed in iPSC-derived neurons differentiated via dual SMAD inhibition, reflecting the identity of deep-layer cortical neurons [170, 171].

While the expression of Satb2 has also been shown to persist in the adult cortex, we were unable to detect Satb2 expression in either mouse cortex or iPSC-derived neurons [174]. Satb2 expression, associated with later-forming upper-layer cortical neurons, has been shown to appear at later stages in iPSC-derived neurons generated via dual SMAD inhibition (as late as 90 days post terminal differentiation) [170]. Although we were unable to detect Satb2 expression at 90 days post terminal differentiation, it is possible that evidence of Satb2 expression would emerge at later time points had these neurons aged longer.

To consider the possibility of cell-type heterogeneity in our cultures, we also immunoblotted lysates from iPSC-derived neurons for GFAP as a marker of astrocytes. As neurons and astrocytes share a common cell lineage, it is unsurprising that we detected markers for these glial cells in our cultures [175]. Indeed, the presence of astrocytes in neuronal cultured obtained through dual SMAD inhibition has been previously documented [171, 176]. Considering the critical role astrocytes play in promoting the survival of neurons as well as in the formation and maintenance of synapses, the presence of astrocytes in these cultures is encouraging [177].

While immunoblotting confirmed the expression of pre- and post-synaptic markers SV2A and PSD-95, we also sought to confirm the presence of morphological synaptic structures through immunocytochemistry. Mature iPSC-derived neurons 95 days post terminal differentiation cultured on glass coverslips were immunolabeled with antibodies for MAP2, to visualize dendritic microtubules, as well as synaptophysin and PSD-95 to visualize pre- and post-synaptic structures, respectively. MAP2 immunolabeling of iPSC-derived neurons revealed healthy 2D neuronal morphology, while synaptophysin and PSD-95 immunolabeling revealed juxtaposed areas of pre- and post-synaptic makers along MAP2-positive dendritic arbors (**Fig. 3**) previously associated with functional synapses [170]. Qualitatively, areas of highest PSD-95 immunoreactivity were commonly surrounded by areas of dense synaptophysin immunoreactivity, suggesting the presence of morphological synapses in these cultures. Indeed, previous reports of iPSC-derived neurons generated via dual SMAD inhibition have confirmed the presence of physical synapses as early as 28 days post terminal differentiation, with electrophysiological evidence of functional chemical synapses appearing as early as 45 days post terminal differentiation [170, 171].

Mature iPSC-derived human neurons display evidence of canonical Aβo-induced signaling events

It is well-documented that toxic Aβ signaling leads to a number of aberrant molecular signaling events in neurons including the phosphorylation of eEF2 at T56 and Tau at multiple pathophysiologically-relevant residues [77, 93, 126, 178, 179]. In order to validate our iPSC-derived neurons as a model that can be used to study toxic Aβ signaling, we assessed whether Aβo administration would also induce aberrant phosphorylation of eEF2 and Tau (**Fig. 4**). Mature iPSC-derived neurons 90 days post terminal differentiation were treated for 30 min at 37°C with various concentrations of Aβo. 1 μM Aβo treatment was sufficient to induce phosphorylation of eEF2 at T56 (**Fig. 4A, B**), while 2 μM Aβo treatment led to a ~6-fold increase in eEF2 phosphorylation at T56. 1 and 2 μM Aβo treatment also led to a significant increase in Tau phosphorylation at S202/T205 (AT8), though only 1 μM Aβo administration caused a significant increase in Tau phosphorylation at S199/S202. Whether 2 μM Aβo activates compensatory mechanisms that limit the phosphorylation of Tau at S199/S202 has yet to be determined. Overall, the observation that Aβo administration induces canonical, aberrant signaling events in iPSC derived human neurons suggests that these neurons can be used in future experiments designed to evaluate strategies of disrupting Aβo toxicity.

DISCUSSION

Considering many substantial and currently unresolved species-specific challenges associated animal models of AD, iPSC-derived human neurons represent a powerful in vitro tool for elucidating the pathophysiological mechanisms of this uniquely human neurodegenerative disease. Validating the methodology by which iPSC-derived neurons are

generated, however, remains crucial given the possibility of user variability associated with any protocol used to differentiate neurons from iPSCs.

Here we show that a well-described and previously validated protocol for generating iPSC-derived human cortical neurons via dual SMAD inhibition produces neurons that express critical Aβ-signaling factors, demonstrate morphological evidence of physical synapses and an express biochemical marker suggestive of co-cocultured astrocytes, necessary for the maintenance of neuronal health and survival. Furthermore, we demonstrate that mature iPSC-derived neurons treated with Aβo recapitulate canonical Aβ-induced signaling events through the increased phosphorylation of both eEF2 and Tau, suggesting that these neurons could be used to explore both Aβ signaling and Tau processing.

FIGURES

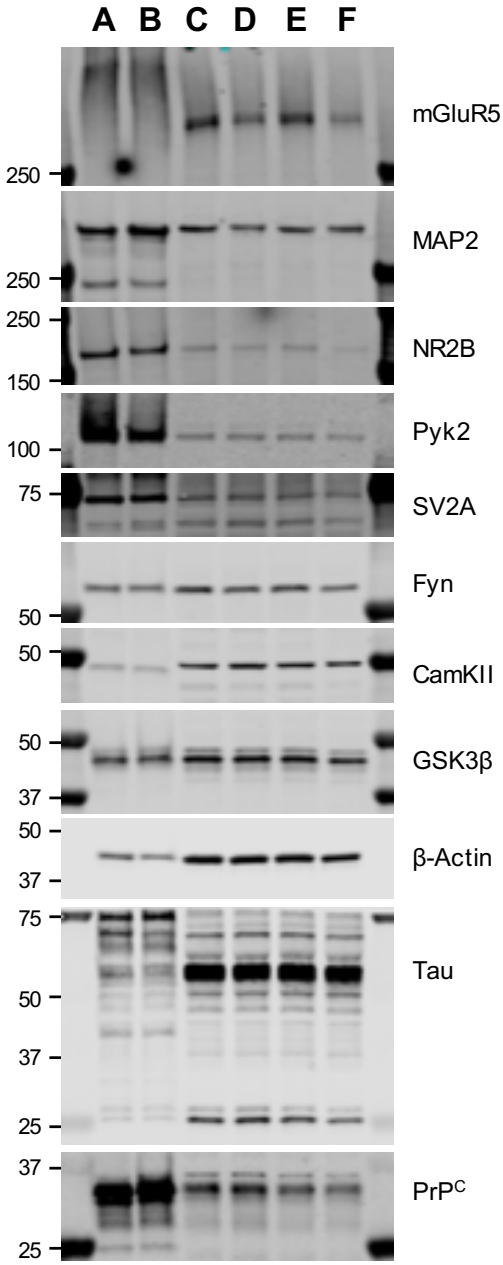

Figure 1. Mature human iPSC-derived neurons express critical Aβ-signaling proteins. Lysates from mouse hippocampus (**A**) and cortex (**B**). **C–F**, lysates from iPSC-derived neurons 50 days post terminal differentiation express detectable levels of mGluR5, MAP2, NRB2, Pyk2, SV2A, Fyn, CamKII, GSK3β, β-Actin, Tau and PrP^{C}.

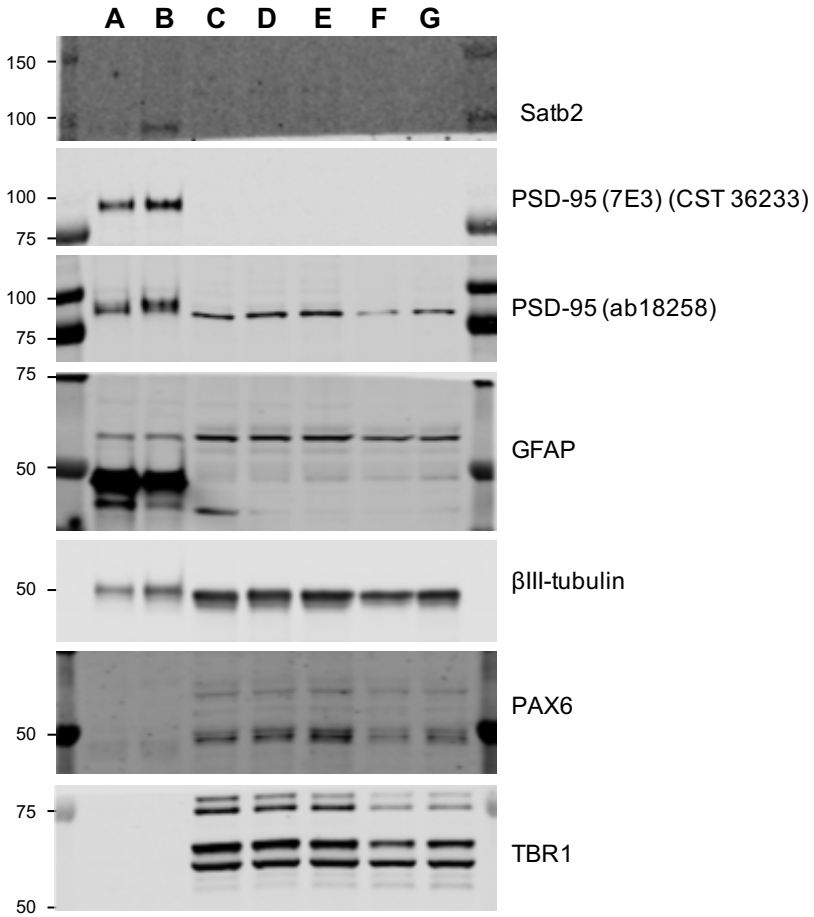

Figure 2. Mature human iPSC-derived neurons express synaptic and astrocytic proteins as well as key cortical transcription factors. Lysates from mouse hippocampus (**A**) and cortex (**B**). **C–E**, lysates from iPSC-derived neurons 65 days post terminal differentiation. **F** and **G**, lysates from iPSC-derived neurons 90 days post terminal differentiation. iPSC-derived neurons express detectable levels of PSD-95, GFAP, βIII-tubulin, PAX6 and TBR1.

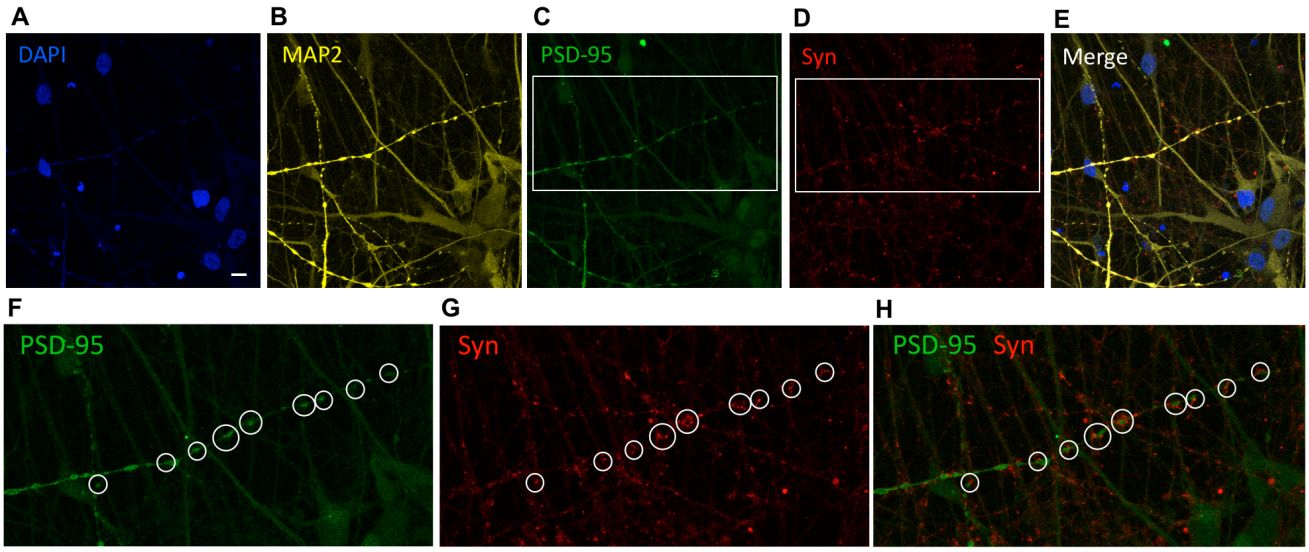

Figure 3. Mature iPSC-derived neurons colocalization of post- and pre-synaptic markers. Images of mature iPSC-derived neurons 95 days post terminal differentiation showing immunofluorescence of DAPI (**A**), MAP2 (**B**), PSD-95 (**C**) and synaptophysin (**D**). **E**, merge of **A–B**. **F–H**, enlargements of **C** and **D**, showing synaptic colocalization of PSD-95 (**F**) and synaptophysin (**G**) (white circles). **H**, merge of **F** and **G**. Scale bar, 10 μm.

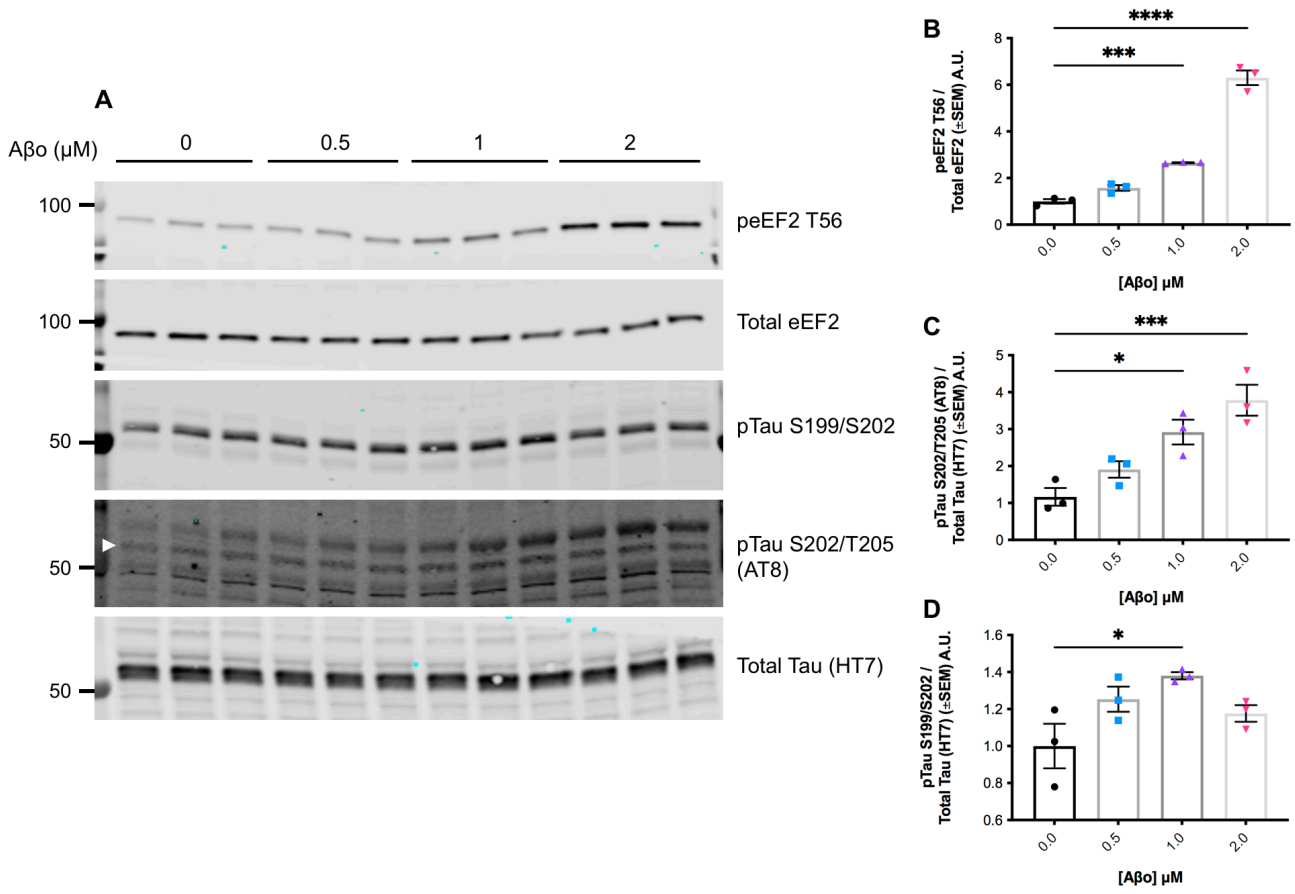

Figure 4. Aβo administration increases phosphorylation of eEF2 and Tau in mature iPSC-derived neurons. iPSC-derived neurons 90 days post terminal differentiation were treated with various concentrations of synthetic Aβo. **A**, representative immunoblots of lysates from iPSC-derived neurons. **B–D**, quantification of **A**. Aβo-treated iPSC-derived neurons display increased phosphorylation of eEF2 at T56 (**B**), Tau at S202/T205 (AT8) (white arrowhead) (**C**) and pTau S199/S202 (**D**). Data are graphed as mean ± SEM, one-way ANOVA with Dunnett's multiple comparisons test, *p<0.05, ***p<0.001, ****p<0.0001, n = 3.

MATERIALS AND METHODS

Neural Induction and Terminal Differentiation

Mature cortical neurons were obtained from human iPSCs with the methodology described in Chapter 4.

Synthetic Aβo Preparation

Synthetic, lyophilized 1-42 Aβ peptide (5 µg) was resuspended in 20 µl DMSO, vortexed and incubated at room temperature for 20 min. Following incubation, 20 µl of resolubilized Aβ were transferred to 1 ml DMEM F12 and incubated overnight at room temperature to allow for peptide oligomerization. Following oligomerization, samples were spun down to remove insoluble Aβ and the supernatant transferred to 3K cutoff spin tubes for buffer exchange to PBS. Following buffer exchange, Aβo concentration (monomer equivalent) was determined using a NanoDrop spectrophotometer with a molar extinction coefficient of 1490 $cm^{-1}M^{-1}$ at 280 nm absorbance. Samples were flash frozen in liquid nitrogen and stored at -80°C until usage.

Aβo Treatment

1 hr prior to Aβo treatment, terminal neural differentiation medium was completely replaced with fresh medium of the same composition. Following pre-incubation, neurons were treated with terminal differentiation media supplemented with synthetic Aβo of various concentrations or PBS vehicle for 30 min at 37°C. Cells were immediately harvested after treatment.

Cell Harvesting

Neurons were harvested on ice in 100 µl/well RIPA (from a 24-well plate) with 1% SDS and protease/phosphatase inhibitors. Samples from adjacent wells were pooled (pooled sample volume, 200 µl from 2 wells), briefly vortexed and spun at 100,000 × g for 30 min at 4°C. SDS-soluble supernatants were boiled in Laemmli sample buffer with 5% β-mercaptoethanol at 95°C for 5 min.

Brain Tissue Collection and Processing

5-month-old WT C57BL/6J mice were sacrificed via live decapitation and hemispheres separated medially on ice using a sharp razor blade. Hippocampi and cortices were immediately dissected from right hemispheres on ice. Hippocampi and cortices were homogenized in 150 µl and 300 µl, respectively, RIPA with 1% SDS containing protease and phosphatase inhibitors using a polypropylene pellet pestle on ice. Homogenates were spun at 100,000 × g for 30 min at 4°C. Supernatants were boiled in Laemmli sample buffer with 5% β-mercaptoethanol at 95°C for 5 min.

Immunoblotting

Samples were separated via SDS-PAGE through 4-20% Tris-glycine gels and transferred onto nitrocellulose membranes using an iBlot 2 Gel Transfer Device. Loaded sample volumes were normalized to total protein concentration via BCA protein assay. Nitrocellulose membranes were blocked while rocking at room temperature for 1 hr and incubated with blocking buffer containing primary antibodies overnight at 4°C. All primary antibodies were diluted to a concentration of 1:1000 (except for β-Actin, which was diluted to a concentration of 1:10,000). After primary antibody incubation, membranes were washed (3

X 5-min in TBST) and incubated with appropriate secondary antibodies for 1 hr at room temperature. After final washes (5 X 5-min in TBST), immunoblots were scanned with a LI-COR Odyssey infrared imaging system and protein bands quantified using LI-COR Image Studio Lite software, version 5.2.5.

Immunocytochemistry

iPSC-derived neurons cultured on PDL/laminin pre-coated glass coverslips were fixed in 4% PFA for 15 min and blocked with PBS containing 0.1% Triton X-100 and 1% BSA for 1 hr at room temperature. Sections were then incubated in primary antibody diluted in PBS with 0.1% Triton X-100 and 1% BSA for 48 hr at 4°C. All primary antibodies were used at a concentration of 1:500. Following primary antibody incubation, sections were washed in PBS and incubated in appropriate secondary antibodies diluted 1:500 in PBS with 0.1% Triton X-100 and 1% BSA overnight at 4°C.

Image Acquisition

Images were obtained using a Leica SP8 confocal microscope. Coverslips were imaged with a 63X 1.4 numerical aperture oil-immersion objective and 5 image slices (1 µm apart) were z-stack compressed via maximum orthogonal projection.

Statistical Analysis

One-way ANOVA with post hoc Dunnett's multiple comparisons tests were performed using GraphPad Prism software. Group means ± SEM and samples sizes (n) are reported in each figure legend. Data were considered to be statistically significant if $p<0.05$. For all figures, all statistically significant group differences are labeled. For any given group comparison, the

lack of any indication of significant difference implies lack of significance by the applied statistical test.

CHAPTER 3

Alzheimer Risk Gene Product Pyk2 Suppresses Tau Phosphorylation and Phenotypic Effects of Tauopathy

ABSTRACT

Background. Genetic variation at the *PTK2B* locus encoding the protein Pyk2 influences Alzheimer's disease (AD) risk. Neurons express Pyk2 and the protein is required for Amyloid-β (Aβ) peptide-driven deficits in synaptic function and memory in mouse models, but has minimal effect on neuro-inflammation. Previous *in vitro* data suggested that Pyk2 activity might enhance GSK3β-dependent Tau phosphorylation and be required for tauopathy. Here, we examine the influence of Pyk2 on Tau phosphorylation and associated pathology.

Methods. The effect of Pyk2 on Tau phosphorylation was examined in cultured Hek cells through protein over-expression and in iPSC-derived human neurons through pharmacological Pyk2 inhibition. PS19 mice overexpressing the P301S mutant of human Tau were employed as an in vivo model of tauopathy. Phenotypes of PS19 mice with a targeted deletion of Pyk2 expression were compared with PS19 mice with intact Pyk2 expression. Phenotypes examined included Tau phosphorylation, Tau accumulation, synapse loss, gliosis, proteomic profiling and behavior.

Results. Over-expression experiments from Hek293T cells indicated that Pyk2 contributed to Tau phosphorylation, while iPSC-derived human neuronal cultures with endogenous protein levels supported the opposite conclusion. *In vivo*, multiple phenotypes of PS19 were exacerbated by Pyk2 deletion. In Pyk2-null PS19 mice, Tau phosphorylation and accumulation increased, mouse survival decreased, spatial memory was impaired and

hippocampal C1q deposition increased relative to PS19 littermate controls. Proteomic profiles of Pyk2-null mouse brain revealed that several protein kinases known interact with Tau are regulated by Pyk2. Endogenous Pyk2 suppresses LKB1 and p38 MAPK activity, validating one potential pathway contributing to increased Tau pathology.

Conclusions. The absence of Pyk2 results in greater mutant Tau-dependent phenotypes in PS19 mice, in part via increased LKB1 and MAPK activity. These data suggest that in AD, while Pyk2 activity mediates Aβ-driven deficits, Pyk2 suppresses Tau-related phenotypes.

Keywords. Alzheimer's disease, Fronto-Temporal Dementia, tauopathy, *PTK2B*, Pyk2, C1q

BACKGROUND

Alzheimer's disease (AD), the most common cause of dementia, is the 6th leading cause of death overall and the 5th leading cause of death in individuals 65 years and older in the United States [180]. Currently, there are an estimated 6.2 million individuals living with AD in the US, a number that is expected to increase more than two-fold by 2050 [180]. With no therapeutic interventions known to slow or halt AD progression, AD is situated to overwhelm existing global health care infrastructure.

The tyrosine kinase Pyk2 (*PTK2B*) has been identified in multiple genome wide association studies (GWAS) as a risk factor for late-onset AD (LOAD) [132, 133, 181-184], and at least one AD-associated *PTK2B* variant (rs28834970) results in increased Pyk2 expression in human peripheral blood monocytes [185]. Biochemically, Pyk2 demonstrates increased

activity in both wild-type mouse brain slices treated with oligomeric amyloid beta (Aβo) and in brain lysates from aged APPswe/PS1ΔE9 (APP/PS1) transgenic mice [94, 95].
Recently, our group reported that genetic deletion of Pyk2 rescues a number of Aβ-associated phenotypes in APP/PS1 animals including memory impairment, synapse loss, astrogliosis and impaired synaptic plasticity [186]. Mechanistically, Aβo-induced dendritic spine loss in mouse primary hippocampal neurons was dependent on the expression of Pyk2 [187]. In the presence of Aβo, the Aβo receptor PrP^C increases its association with the Aβo co-receptor mGluR5, which triggers the intracellular release of Pyk2 from the PrP^C-mGluR5 signaling complex [66, 93, 95]. Once dissociated from mGluR5, activated Pyk2 participates in aberrant, downstream Aβo-induced signaling events, including the activation of RhoA and JNK, contributing to spine loss and apoptosis, respectively [187-193].

While Pyk2's contribution to pathological Aβ signaling is relatively well-described, Pyk2's role in regulating Tau is less defined, despite strong correlative evidence for such a role. GSK3β, for example, a kinase known to phosphorylate Tau at a number of pathophysiologically-relevant residues [194-199], is activated by Pyk2 [145, 146, 200]. Pyk2 has also been shown to interact biochemically with Tau in Hek293 cells and to colocalize with hyperphosphorylated Tau fibrils in both AD brains and Tau transgenic mice [201]. Additional evidence suggests that Pyk2 may phosphorylate Tau directly. Pyk2 co-localizes with Tau in mouse primary hippocampal neurons, phosphorylates Tau at Y18 *in vitro* and augments the phosphorylation of Tau at Y18 when over-expressed in MAPT P301L transgenic mice [202].

Notwithstanding an abundance of correlative data suggesting a role for Pyk2 in regulating Tau, existing evidence of Pyk2's ability to phosphorylate Tau either directly or indirectly has relied exclusively on Pyk2 over-expression. To the best of our knowledge, the results

reported here represent the first attempt at elucidating Pyk2's ability to regulate Tau phosphorylation and Tau pathology through the modulation of endogenous Pyk2. While our results confirm that, when over-expressed, Pyk2 contributes to Tau phosphorylation, suppression of Pyk2 activity through either pharmacological inhibition or genetic deletion *increases* the phosphorylation of Tau at a number of pathophysiologically-relevant residues. When crossed with $Pyk2^{-/-}$ animals, hemizygous PS19 (MAPT P301S, 1N4R) transgenic mice demonstrate augmented Tau pathology, decreased survival, impaired spatial memory and increased hippocampal C1q deposition. Phospho-proteomic analysis of hippocampal synaptosomes reveals a number of putative Pyk2-modulated regulators of Tau, one of which (LKB1) is validated here. LKB1 positively regulates the activity of the Tau kinase p38 MAPK [203-209], and the activities of both kinases are suppressed by endogenous levels of Pyk2. Together, these results suggest a protective role for Pyk2 against Tau phosphorylation, Tau pathology and Tau-induced behavioral deficits, in part through the suppression of LKB1 and p38 MAPK activity.

METHODS

Plasmid DNA Constructs

Tau and Pyk2 sequences were subcloned into an AAV-CAG-GFP vector (RRID:Addgene_28014) and GSK3β and Fyn sequences subcloned into a pcDNA3.0 vector which served as a negative transfection control.

Hek293T Cell Culture and Transfection

Human embryonic kidney 293T (Hek293T, RRID:CVCL_QW54) cells were cultured in DMEM (Gibco #11965092) with 10% FBS (Gibco #16000044) and incubated at a constant 37°C with

5% CO_2. For protein over-expression, Hek293T cells were transfected with appropriate DNA constructs (0.5 µg DNA/well in a 12-well plate) using Lipofectamine 3000 reagent (Invitrogen #L3000001). Cells were harvested in 1% Triton X-100 containing 50 mM Tris, 150 mM NaCl and 1 mM EDTA with protease (Roche #11836170001) and phosphatase (Roche #4906845001) inhibitors. Lysates were spun at 14,000 × *g* for 10 min at 4°C and Triton-X100-soluble supernatants were boiled in Laemmli sample buffer (Bio-Rad #1610747) at 95°C for 10 min.

Animals

B6;C3-Tg (Prnp-MAPT*P301S) PS19Vle/J (RRID:IMSR_JAX:008169) mice purchased from Jackson Laboratories (JAX) were backcrossed over 5 generations to a C57BL/6J background to obtain hemizygous $PS19^{0/+}$ animals. $Pyk2^{-/-}$ mice, backcrossed to a C57BL/6J background over 10 generations by Schlessinger and colleagues [210] (RRID:MGI_3584536), were generously provided by Dr. David Schlaepfer (University of California–San Diego). Hemizygous $PS19^{0/+}$ and $Pyk2^{+/-}$ mice were paired to obtain WT, $Pyk2^{-/-}$, $PS19^{0/+}$ and $Pyk2^{-/-}$; $PS19^{0/+}$ mice. All experiments used littermate control mice with no preference for either female or male animals. Comparisons of male and female outcomes by group were conducted *post hoc*. All protocols including animal husbandry, genotyping, behavioral testing and euthanasia were approved by the Yale University Institutional Animal Care and Use Committee (IACUC). Animals were housed in groups of 2–5 mice per cage with access to food and water *ad libitum*. 12-hr light/dark cycles were maintained throughout the duration of animal housing with light periods beginning consistently at 7am.

Acute Brain Slice Pharmacology

4.5–5.5-month-old $PS19^{0/+}$ mice were sacrificed via live decapitation in accordance with Yale University's Institutional Animal Care and Use Committee standards. Brains were dissected on ice and sectioned using a Leica WT1000S Vibratome in ice-cold, oxygenated (95% O_2, 5% CO_2) artificial cerebrospinal fluid (aCSF) containing 119 mM NaCl, 2.5 mM KCl, 2.7 mM $MgSO_4$, 26 mM $NaHCO_3$, 11 mM D-glucose and 1.25 mM NaH_2PO_4. Three 400-µm-thick coronal sections (containing the three most rostral sections of hippocampus) were collected per brain. The two hemispheres of each section were divided medially and slices enriched for hippocampal tissue by removal of the ventral half of each section using a sharp razor blade. Hippocampal-enriched brain slices were transferred to a radial-arm incubation chamber (Scientific Systems Designs Inc #BSK6-6) containing room temperature aCSF supplemented with 2.4 mM $CaCl_2$ and continuously oxygenated with 95% O_2 and 5% CO_2. After a 30 min recovery, slices were treated with either 1 µM PF-719 (Chinglu Pharmaceutical Research) or equal volume of DMSO for 2 hr at room temperature. After treatment, slices were immediately homogenized on ice in 100 µl RIPA (EMD Millipore #20-188) with protease and phosphatase inhibitors (Thermo Scientific #1861281) using a polypropylene pellet pestle and spun at 100,000 × *g* for 30 min at 4°C. RIPA-soluble supernatants were boiled in Laemmli sample buffer with 5% β-mercaptoethanol and 1% SDS at 95°C for 5 min.

iPSC-Derived Human Cortical Neurons

Neural Induction and Terminal Differentiation. iPSC-derived human cortical neurons were derived from zero-footprint Gibco Episomal hiPSCs (Gibco #A18945) using a previously described and validated dual SMAD inhibition protocol [211]. hiPSCs were cultured in Essential 8 Flex Medium (Gibco #A2858501) on vitronectin (Gibco #A14700)-coated plates

and regularly passaged using Gentle Dissociation Medium (Stemcell Technologies #07174). When confluent, hiPSCs were dissociated using Accutase (Stemcell Technologies #07920) and re-plated at a density of $2*10^5$ cells per well on a vitronectin-coated 12-well plate with 2 μM thiazovivin (Stemcell Technologies #72252) to improve cell-survival. One day after plating (at ~75% confluence), Essential 8 Flex Medium was replaced with a neural induction medium [a 1:1 mixture of DMEM/F12 (Gibco #11330) and Neurobasal-A Medium (Gibco #10888022) containing N-2 1:100 (Gibco #17502048), B-27 1:50 (Gibco #17504044), 20 μg/ml insulin (Sigma-Aldrich #I0516), 1 mM L-glutamine (Gibco #25030081), 100 μM MEM Non-Essential Amino Acids (Gibco #11140050), 0.1 mM β-mercaptoethanol (Gibco #21985), 100 nM LDN-193189 (Cayman Chemical #19396), 10 μM SB-431542 (Cayman Chemical #13031) and 2 μM XAV-939 (Tocris #3748)] replaced daily for 12 days. On day 13, cells were dissociated using Accutase and seeded onto 24-well poly-D-lysine plates (Corning #354414) additionally coated with 5 μg/ml laminin (Gibco 23017015) in neural induction medium with 2 μM thiazovivin at a density of $4*10^4$ cells/well. Neural induction medium was replaced 2 to 3 days after seeding with terminal neural differentiation medium (Neurobasal-A Medium containing N-2 1:100, B-27 1:50, 1 mM L-glutamine and 30 ng/ml BDNF (Gibco #PHC7074). Cells were maintained in terminal neural differentiation medium, ¾ of which was replenished twice-weekly for more than 120 days. To prevent detachment, terminal neural differentiation medium was supplemented with 2.5 μg/ml laminin once-weekly.

hiPSC-Derived Neuron Pharmacology. 1 hr prior to treatment, ¾ of medium was replaced with fresh terminal neural differentiation medium. For treatment, cells were administered either PF-719 or DMSO vehicle diluted in terminal neural differentiation medium. For each treatment condition, volumes of DMSO vehicle and DMSO-solubilized PF-719 were kept constant to control for DMSO-induced modulation of cellular signaling events. Neurons were

treated for 2 hr at 37°C and, following treatment, immediately harvested on ice in 100 µl/well RIPA (from a 24-well plate) with 1% SDS and protease/phosphatase inhibitors. Samples from adjacent wells were pooled (pooled sample volume, 200 µl from 2 wells), briefly vortexed and spun at 100,000 × *g* for 30 min at 4°C. SDS-soluble supernatants were boiled in Laemmli sample buffer with 5% β-mercaptoethanol and 1% SDS at 95°C for 5 min.

Brain Tissue Collection and Processing

9.5–10.5-month-old animals were sacrificed via live decapitation and hemispheres separated medially on ice using a sharp razor blade. For immunohistology, left hemispheres were post-fixed in PBS with 4% paraformaldehyde (PFA) for 48 hr at 4°C. Post-fixed hemispheres were then transferred to PBS with 0.05% sodium azide and stored at 4°C until sectioning. For biochemistry, hippocampi and cortices were immediately dissected from right hemispheres on ice. To obtain TBS-soluble fractions, hippocampi and cortices were homogenized in 150 µl and 300 µl, respectively, TBS with protease and phosphatase inhibitors using a polypropylene pellet pestle on ice. Homogenates were spun at 100,000 × *g* for 30 min at 4°C. TBS-soluble supernatants were boiled in Laemmli sample buffer with 5% β-mercaptoethanol and 1% SDS at 95°C for 5 min, while TBS-insoluble hippocampal and cortical pellets were resolubilized on ice in 150 µl and 300 µl, respectively, RIPA with 1% SDS and protease/phosphatase inhibitors. Homogenates were spun at 100,000 × *g* for 30 min at 4°C and SDS-soluble supernatant boiled in Laemmli sample buffer with 5% β-mercaptoethanol and 1% SDS at 95°C for 5 min.

Immunoblotting

Samples were separated via SDS-PAGE through 4-20% Tris-glycine gels (Bio-Rad #5671095) and transferred onto nitrocellulose membranes (Invitrogen #IB23001) using an iBlot 2 Gel Transfer Device (Invitrogen #IB21001). Loaded sample volumes were normalized to total protein concentration via BCA protein assay (Thermo Scientific #23225). Nitrocellulose membranes were blocked while rocking at room temperature for 1 hr (Rockland #MB-070-010TF) and incubated with blocking buffer containing primary antibodies overnight at 4°C. The following antibodies were employed for immunoblotting: anti-Tau (HT7) (Thermo Fisher Scientific #MN1000, 1:1000, RRID:AB_2314654), anti-pTau S202/T205 (AT8) (Thermo Fisher Scientific #MN1020, 1:1000, RRID:AB_223647), anti-pTau S396/S404 (PHF-1) (Peter Davies personal request, 1:1000, RRID:AB_2315150), anti-pTau S199/S202 (Thermo Fisher Scientific #44-768G, 1:1000, RRID:AB_2533749), anti-pTau T181 (AT270) (Thermo Fisher Scientific #MN1050, 1:1000, RRID:AB_223651), anti-pTau S262 (Thermo Fisher Scientific #44-750G, 1:1000, RRID:AB_2533743), anti-Pyk2 (Cell Signaling Technology #3480, 1:1000, RRID:AB_2174093), anti-pPyk2 Y402 (Cell Signaling Technology #3291, 1:1000, RRID:AB_2300530), anti-GSK3β (Cell Signaling Technology #9315, 1:1000, RRID:AB_490890), anti-GSK3β Y216/pGSK3α Y279 (Abcam #ab68476, 1:1000, RRID:AB_10013745), anti-GSK3β S9 (Cell Signaling Technology #9336, 1:1000, RRID:AB_331405), anti-Fyn (Cell Signaling Technology #4023, 1:1000, RRID:AB_10698604), anti-pSrc Family Y216 (Cell Signaling Technology #6943, 1:1000, RRID:AB_10013641), anti-PSD-95 (Cell Signaling Technology #36233, 1:1000, RRID:AB_2721262), anti-C1q (Abcam #ab182451, 1:1000, RRID:AB_2732849), anti-p38 MAPK (Cell Signaling Technology #9212, 1:1000, RRID:AB_330713), anti-pp38 MAPK T180/Y182 (Cell Signaling Technology #4511, 1:1000, RRID:AB_2139682), anti-LKB1 (Cell

Signaling Technology #3047, 1:1000, RRID:AB_2198327), anti-pLKB1 S428 (Cell Signaling Technology #3482, 1:1000, RRID:AB_2198321), anti-MAPK1 (Cell Signaling Technology #4696, 1:1000, RRID:AB_390780), anti-pMAPK1 T185/Y187 (Cell Signaling Technology #9101, 1:1000, RRID:AB_331646) and anti-β-Actin (Cell Signaling Technology #3700, 1:10,000, RRID:AB_2242334). For experiments shown in Figure 1, all primary antibodies were the same as above accept for the following: anti-GSK3β (Cell Signaling Technology #12456, 1:2000, RRID:AB_2636978), anti-pGSK3β Y216/pGSK3α Y279 (Abcam #ab52188, 1:1000, RRID:AB_880261), anti-Pyk2 (Cell Signaling Technology #3292, 1:1000, RRID:AB_2174097) and anti-β-Actin (Cell Signaling Technology #8457, 1:1000, RRID:AB_10950489). After primary antibody incubation, membranes were washed (3 X 5-min in TBST) and incubated with appropriate secondary antibodies for 1 hr at room temperature. The following secondary antibodies were used for immunoblotting: anti-mouse IRDye 800CW (LI-COR Biosciences #926-32212, 1:20,000, RRID:AB_621847) and α-rabbit IRDye 680CW (LI-COR Biosciences #926-68023, 1:20,000, RRID:AB_10706167). After final washes (5 X 5-min in TBST), immunoblots were scanned with a LI-COR Odyssey infrared imaging system and protein bands quantified using LI-COR Image Studio Lite software, version 5.2.5 (RRID:SCR_013715).

Immunohistology

Immunofluorescence. Brains post-fixed in 4% PFA for 48 hr were vibratome sectioned into 40 µm, free-floating sections, washed in PBS with 0.05% sodium azide and blocked with PBS containing 0.1% Triton X-100 (American Bio #AB02025) and 1% BSA for 1 hr at room temperature. Spinal cord lumbar enlargements were post-fixed and, following embedment in gelatin, sectioned and blocked as described above. Sections were incubated in primary

antibody diluted in PBS with 0.1% Triton X-100 and 1% BSA for 48 hr at 4°C. The following primary antibodies were used for immunohistology: anti-Pyk2 (Santa Cruz Biotechnology #SC-1515, 1:250, RRID:AB_632286), anti-Tau (Agilent #A0024, 1:500, RRID:AB_10013724), anti-pTau S202/T205 (AT8) (Thermo Fisher Scientific #MN1020, 1:1500, RRID:AB_223647), anti-pTau S199/S202 (Thermo Fisher Scientific #44-768G, 1:100, RRID:AB_2533749), anti-NeuN (Abcam #ab104225, 1:500, RRID:AB_10711153), anti-GFAP (Abcam #ab4674, 1:500, RRID:AB_304558), anti-Iba1 (FUJIFILM Wako Shibayagi #019-19741, 1:250, RRID:AB_839504), anti-CD68 (Bio-Rad #MCA1957, 1:500, RRID:AB_322219), anti-PSD-95 (Thermo Fisher Scientific #51-6900, 1:250, RRID:AB_2533914) and anti-C1q (Abcam #ab182451, 1:1000, RRID:AB_2732849). Anti-PSD-95 immunolabeling required an antigen retrieval step prior to primary antibody incubation. For antigen retrieval, sections were transferred to PBS with 1% SDS and heated at 90°C for 5 min. Following primary antibody incubation, sections were washed (3 X in PBS) and incubated in appropriate secondary antibodies diluted in PBS with 0.1% Triton X-100 and 1% BSA overnight at 4°C. The following Alexa Fluor secondary antibodies were employed: anti-goat 488 (Thermo Fisher Scientific #A11055, 1:500, RRID:AB_2534102), anti-mouse 488 (Thermo Fisher Scientific #A-21202, 1:500, RRID:AB_141607), anti-rabbit 568 (Thermo Fisher Scientific #A10042, 1:500, RRID:AB_2534017), anti-rabbit 488 (Thermo Fisher Scientific #A-11008, 1:500, RRID:AB_143165), anti-chicken 647 (Thermo Fisher Scientific #A32933, 1:500, RRID:AB_2762845) and anti-rat 488 (Thermo Fisher Scientific #A-21208, 1:500, RRID:AB_2535794). To minimize lipofuscin autofluorescence, sections were washed after secondary antibody incubation (3 X in PBS), dipped briefly in ddH_2O and incubated in ammonium acetate with 10 mM $CuSO_4$ for 15 min at room temperature. Samples were briefly

returned to ddH_2O, washed in PBS and mounted onto glass slides using Vectashield mounting medium with DAPI (Vector #H-1200).

Cresyl Violet Staining. Post-fixed brain sections were obtained as described above and stained in filtered, pre-warmed 0.1% cresyl violet solution for 10 min. Sections were then washed in ddH_2O for 3 min and de-stained in 95% and 100% ethanol for 10 and 5 min, respectively. Sections were submerged in fresh 100% ethanol for an additional 5 min, placed in xylene for 5 min, removed and placed in fresh xylene for an additional 5 min. Sections were left in xylene overnight and then mounted to glass slides with Cytoseal 60 (Thermo Fisher Scientific #8310-4).

Imaging and Immunohistological Analysis

Image Acquisition. Images of Pyk2, total Tau, phospho-Tau, NeuN, Iba1, CD68 and C1q-immunolabeled sections were captured using a Leica SP8 confocal microscope. Pyk2-immunolabeled sections were imaged using a 10X 0.4 numerical aperture air-objective lens. 4 image slices were acquired throughout the thickness of each section and z-stack compressed via maximum orthogonal projection. 12 contiguous, tiled images (3 × 4) were stitched together to image the hippocampus and cortex. Tau-immunolabeled sections were imaged with a 10X 0.4 numerical aperture air-objective lens. 20 image slices were acquired throughout the entire thickness of each section and z-stack compressed via maximum orthogonal projection. NeuN- and AT8-immunolabled spinal cord sections were imaged with a 10X 0.4 numerical aperture air-objective lens. 10 image slices were acquired throughout the thickness of each section and z-stack compressed via maximum orthogonal projection. To image the entire spinal cord lumbar enragement, 6 contiguous, tiled images (2 × 3) were

stitched together. Iba1 and CD68-immunolabed sections were imaged using a 20X 0.75 numerical aperture air objective and 15 image slices, acquired throughout the thickness of each section, z-stack compressed via maximum orthogonal projection. To image the entire hippocampus, 4 contiguous, tiled images (1 × 4) were stitched together. For C1q imaging, sections were imaged with a 63X 1.4 numerical aperture oil-immersion objective and 5 image slices (1 µm apart) were z-stack compressed via maximum orthogonal projection. For PSD-95 and GFAP imaging, section images were captured using a Zeiss LSM 800 confocal microscope. PSD-95-immunolabeled sections were imaged using a 63X 1.4 numerical aperture oil-immersion objective at the z-level of greatest immunofluorescence for each section. GFAP-labeled sections were imaged with a 20X 0.8 numerical aperture air objective and 10 image slices taken throughout the thickness of the section were z-stack projected via maximum orthogonal projection. To image the entire dentate gyrus, 3 × 5 tiled images were stitched together. For all image acquisition, pinholes were set to 1 AU. Cresyl violet-stained sections were scanned using an Aperio scanner (Aperio CS2, Leica Biosystems).

Image Analysis. Image analysis was conducted using CellProfiler Image Analysis software, version 3.1.8 (RRID:SCR_007358). Macros to identify positive immunofluorescence signal for cell bodies or synaptic puncta were developed and applied uniformly for each immunolabeled epitope. Hippocampal cell layer thickness of cresyl violet-stained sections was determined using Aperio ImageScope, version 12.4.3.5008 (RRID:SCR_020993). All images were acquired, processed and analyzed by an experimenter blinded to animal genotype.

Behavioral Assays

Behavioral assays were administered in the following order: rotarod, wire hang and Morris Water maze (MWM). Noldus CatWalk XT gait analysis was administered to a separate cohort of animals naïve to rotarod, wire hang and MWM. All animals were 9–10 months old at the time of behavioral testing. Exclusion criteria, described below, were applied independently to each assay. Animal handling and analyses (including application of exclusion criteria) were completed by an experimenter blinded to animal genotype. In order to habituate animals to experimenter handling, mice were handled for at least 2 min over 4 days prior to the first behavioral assay. For each assay, mice were habituated to the testing room for 1 hr prior to behavioral testing.

Rotarod. Animals were positioned on the drum of a 4-lane Rotarod device (Economex, Columbus Instruments) set to accelerate 0.1 rotations/min/sec until reaching a top speed of 4 rpm. Trials began at the start of drum rotation. Latency to fall onto a foam pad placed beneath the spinning drum was recorded across five trials with 1 min inter-trial rest periods.

Wire Hang. Animals were placed in the center of a wire grid (wire spacing, 1 cm x 1 cm) which, at the beginning of each trial, was inverted over a foam pad. The latency to fall from the grid was recorded (maximum trial duration, 120 sec) across two trials with a 1 min inter-trial rest period.

MWM. Testing took place over 5 consecutive days, with acquisition trials taking place over the first 3 days and the probe and visible platform trials taking place on days 4 and 5, respectively. Mice were swum in an open pool ~1 m in diameter adorned with distinct visual cues (white poster board marked with black tape) distributed evenly along the pool perimeter.

Water temperature was set to 25°C at the beginning of each testing day. During acquisition, a clear plexiglass platform submerged 1 cm below water level was placed in the center of the target quadrant where it remained for the duration of the acquisition trials. Acquisition trials took place over 6 sessions, two sessions per day, with each session consisting of 4 trials and 1 min inter-trial rest periods. For each trial, mice were placed (facing away from the pool's center) into the pool at one of four drop zones, the orders of which were varied across each session. The time required to locate the submerged platform was recorded for each trial using Panlab SMART video tracking software, version 2.5.21 (RRID:SCR_002852). A trial was considered successfully completed only if the animal spent 1 sec on the platform. Animals unable to locate the submerged platform within the 60 sec maximum trial period were gently guided to the platform and allowed to rest for 10 sec. 24 hr after the final acquisition trial, animals were reintroduced to the pool with the submerged platform removed. During the single probe trial, animals were placed in the zone farthest from the target quadrant and the time spent in the target quadrant recorded (maximum trial duration, 60 sec). To rule out visual impairment as a potential confound, the latency required to reach a visible platform placed in the center of the pool was determined. Visible platform trials were administered until latencies stabilized (defined as a maximum range in latency of 10 sec across 3 consecutive trials) over a maximum number of 15 trials, and the latencies for the final 3 trials were averaged. Animals that were unable to locate the visible platform (1 $PS19^{0/+}$ and 1 $PS19^{0/+}$;$Pyk2^{-/-}$ mouse), were statistical outliers (1 $Pyk2^{-/-}$ mouse) or whose latencies failed to stabilize over 15 trials (1 $Pyk2^{-/-}$ mouse) were excluded from all MWM analyses.

Noldus CatWalk XT. Prior to behavioral testing, animals were habituated and trained to the CatWalk by placing their home-cage beneath a platform located at the target end of the

CatWalk unit. The home-cage was accessible to the animals through an aperture in the platform. Animals were placed onto the target end platform and permitted to explore until they attempted to enter their home-cage through the platform aperture. After 3 successful attempts, a housing-unit was placed over the aperture bridging the end of the CatWalk and the home-cage entrance. Testing began after 3 successful attempts to enter the housing unit from the target end of the CatWalk. Animals were placed at the far end of the CatWalk unit and gait parameters recorded during each successful transverse of the ~1 m long platform track in either direction. Trials were repeated until animals achieved 3 successful runs (maximum run duration, 10 sec; maximum run variation, 75%). Animals unable to ambulate across the platform track were excluded from analysis.

Label-Free Quantitative Proteomics

Sample Preparation. P2' crude synaptosomal pellets from mouse brain (4 biological replicates / genotype) were homogenized by sonication in a buffer containing urea (8 M), ammonium bicarbonate (0.4 M), and protease (Pierce #87786 at 1% of lysis buffer) and phosphatase inhibitor cocktails (Pierce #78420 at 2.5% of lysis buffer). Samples were then centrifuged to pellet cellular debris and supernatant collected for downstream global proteomics sample preparation with slight modification from a previously published protocol [212]. Briefly, proteins were first extracted using cold (-20°C) acetone. A 1:4 ratio of protein solution to cold acetone was incubated for 1 hr at -20°C, then centrifuged at 15,000 $\times$ *g* to pellet out the protein precipitate. Protein pellets were reconstituted in a final solution containing 2 M urea and 25 mM ammonium bicarbonate. Cysteines were reduced with dithiothreitol (DTT) at 37°C for 20 min, cooled and then alkylated with iodoacetamide (IAM) at room temperature in the dark for 20 min. Dual enzymatic digestion was carried out first with

LysC at 37°C for 4 hr and subsequently with Trypsin overnight at 37°C. Digestion was quenched with 0.5% formic acid. Samples were desalted using MiniSpin SPE columns (The Nest Group #HMM S18V) and dried via SpeedVac (Thermo Scientific SAVANT RVT-4104). Pellets were dissolved in a solution containing 70 mM L-glutamic acid, 65% ACN and 2% TFA in water (loading/conditioning buffer for TopTip). Samples were then subjected to titanium dioxide (TiO_2) phospho-peptide enrichment using TopTip (Glygen #TT2TIO). Phospho-peptide enrichment was carried out according to manufacturing specification with the exception of the initial loading/conditioning buffer indicated above. Flow Through peptide eluate (FT, non-bound) was collected and stored at -80°C for mass spectrometry analysis of total proteins. Enriched phospho-peptides (EN, bound) were eluted from each TopTip in three aliquots of 30 µL 28% high-purity ammonium hydroxide. The eluted fraction was dried and re-dried with 2 × 30 µL water by SpeedVac. Enriched fractions were dissolved in 10 µL of 70% formic acid and 30 µL of 50 mM sodium phosphate. Peptide concentrations were determined by NanoDrop spectrophotometer (Thermo Scientific NanoDrop 2000) to load 0.3 µg / 5 µL of each sample for analysis (3 injections / biological replicate) and, for WT vs $Pyk2^{-/-}$ analysis, LC-MS/MS was conducted using an Orbitrap Fusion LC-MS/MS mass spectrometer equipped with a Waters nanoACQUITY Ultra Performance Liquid Chromatography (UPLC) System. For $PS19^{0/+}$ vs $PS19^{0/+}$;$Pyk2^{-/-}$ analysis, LC-MS/MS was conducted using a Q Exactive HF-X Quadrupole-Orbitrap MS system.

Proteomics Data Analysis. Online chromatographic separation was conducted as described previously [213]. Peaks were selected and the generated peak list files were used for phospho-peptide identification using SEQUEST search algorithm in Proteome Discoverer, version 2.2 (RRID:SCR_014477). Searches were conducted against the SwissProt Protein Database (Version SwissProt_2017_01, *Mus musculus*) (RRID:SCR_017486). Search

parameters included: fragment ion mass tolerance of 0.020 Da; parent ion tolerance of 10.0 pp; strict trypsin fragments (enzyme cleavage after the C-terminus of Lysine or Arginine, but not if followed by Proline); variable modification of phospho- Ser, Thr, and Tyr; oxidation of Met; deamidation of Asn and Gln; and carbamidomethlyation of Cys. A decoy search (based on the reverse sequence search) was performed to estimate the false discovery rate (FDR), with a setting of acceptable protein ID having an FDR of <1%. A protein was considered to be positively identified if there were two or more significantly labeled unique peptides. Scaffold Proteome Software, version 4.8.6 (RRID:SCR_014345) was used to obtain quantitative abundance values for comparison between WT and Pyk2$^{-/-}$ genotypes. Abundance values for phospho-enriched samples were normalized to total (FT) values. Proteins significantly differentiated between genotypes were identified using two-tailed *t*-test ($p<0.05$). Two-tailed *t*-tests were conducted and z-scores determined using Microsoft Excel software, version 16.16.27 (RRID:SCR_016137). Enrichment of Gene Ontology terms amongst lists of DEPs were assessed using ClueGO in Cytoscape ([214], RRID: SCR_005748) A protein-protein association network between significantly differentially regulated phospho-proteins was obtained using STRING ([215], RRID:SCR_005223).

Synaptosomal Fractionation

Animals were sacrificed and brain tissue dissected on ice as described above. Hippocampi and cortices from a single hemisphere were homogenized in 200 µl and 400 µl, respectively, Syn-PER Reagent (Thermo Scientific #87793) with protease and phosphatase inhibitors using a polypropylene pellet pestle. Homogenates were centrifuged at 1200 × *g* for 10 min at 4°C. Supernatants were collected and spun again at 15,000 × *g* for 20 min at 4°C. The crude

synaptosomal (P2') pellets were resolubilized in RIPA with 1% SDS and boiled in Laemmli sample buffer with 5% β-mercaptoethanol and 1% SDS at 95°C for 5 min.

Experimental Design and Statistical Analysis

One-way ANOVA with *post hoc* Tukey's multiple comparisons tests, One-way ANOVA with *post hoc* Dunnett's multiple comparisons tests, Log-rank (Mantel-Cox) test and unpaired two-tailed *t*-tests were performed using GraphPad Prism software, versions 8 and 9 (RRID:SCR_002798). Repeated measures ANOVA with *post hoc* Tukey HSD multiple comparisons tests were performed using IBM SPSS Statics software, version 26 (RRID:SCR_019096). For the MWM visible platform test, statistical outliers were identified using the ROUT method (Q = 1%) in GraphPad Prism. Group means ± SEM and samples sizes (*n*) are reported in each figure legend. Data were considered to be statistically significant if $p<0.05$. For all figures, all statistically significant group differences are labeled. For any given group comparison, the lack of any indication of significant difference implies lack of significance by the applied statistical test.

RESULTS

Pyk2 phosphorylates Tau via GSK3β in an *in vitro* over-expression system

The ability of GSK3β to phosphorylate pathophysiologically-relevant resides of Tau is well-documented [194-199], and Pyk2 has been shown activate GSK3β through the phosphorylation of Y216 in GSK3β's activation loop [145, 146, 200]. Although it has previously been demonstrated that Pyk2 can directly phosphorylate Tau at Y18 [202], whether Pyk2 can augment GSK3β's ability to phosphorylate Tau at disease-relevant residues has not been clarified. We over-expressed combinations of GSK3β, Pyk2, Tau and

Fyn in Hek293T cells and measured the phosphorylation of GSK3β at Y216 and Tau at S202/T205 (AT8) (**Fig. 1A–C**). Pyk2 co-transfection with GSK3β led to a significant increase in GSK3β activation, and this activation was further augmented with the addition of Fyn, a kinase known to synergistically co-activate Pyk2 [94, 144, 216, 217] (**Fig. 1A, B**). Over-expression of GSK3β and Pyk2 together led to a significant increase in Tau phosphorylation at S202/T205 compared Tau co-transfected with either kinase alone (**Fig 1A, C**). Over-expression of GSK3β, Pyk2 and Fyn together also led to robust Tau phosphorylation at S202/T205, however this signal failed to reach a level significantly higher than that seen with both GSK3β and Pyk2, suggesting that a ceiling to GSK3β-mediated S202/T205 phosphorylation may have been achieved in this system.

Basal levels of Pyk2 activity suppress Tau phosphorylation in neurons

In order to confirm whether Pyk2 activity positively correlates with Tau phosphorylation at physiological levels of expression in neurons *ex vivo*, we conducted an acute brain slice assay in which we pharmacologically inhibited Pyk2 in mouse hippocampal slices with the selective Pyk2 inhibitor PF-719 (**Fig. 2A–D**). Since basal levels of AT8 Tau phosphorylation were undetectable in WT mice (**Fig. 3A, G**), we used tissue from transgenic PS19$^{0/+}$ mice that express a mutant form of human Tau (MAPT P301S) associated with FTD and are a well-described animal model of tauopathy [218, 219]. Unexpectedly, inhibition of Pyk2 with 1 μM PF-719 resulted in an increase of Tau phosphorylation at S202/T205 (**Fig. 2A, B, D**). Importantly, this increase in Tau phosphorylation occurred independently of any changes in GSK3β activity (**Fig. 2A, C**), suggesting that basal levels of Pyk2 activity suppress Tau phosphorylation through a GSK3β-independent mechanism.

To confirm these results in a second neuronal system, we pharmacologically inhibited Pyk2 in mature iPSC-derived human cortical neurons differentiated from iPSCs via dual SMAD inhibition and patterned into forebrain cortical neurons via Wnt inhibition. This well-described and previously validated method of obtaining cortical neurons from iPSCs has the benefit of recapitulating the differentiation of cortical neurons in the developing human brain without relying on the induced overexpression of transgenic transcription factors such as Ngn2 [211]. While Pyk2 inhibition failed to result in any measurable modulation of GSK3β activity in these neurons, the inhibition of basal Pyk2 activity with PF-719 led to significant increases in Tau phosphorylation at two pathophysiologically-relevant epitopes of Tau, S396/S404 (PHF-1) and S202/T205 (AT8) (**Fig. 2E–I)**. Together, these results suggest that while Pyk2 can phosphorylate Tau through GSK3β when over-expressed at supra-physiological stoichiometries, basal levels of neuronal Pyk2 activity suppress Tau phosphorylation through a mechanism independent measurable changes in the activity of GSK3β.

Pyk2 expression is protective against Tau phosphorylation and pathology *in vivo*

To determine whether Pyk2 expression is protective against Tau phosphorylation in an *in vivo* mammalian system, we again employed $PS19^{0/+}$ transgenic mice, this time crossed with a $Pyk2^{-/-}$ line. To assess the influence of Pyk2 genetic deletion on Tau phosphorylation biochemically, we obtained TBS-insoluble, SDS-soluble fractions from both hippocampi and cortices of 9.5–10.5-month-old WT, $Pyk2^{-/-}$, $PS19^{0/+}$ and $PS19^{0/+}$;$Pyk2^{-/-}$ animals (**Fig. 3A–L**). While there were no detectable levels of TBS-insoluble, SDS-soluble Tau phosphorylated at any disease-relevant epitope analyzed biochemically in WT or $Pyk2^{-/-}$ mice, $PS19^{0/+}$;$Pyk2^{-/-}$ animals demonstrated a significantly higher level of hippocampal Tau phosphorylation at S393/S404 (PHF-1), S262 and S199/S202 compared to $PS19^{0/+}$ mice (**Fig. 3A–F**). Of

phospho-Tau epitopes analyzed in the cortex, only pTau T181 (AT270) demonstrated higher phosphorylation in PS19$^{0/+}$;Pyk2$^{-/-}$ compared to PS19$^{0/+}$ animals, suggesting that Pyk2's influence on regulating Tau phosphorylation may be greater in hippocampus compared to cortex (**Fig. 3G–L**). In support of a region-specific influence of Pyk2 in suppressing Tau phosphorylation, we observed significantly greater Pyk2 expression in the hippocampus compared to cortex both immunohistologically and biochemically (**Fig. S1A–C**). Pyk2 activation was also significantly higher in WT and PS19$^{0/+}$ hippocampus compared to cortex, while Tau-induced activation of Pyk2 in PS19$^{0/+}$ animals was restricted to the hippocampus (**Fig. S1D**). Higher levels of expression and activity of Pyk2 in the hippocampus suggest that its genetic deletion from PS19$^{0/+}$ animals would likely have a greater magnitude of effect on Tau phosphorylation in this region compared to cortex.

The ability of Pyk2 expression to suppress Tau phosphorylation, however, extends beyond hippocampus and cortex. Histological analysis of 9.5–10.5-month-old PS19$^{0/+}$ and PS19$^{0/+}$;Pyk2$^{-/-}$ amygdala also revealed significant increases in immunofluorescent signal of pTau S202/T205 (AT8) in both the number of AT8-positive cell bodies, as well as the area occupied by those cell bodies, and pTau S199/S202 by mean image intensity of immunofluorescent signal (**Fig. 4A–G**). While sexual dimorphism with respect to severity of Tau pathology has been previously reported in PS19 transgenic mice, we observed no differences in amygdalar Tau pathology between PS19$^{0/+}$ and PS19$^{0/+}$;Pyk2$^{-/-}$ animals by any measure when segregated by sex (**Fig. S2**) [220]. No changes were observed in total Tau immunofluorescence between PS19$^{0/+}$ and PS19$^{0/+}$;Pyk2$^{-/-}$ animals, suggesting that Pyk2's ability to suppress Tau pathology is specific to Tau phosphorylation rather than total Tau expression (**Fig. S3**). Taken together, these results provide both biochemical and histological

evidence of Pyk2's role in suppressing Tau phosphorylation in a well-described animal model of tauopathy *in vivo*.

Pyk2 expression is protective against Tau-induced early death and memory impairment in PS19 transgenic mice

We sought to determine whether genetic deletion of Pyk2, found here to exacerbate Tau pathology in $PS19^{0/+}$ mice, would result in appreciable changes in Tau-induced early-death or behavioral deficits in the same model. While, as expected, $PS19^{0/+}$ animals demonstrated a marked reduction in survival compared to WT and $Pyk2^{-/-}$ animals, $PS19^{0/+}$;$Pyk2^{-/-}$ mice showed a significant reduction in survivorship compared to $PS19^{0/+}$ animals (**Fig. 5A**), and segregating survivorship data by sex suggests that this effect is primarily driven by female rather than male mice (**Fig. S4**). Immediately preceding death, $PS19^{0/+}$ and $PS19^{0/+}$;$Pyk2^{-/-}$ animals displayed a rapid, stereotyped deterioration in condition marked by hindlimb paralysis, hunched posture and reduced body weight, all of which have been previously described in this transgenic line [218]. Immunofluorescent labeling of NeuN and pTau S202/T205 (AT8) reveals substantial Tau accumulation in the lumbar enlargement of $PS19^{0/+}$ and $PS19^{0/+}$;$Pyk2^{-/-}$ spinal cord, with AT8-positive immunofluorescent signal colocalizing with NeuN-positive motor neurons in the ventral horn of $PS19^{0/+}$ spinal cord (**Fig. S5**). In $PS19^{0/+}$;$Pyk2^{-/-}$ spinal cord, AT8 immunofluorescence is considerably more diffuse, with marked loss of NeuN-positive motor neurons in the ventral horn (**Fig. S5B**). The presence of Tau inclusions within motor neurons of the lumbar enlargement has been previously suggested as a causal mechanism of hindlimb paralysis in $PS19^{0/+}$ mice, thus the reduced survivorship of $PS19^{0/+}$;$Pyk2^{-/-}$ compared to $PS19^{0/+}$ mice, all of which succumbed to hindlimb

paralysis, likely reflects an acceleration of PS19-mediated Tau pathology in these animals [218].

To assess the influence of Pyk2 expression on Tau-induced spatial memory impairment in $PS19^{0/+}$ animals, we subjected 9–10-month-old animals from all four genotypes to the Morris water maze (MWM) test. While $PS19^{0/+}$ mice of this age demonstrated no significant impairment in learning during MWM acquisition sessions, genetic deletion of Pyk2 significantly impaired MWM spatial memory acquisition in $PS19^{0/+}$;$Pyk2^{-/-}$ compared to WT animals (**Fig. 5B**). Pyk2 deletion on the WT background did not alter performance, as reported previously [186]. To assess long-term spatial memory, animals were subjected to a probe trial 24 hr after the final acquisition session. WT, $Pyk2^{-/-}$ and $PS19^{0/+}$ animals all spent a significantly greater amount of time in the target quadrant compared to the opposite quadrant during the MWM probe trial. $PS19^{0/+}$;$Pyk2^{-/-}$ animals, however, failed to spend significantly more time the target quadrant compared to the opposite quadrant, suggesting that Pyk2 expression is necessary to protect against Tau-induced impairment of long-term spatial memory (**Fig. 5C**). Impaired spatial memory observed in $PS19^{0/+}$;$Pyk2^{-/-}$ mice during MWM acquisition and probe trials could not be explained by visual impairment, as animals from all genotypes were able to effectively locate a visible platform during visual assessment (**Fig. 5D**). Notably, impaired spatial memory in $PS19^{0/+}$;$Pyk2^{-/-}$ mice occurs prior to frank hippocampal neurodegeneration in these animals, as there were no significant reductions in hippocampal cell layer thickness across genotypes (**Fig. S6**).

While both $PS19^{0/+}$ and $PS19^{0/+}$;$Pyk2^{-/-}$ mice weighed significantly less than WT animals, Pyk2 deletion failed to result in any measurable modulation of Tau-induced body mass reduction in $PS19^{0/+}$ mice (**Fig. 5E**). To assess possible Tau-induced impairments in motor

coordination, grip strength and gait patterns, animals were subjected to Rotarod, wire hang and CatWalk XT assays (**Fig. 5F–J**). There were no observable differences across genotypes by any of these measures, suggesting that while Pyk2's suppression of Tau pathology is concomitant with an exacerbation of Tau-induced early death and spatial memory impairment in $PS19^{0/+}$;$Pyk2^{-/-}$ animals, these results are not associated with any measurable sensorimotor deficits.

Proteomic analysis reveals Pyk2's role in regulating synaptic translational machinery, C1q expression and MAPK1 activity in PS19 mice

To more completely elucidate the effect of genetic Pyk2 deletion on $PS19^{0/+}$ transgenic animals and to reveal the possible mechanisms by which Pyk2 suppresses Tau phosphorylation, pathology and Tau-associated phenotypes, we conducted LC-MS/MS label-free profiling of $PS19^{0/+}$ and $PS19^{0/+}$;$Pyk2^{-/-}$ hippocampal tryptic peptides. Since we measured no discernable changes in either hippocampal astrogliosis or microgliosis across WT, $Pyk2^{-/-}$, $PS19^{0/+}$ and $PS19^{0/+}$;$Pyk2^{-/-}$ animals (**Fig. S7**), we focused our analysis on neuronal, cell-autonomous mechanisms and enhanced our analysis by utilizing hippocampal synaptosomal fractions as starting material.

Proteomic analysis revealed 338 significantly differentially regulated proteins between $PS19^{0/+}$ and $PS19^{0/+}$;$Pyk2^{-/-}$ hippocampal synaptosomes (**Fig. 6A, B**). Intriguingly, 32 (9.5%) of the identified hits were either 40S or 60S ribosomal proteins, while an additional 6 (1.8%) of identified hits were either eukaryotic translation initiation or elongation factors, all of which were upregulated in $PS19^{0/+}$;$Pyk2^{-/-}$ compared to $PS19^{0/+}$ animals (**Fig. 6B**). Dysregulation of protein translational machinery, including altered expression of ribosomal proteins, has been

observed across multiple Tau transgenic lines, and the aberrant association of Tau with ribosomal proteins, as seen in both MAPT P301L mice and AD brains, has been shown to disrupt synthesis of proteins critical for synaptic function including PSD-95 [221-224]. Notably, the expressions of both C1qa and C1qb, two components of the classical complement system, were also significantly upregulated in $PS19^{0/+}$;$Pyk2^{-/-}$ synaptosomes, suggesting that endogenous Pyk2 expression may protect against synaptic dysfunction through the suppression of synaptic C1q deposition (**Fig. 6B**).

Since Pyk2 is a protein kinase and Tau phosphorylation is correlated with pathophysiology, we specifically assessed phospho-enriched peptides obtained from $PS19^{0/+}$ and $PS19^{0/+}$;$Pyk2^{-/-}$ hippocampal synaptosomes through LC-MS/MS label-free profiling. For each experimental replicate, relative abundance values for phospho-enriched hippocampal synaptosomal proteins were normalized to their respective total protein values to determine relative normalized phospho-protein abundance. We identified 50 significantly differentially regulated phospho-proteins between $PS19^{0/+}$ and $PS19^{0/+}$;$Pyk2^{-/-}$ hippocampal synaptosomes (**Fig. 6C, D**). Of interest, the phosphorylation of MAPK1 (ERK2), a known regulator of Tau phosphorylation [206, 225-227], was significantly decreased at residue Y187 in $PS19^{0/+}$;$Pyk2^{-/-}$ compared to $PS19^{0/+}$ hippocampal synaptosomes. The phosphorylation of Y187 and T185, two residues present on the activation loop of MAPK1, are required for full activation of the kinase [228, 229], and thus a decrease in MAPK1 phosphorylation at Y187 suggests a decrease in MAPK1 kinase activity in $PS19^{0/+}$;$Pyk2^{-/-}$ animals.

Pyk2 expression is protective against Tau-induced C1q deposition

From the proteomic changes, we focused our initial attention on C1q, which is a key component of the classical complement system and, in the CNS, plays a critical role in microglia-mediated synaptic pruning during development [230]. Levels of C1q are known to increase with age, and AD brains show increased neuronal deposition of C1q in both the hippocampus and frontal cortex [231]. Expression of C1q is augmented in response to both injury and Aβ exposure, and increased levels of C1q deposition at synapses are associated with microglia-mediated synaptic engulfment and synapse loss in models of neurogenerative diseases such as AD and FTD [232, 233]. We sought to biochemically validate the proteomics-based observation of increased C1qa and C1qb expression in $PS19^{0/+}$;$Pyk2^{-/-}$ hippocampal synaptosomes and assessed whether genetic Pyk2 deletion modulated Tau-induced C1q deposition in a manner that reflects Pyk2's role in suppressing Tau-associated memory impairment in $PS19^{0/+}$ mice. We obtained crude synaptosomal fractions from both hippocampus (**Fig. 7A–D**) and cortex (**Fig. 7E–H**) and found that $PS19^{0/+}$;$Pyk2^{-/-}$ mice displayed significantly higher levels of hippocampal, synaptosomal C1q (normalized to β-Actin) compared to WT, $Pyk2^{-/-}$ and $PS19^{0/+}$ animals. In the cortex, levels of synaptosomal C1q were significantly higher in $PS19^{0/+}$;$Pyk2^{-/-}$ compared to WT and $PS19^{0/+}$ mice.

Although reduced PSD-95 expression observed in $PS19^{0/+}$;$Pyk2^{-/-}$ hippocampal synaptosomes only reached significance when compared to $Pyk2^{-/-}$ mice (**Fig. 7A, B**), histological analysis revealed significant decreases in PSD-95-positive puncta in both $PS19^{0/+}$ and $PS19^{0/+}$;$Pyk2^{-/-}$ dentate gyrus compared to WT and $Pyk2^{-/-}$ mice (**Fig. 7I, J**). In the CA3 region of the hippocampus, C1q immunofluorescence signal was significantly increased in both $PS19^{0/+}$ and $PS19^{0/+}$;$Pyk2^{-/-}$ animals compared to WT and $Pyk2^{-/-}$ mice (**Fig. 7K, L**). However, in the dentate gyrus C1q immunofluorescence was significantly increased in

PS19$^{0/+}$;Pyk2$^{-/-}$ animals (compared to WT), while no such increase was observed in PS19$^{0/+}$ mice (**Fig. 7M, N**).

Proteomic analysis reveals several possible regulators of Tau phosphorylation modulated by Pyk2 expression

Our observations of exacerbated Tau pathology, early death and memory impairment in PS19$^{0/+}$;Pyk2$^{-/-}$ animals suggest that Pyk2 deletion accelerates disease progression in PS19$^{0/+}$ transgenic mice. Identifying mechanisms by which Pyk2 may suppress Tau phosphorylation from proteomics-based comparison of aged-matched PS19$^{0/+}$ and PS19$^{0/+}$;Pyk2$^{-/-}$ animals is therefore complicated by the fact that PS19$^{0/+}$;Pyk2$^{-/-}$ animals likely represent a more advanced stage of disease. Alterations to protein translational machinery, which likely result in substantial differences in global protein translation between PS19$^{0/+}$ and PS19$^{0/+}$;Pyk2$^{-/-}$ mice, further complicate the use of these animals for the identification of Pyk2-modulated regulators of Tau phosphorylation through phospho-proteomic analysis. Considering these limitations, we also conducted LC-MS/MS label-free profiling of WT and Pyk2$^{-/-}$ hippocampal synaptic peptides, as any observed changes in the synaptic proteome between animals of these genotypes would more likely reflect the influence of Pyk2 expression *per se*, as opposed to differences in the stage of PS19-driven pathology.

Proteomic analysis of relative protein abundance revealed 170 significantly differentially regulated proteins between WT and Pyk2$^{-/-}$ mice (**Fig. 8A, B**). Many of these hits represent potentially intriguing avenues for further exploration and may help elucidate Pyk2's role in synaptic development and function [Dlg1, Dlg2, Dlg4 (PSD-95), Homer1, Camk2b, Camk2d, Nrxn1, Syt2, Gria2 (GluR2), Arhgef7 and Cask] and disease [Snca (α-synuclein) and Snca (β-

synuclein)]. However, for the purposes of this paper, and in order explain Pyk2's role in regulating signaling events that influence Tau phosphorylation, we focused our analysis on differential levels of phospho-peptides from the synaptosomal proteins with all values normalized to total protein abundance (**Fig. 8C–E**). We identified a total of 38 phospho-proteins that were significantly differentially regulated between WT and Pyk2$^{-/-}$ animals (**Fig. 8C**).

In order to identify candidate regulators of Tau phosphorylation modulated by Pyk2 expression, we used STRING to generate a functional protein association network that included all 38 phospho-protein hits as well as MAPT (Tau) (**Fig. 8E**). Proximate regulators of Tau phosphorylation were defined *a priori* as kinases or phosphatases positioned one or two degrees from MAPT in the association network. Using this definition, we identified 6 possible Pyk2-modulated regulators of Tau phosphorylation (6 kinases, 0 phosphatases): Gsk3α, Gsk3β, Brsk1, Mapk1, Mark2 and Lkb1 (Stk11). Interestingly, the phosphorylation of MAPK1, the only proximate regulator of Tau phosphorylation identified in both the WT vs Pyk2$^{-/-}$ and the PS19$^{0/+}$ vs PS19$^{0/+}$;Pyk2$^{-/-}$ phospho-proteomic analyses, was also decreased in Pyk2$^{-/-}$ hippocampal synaptosomes. However, since the activity of this kinase was decreased (rather than increased) with Pyk2 deletion, it is unlikely that this putative Tau kinase would explain Pyk2's ability to suppress Tau phosphorylation.

GO enrichment analysis reveals Pyk2-dependent modulation of multiple biological pathways unique to PS19 animals

To further understand the pattern of differential protein abundance and phosphorylation in hippocampal synaptosomes, we conducted Gene Ontology (GO) enrichment analysis and

generated functionally-grouped network maps of significantly differentially regulated synaptic proteins identified across each proteomic and phospho-proteomic analysis. Network maps showing clusters of significantly enriched pathways (p<0.05) were generated in ClueGO using the GO Biological Process ontology with network parameters for each analysis kept constant for proteomic (total protein) and phospho-proteomic (normalized phospho-enriched protein) hits, respectively (**Fig. 9A, B, D, E**). Across proteomic analyses of total hippocampal synaptosomal proteins, 25 proteins were shared between WT vs Pyk2$^{-/-}$ and PS19$^{0/+}$ vs PS19$^{0/+}$;Pyk2$^{-/-}$ animals, representing 14.7% of hits identified in the WT vs Pyk2$^{-/-}$ analysis (**Fig. 9C**). GO enrichment of total proteins reveals several biological pathways conserved between WT vs Pyk2$^{-/-}$ and PS19$^{0/+}$ vs PS19$^{0/+}$;Pyk2$^{-/-}$ proteomic analyses, reflecting Pyk2's role in regulating neuronal projection (GO terms: regulation of neuron projection development; regulation of plasma membrane bounded cell projection organization; regulation of plasma membrane bounded cell projection organization) and exocytosis (GO terms: regulated exocytosis; exocytosis) (**Fig. 9A, B**, **Table 1**).

Several additional pathways, however, were unique to the PS19$^{0/+}$ vs PS19$^{0/+}$;Pyk2$^{-/-}$ analysis, likely reflecting Pyk2's role in regulating aberrant, Tau-associated cellular processes specific to PS19$^{0/+}$ mice, including pathways involved in protein translation and processing (GO terms: regulation of translation; protein polymerization; negative regulation of protein metabolic process; negative regulation of cellular protein metabolic process) (**Fig. 9B**). Also unique to the PS19$^{0/+}$ vs PS19$^{0/+}$;Pyk2$^{-/-}$ analysis are pathways involved in glial development (GO terms: glial cell development, glial cell differentiation; gliogenesis), myelination (GO term: myelination) and synaptic homeostasis (GO terms: positive regulation of synaptic transmission; regulation of synaptic plasticity; regulation of trans-synaptic signaling; chemical synaptic transmission), the latter of which may reflect impaired synaptic function in

PS19$^{0/+}$;Pyk2$^{-/-}$ animals. Using Kyoto Encyclopedia of Genes and Genomes (KEGG) enrichment ontology for total protein hits identifies a single node for the PS19$^{0/+}$ vs PS19$^{0/+}$;Pyk2$^{-/-}$ proteomic analysis (GO term: pathways of neurodegeneration), while no pathways were identified for the WT vs Pyk2$^{-/-}$ analysis using the same parameters, suggesting that Pyk2 deletion alters pathways related to neurodegeneration uniquely in PS19$^{0/+}$, but not WT animals (**Table S1**).

We also generated functionally-grouped network maps for normalized phospho-enriched protein hits across phospho-proteomic analyses (**Fig. 9 D, E**). Encouragingly, GO enrichment analysis of WT vs Pyk2$^{-/-}$ hits revealed significant enrichment for multiple biological pathways involved in protein phosphorylation (GO terms: tau-protein kinase activity; protein serine kinase activity; protein threonine kinase activity; regulation of protein phosphorylation; peptidyl-serine phosphorylation; protein phosphorylation), with “tau-protein kinase activity” having the highest percentage of associated genes of any identified pathway (11.43%) (**Table 2**). Using the same network parameters, we found considerably fewer enriched pathways from hits identified from the PS19$^{0/+}$ vs PS19$^{0/+}$;Pyk2$^{-/-}$ analysis, with all significantly enriched pathways relating to cation homeostasis (GO terms: regulation of calcium ion transport; cellular calcium ion homeostasis; cation channel activity), likely reflecting Pyk2’s role in regulating calcium homeostasis in PS19$^{0/+}$ transgenic mice (**Fig. 9E**). Only 3 hits (7.9% of WT vs Pyk2$^{-/-}$ hits) were shared between phospho-proteomic analyses (**Fig. 9F**). The lack of enriched pathways relating to protein phosphorylation in the PS19$^{0/+}$ vs PS19$^{0/+}$;Pyk2$^{-/-}$ analysis further suggests that phospho-proteomic hits that may mechanistically explain Pyk2’s role in suppressing Tau phosphorylation are likely masked in PS19$^{0/+}$ animals as pathology progresses.

Pyk2 inhibits LKB1 (SKT11) and p38 MAPK activity

Because LKB1 is implicated in both Aβ processing as well as Tau phosphorylation, and thus, like Pyk2, is well-positioned to serve as possible mechanistic link between Aβ and Tau, we selected this kinase for further validation [234-236]. To confirm whether Pyk2 modulates LKB1 (STK11) activity, we inhibited Pyk2 pharmacologically in mature iPSC-derived human cortical neurons and measured the phosphorylation of LKB1 biochemically at S428. The phosphorylation of this serine residue, located within the C-terminal domain of LKB1, is required for LKB1 nuclear export, substrate biding and activation [237-239]. Since evidence of LKB1's ability to directly phosphorylate Tau is lacking, we also measured the activity of p38 MAPK, a known downstream effector of LKB1 signaling [203, 204] and a direct kinase of Tau [205-207], through the phosphorylation of T180/Y182. The phosphorylation of p38 MAPK at T180/Y182, two auto-phosphorylated residues present in the protein's activation loop required for catalytic activity and substrate binding, are well-validated markers of p38 MAPK activity [240-243].

In iPSC-derived human cortical neurons, Pyk2 inhibition with PF-719 significantly increased both the phosphorylation of LKB1 at S428 as well as the phosphorylation of p38 MAPK at T180/Y182, suggesting that basal levels of neuronal Pyk2 activity suppress the activation of both LKB1 and p38 MAPK in a manner that reflects Py2k's ability to inhibit Tau phosphorylation (**Fig. 10A–C**). Since the phosphorylation of MAPK1 was significantly differentially regulated in both WT vs $Pyk2^{-/-}$ and $PS19^{0/+}$ vs $PS19^{0/+}$;$Pyk2^{-/-}$ phospho-proteomic analyses, we also assessed whether pharmacological Pyk2 inhibition would modulate MAPK1 activity via phosphorylation of its activation loop at T185/Y187 in iPSC-derived human cortical neurons. Consistent with our phospho-proteomic results suggesting decreased phosphorylation of MAPK1 in both Pyk2 and $PS19^{0/+}$;$Pyk2^{-/-}$ hippocampal

synaptosomes, we observed significant inhibition of MAPK1 phosphorylation at T185/Y187 with pharmacological inhibition of Pyk2, suggesting that Pyk2 positively regulates the activity of MAPK1 (**Fig. S8**).

We also assessed the activation of LKB1 and p38 MAPK in hippocampal tissue from 9.5–10-month old WT, Pyk2$^{-/-}$, PS19$^{0/+}$ and PS19$^{0/+}$;Pyk2$^{-/-}$ animals (**Fig. 10D–K**). TBS-soluble LKB1 demonstrated significantly higher activation (pLKB1 S428 normalized to total LKB1) in PS19$^{0/+}$;Pyk2$^{-/-}$ animals compared to WT and Pyk2$^{-/-}$ mice, though no changes in TBS-soluble p38 MAPK activity (p38 MAPK T180/Y182 normalized to total p38 MAPK) were observed across genotypes (**Fig. 10D–F**). However, in TBS-insoluble, SDS-soluble fractions that are likely most relevant to aberrant activation and Tau accumulation, the pattern was reversed. While there were no measurable changes in the activity of SDS-soluble LKB1 (pLKB1 S428 normalized to total LKB1) across genotypes, PS19$^{0/+}$;Pyk2$^{-/-}$ animals showed significantly higher activation of SDS-soluble p38 MAPK (p38 MAPK T180/Y182 normalized to total p38 MAPK) compared to WT animals (**Fig. 10G–I**). When normalized to β-Actin, as a measure of total available active kinase, PS19$^{0/+}$;Pyk2$^{-/-}$ animals displayed increased levels of SDS-soluble p38 MAPK T182/Y182 compared to PS19$^{0/+}$ mice, though we observed no changes in levels of active, SDS-soluble LKB1 (pLKB1 S428 normalized to β-Actin) across genotypes (**Fig. 10J–K**).

Taken together, these results are consistent with the activities of LKB1 and p38 MAPK contributing to Pyk2's role in protecting against Tau phosphorylation, Tau pathology, Tau-induced early death, memory impairment and C1q deposition in PS19$^{0/+}$ transgenic animals. While we provide direct evidence for endogenous Pyk2 expression restricting levels of active

p38 MAPK, a known Tau kinase, in PS19$^{0/+}$ hippocampus, it remains possible that additional kinases participate in Pyk2-dependent suppression of mutant Tau phenotypes.

DISCUSSION

The results described here demonstrate a protective role for Pyk2 in suppressing Tau phosphorylation and Tau pathology as well as Tau-induced early death, spatial memory impairment and C1q deposition in PS19$^{0/+}$ transgenic mice. Correlative evidence suggesting a role for Pyk2 in regulating Tau is abundant. Pyk2 (*PTK2B*), which has been repeatedly identified as a genetic LOAD risk factor [132, 133, 182-184], colocalizes with hyperphosphorylated Tau fibrils in AD brains and interacts with Tau when expressed in Hek293 cells [201]. Although at least one group has reported a positive relationship between Pyk2 and Tau phosphorylation in MAPT P301L transgenic mice [202], this association likely depends on Pyk2 over-expression, which in the aforementioned report was driven by the mThy1.2 promoter. Indeed, our results also demonstrate a positive relationship between Pyk2 over-expression and Tau phosphorylation in Hek293T cells, which, as we report here, was dependent on the co-expression of GSK3β.

In order to rule out the potential confound of non-specific kinase-substrate interactions resulting from protein over-expression, we sought to manipulate both the activity and expression of endogenous Pyk2 using iPSC-derived human cortical neurons and PS19$^{0/+}$ (MAPT P301S) transgenic mice. Pharmacological inhibition of basal Pyk2 activity using the selective Pyk2 inhibitor PF-719 increased the phosphorylation of Tau at multiple pathophysiologically-relevant residues in both hippocampal-enriched acute brain slices from PS19$^{0/+}$ mice and in mature iPSC-derived human cortical neurons. As the phosphorylation of

these serine and threonine Tau residues occurred independently of any measurable changes to GSK3β activity, other serine/threonine kinases or phosphatases modulated by Pyk2 are likely to be involved.

In support of a protective role for Pyk2 with respect to Tau phosphorylation, genetic deletion of Pyk2 from $PS19^{0/+}$ animals augmented Tau phosphorylation and Tau pathology while exacerbating Tau-induced early death, spatial memory impairment and C1q deposition at synapses. All $PS19^{0/+}$ and $PS19^{0/+}$;$Pyk2^{-/-}$ animals succumbed to a rapid onset of hindlimb paralysis, followed immediately by dramatic reduction in body weight and death. Although the window between onset of gross motor deficits and animal death was short enough to preclude capture by sensorimotor assays, we observed evidence of pronounced Tau pathology extending into the lumbar enlargement of $PS19^{0/+}$ and $PS19^{0/+}$;$Pyk2^{-/-}$ spinal cord, as described previously [218]. The presence of Tau pathology in the spinal cord and the colocalization of AT8-immunofluorescent signal with NeuN-positive motor neurons in the ventral horn, absent measurable sensorimotor impairment, suggests a high threshold for Tau pathological burden in $PS19^{0/+}$ mice before the rapid emergence of hindlimb paralysis.

No memory impairment was observed in $PS19^{0/+}$ animals via MWM at the ages examined, and we were unable to age these mice further without substantial losses in $PS19^{0/+}$;$Pyk2^{-/-}$ animals whose survivorship was significantly reduced compared $PS19^{0/+}$ mice and likely driven by the spinal cord pathology. Though other groups have observed spatial memory impairment in $PS19^{0/+}$ animals before 9 months, backcrossing these mice to a C57BL/6J background may have resulted in delayed phenotypic onset. Indeed, phenotypic drift in this transgenic line has been previously reported [244, 245]. We suspect, due to the significant reduction in PSD-95-positive puncta observed in the dentate gyrus, that $PS19^{0/+}$ animals

would have likely demonstrated impaired spatial memory if allowed to age further. As no impairments were observed in Pyk2$^{-/-}$ animals, the exacerbations in Tau-induced phenotypes observed in PS19$^{0/+}$;Pyk2$^{-/-}$ animals likely reflect Pyk2's suppression of Tau phosphorylation *per se*, resulting in an acceleration of Tau pathology and PS19-associated phenotypes.

Interestingly, impaired spatial memory observed in PS19$^{0/+}$;Pyk2$^{-/-}$ animals occurred independently of any measurable changes in either hippocampal cell layer thickness or synapse density, suggesting that Pyk2 expression in the setting of Tau accumulation modulates synaptic function without affecting synapse number. Observations of impaired synaptic function without associated reductions in synapse density are not without precedence. Synaptic C1q deposition, for example, has previously been found to impair synaptic transmission independent changes in synapse number [231]. Proteomic and biochemical analysis reveal that Pyk2 deletion significantly increased synaptic C1q deposition in PS19$^{0/+}$ hippocampus and cortex, offering a potential mechanistic explanation for impaired memory in PS19$^{0/+}$;Pyk2$^{-/-}$ mice absent any measurable differences in synapse density between PS19$^{0/+}$ and PS19$^{0/+}$;Pyk2$^{-/-}$ animals.

In addition to increased synaptic C1q expression, we observed evidence of substantial disruption to protein translational machinery in PS19$^{0/+}$ animals with Pyk2 genetic deletion. This, combined with the observation that deletion of Pyk2 likely accelerates the emergence of PS19-associated phenotypes including pathology and early death, confounded the use of PS19$^{0/+}$ animals to identify Pyk2-modulated regulators of Tau phosphorylation. To better elucidate the mechanisms by which Pyk2 suppresses Tau phosphorylation, we conducted phospho-proteomic analysis of hippocampal synaptosomes from WT and Pyk2$^{-/-}$ mice and identified 6 putative, proximate regulators of Tau modulated by Pyk2 expression. Of these,

we selected LKB1 (STK11) for further validation. Although LKB1 is both necessary and sufficient to induce Tau phosphorylation, LKB1 does not phosphorylate Tau directly [234]. Therefore, in addition to LKB1, we also assessed the ability of Pyk2 to modulate the activity of a known LKB1 substrate and direct kinase of Tau, p38 MAPK [203-209].

Pharmacological inhibition of Pyk2 significantly increased LKB1 and p38 MAPK activity in iPSC-derived human cortical neurons, and the activities of both kinases were significantly elevated in $PS19^{0/+}$;$Pyk2^{-/-}$ hippocampus. Furthermore, Pyk2 deletion significantly increased levels of active p38 MAPK in $PS19^{0/+}$ mice, providing direct evidence that Pyk2 may suppress Tau phosphorylation by limiting hippocampal p38 MAPK activity. Whether Pyk2 acts on these kinases directly or indirectly, and whether any of these interactions can be therapeutically modulated for the treatment of AD has yet to be determined.

Although we investigated LKB1 and p38 MAPK here, it is likely that other kinases also play a role in mediating Pyk2's suppression of Tau phosphorylation. Like p38 MAPK, MAPK1 has also been identified as a direct Tau kinase, however at least one report shows decreased Tau phosphorylation at S396 with MAPK1 overexpression [246]. Here, we see evidence of a direct relationship between Pyk2 and MAPK1 activity, raising the possibility that Pyk2-mediated activation of MAPK1 may also lead to decreased Tau phosphorylation in $PS19^{0/+}$ animals. MAPKs, a family of kinases that also include JNK, have long been implicated in the pathogenesis of AD [247-250], and a recent large-scale proteomic analysis of postmortem AD brain tissue from the Accelerated Medicines Partnership for Alzheimer's Disease (AMP-AD) Consortium revealed significant enrichment for proteins related to MAPK signaling and metabolism that strongly correlated with cognitive decline [251].

CONCLUSIONS

The *PTK2B* locus encoding the Pyk2 protein is one of the few validated GWAS risk factors for late-onset Alzheimer's disease expressed primarily in neurons. Here, we show that in PS19 (MAPT P301S) transgenic mice and in human iPSC-derived neurons, reduced Pyk2 activity exacerbates Tau phosphorylation, pathology and Tau-dependent phenotypes including reduced mouse survival, memory impairment and C1q deposition. Proteomic analysis revealed several proximate regulators of Tau phosphorylation modulated by Pyk2 expression, and direct testing supports a role for LKB1 and, more directly, p38 MAPK in mediating Pyk2's ability to suppress Tau phosphorylation.

Our previous work has shown that endogenous Pyk2 activation driven by Aβ signaling alters F-actin dynamics and leads to dendritic spine loss with impairment of memory function such that Pyk2-null animals are protected from transgenes driving Aβ pathology [186, 187]. Thus, Pyk2 activity exhibits divergent effects on Aβ versus Tau driven toxicity in AD mouse models; on the one hand contributing to toxic Aβ signaling and, on the other, protecting against Tau phosphorylation and related pathology. The interaction between these divergent Pyk2 effects during the course of AD is not yet delineated, and whether Aβ signaling disrupts Pyk2's ability to suppress Tau phosphorylation is unknown. As a corollary, any potential therapeutic effect of Pyk2 modulators might depend on disease stage. Pyk2 inhibition, for example, might be most effective during early stages of AD when Aβ-dependent pathophysiology dominates over Tau-dependent pathophysiology.

FIGURES

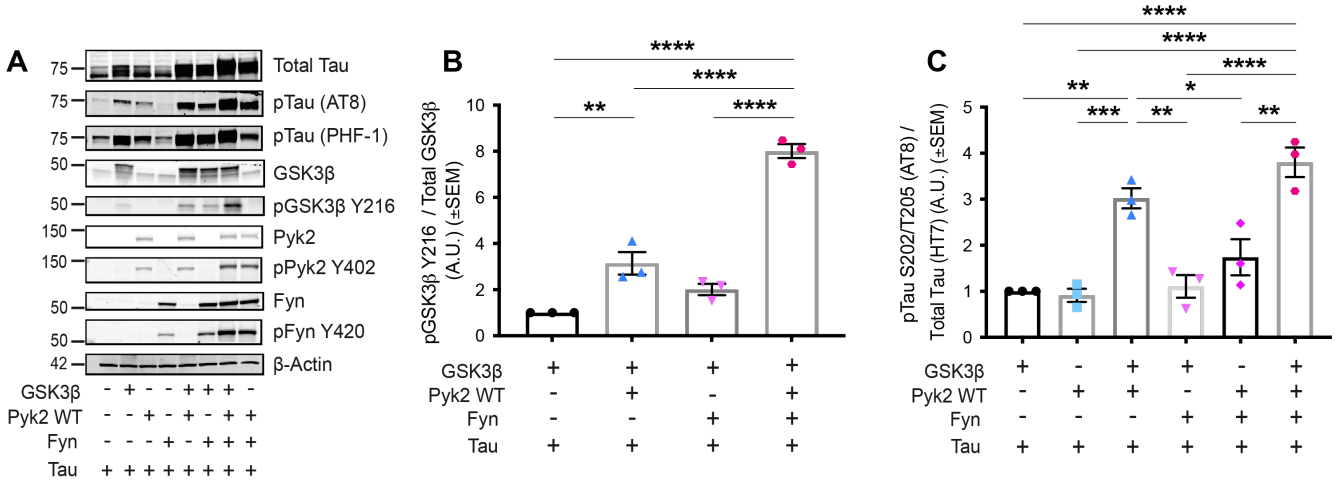

Figure 1. Pyk2 phosphorylates Tau via GSK3β in a Hek293T over-expression system. Hek293T cells were transfected with combinations of the proteins indicated, and lysates separated via SDS-PAGE. Separated lysates were immunoblotted with the antibodies listed. **A**, Representative immunoblot images of transfected Hek293T cells. **B** and **C**, Quantification of **A**. Over-expression of Pyk2 led to a significant increase in the activity of over-expressed GSK3β (pGSK3β Y216 normalized to total GSK3β). This increase was further augmented by the co-transfection of Fyn with GSK3β and Pyk2 (**B**). The phosphorylation of over-expressed Tau at S202/T205 (AT8) normalized to total Tau (HT7) was significantly increased when co-transfected with GSK3β and Pyk2, but not when co-transfected with either kinase alone. No further increase in normalized AT8 signal was observed when Tau, Pyk2 and GSK3β were co-transfected with Fyn. Data are graphed as mean ± SEM, one-way ANOVA with Tukey's multiple comparisons test, *p<0.05, **p<0.01, ***p<0.001, ****p<0.0001, n = 3.

*Data presented in Figure 1, shown here, were collected by Fulin Guan.

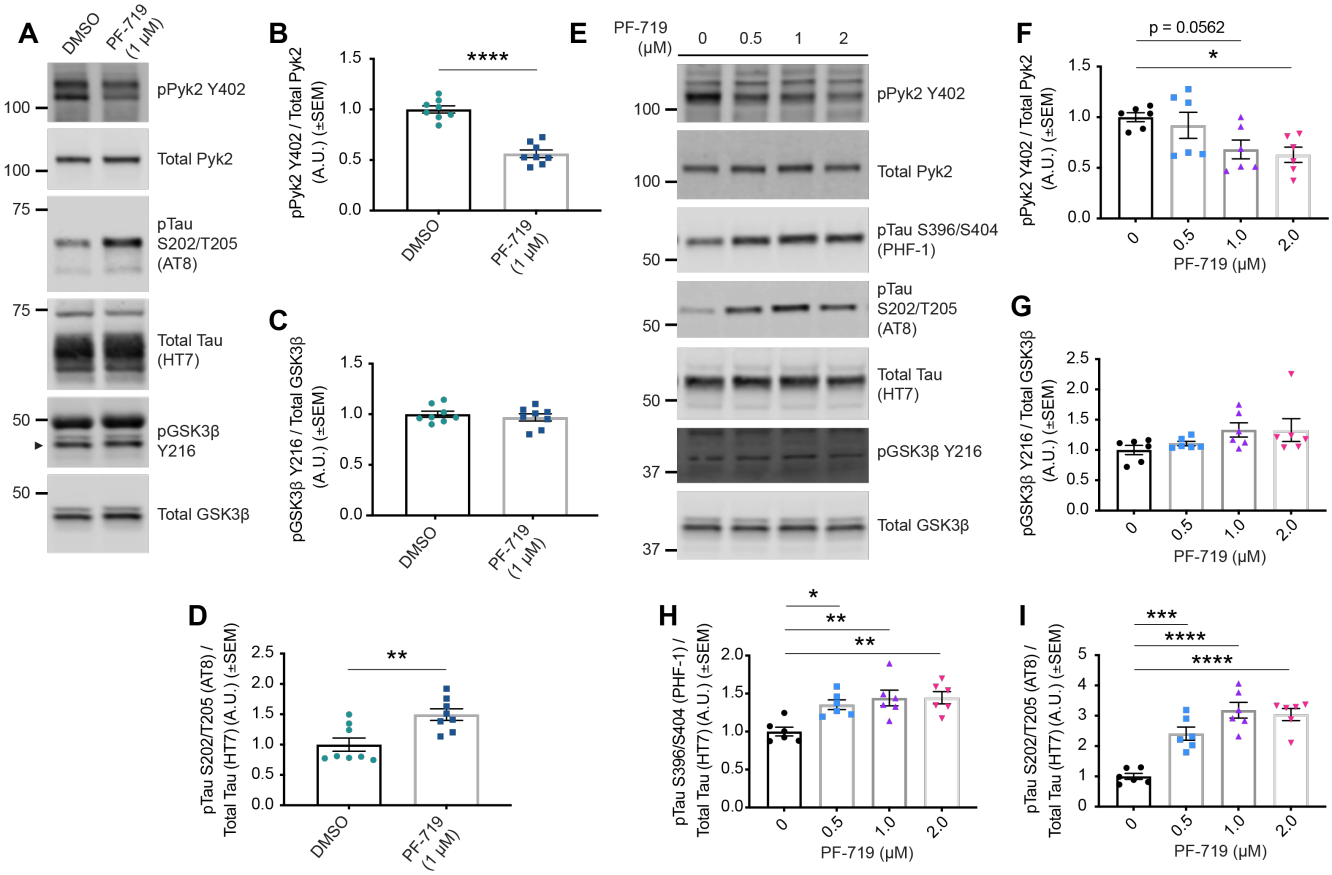

Figure 2. Pharmacological inhibition of Pyk2 increases Tau phosphorylation independent of changes in GSK3β activity. **A**–**D**, Acute hippocampal slices (thickness, 400 μm) from 4.5–5.5-month-old PS19$^{0/+}$ animals were treated with 1 μM Pyk2 inhibitor (PF-719) for 2 hr in oxygenated artificial CSF at room temperature and were homogenized in RIPA immediately following treatment. RIPA-soluble lysates were separated by SDS-PAGE and immunoblotted with the antibodies indicated. **A**, Representative immunoblot images of lysates from PF-719-treated acute hippocampal slices. Arrowhead indicates pGSK3β Y216. **B**–**D**, Quantification of **A**. PF-719 treatment successfully inhibited Pyk2 activity (pPyk2 Y402 normalized to total Pyk2). Pyk2 inhibition significantly increased the phosphorylation Tau at S202/T205 (AT8) normalized to total Tau (HT7) (**D**) while GSK3β activity (pGSK3β Y216 normalized to total GSK3β) remained unchanged (**C**). Data are graphed as mean ± SEM, unpaired two-tailed *t*-test, ***p*<0.01, *****p*<0.0001, *n* = 8. **E**–**I**, iPSC-derived human cortical neurons (90–100 days

post terminal differentiation) were treated with PF-719 at indicated concentrations for 2 hr at 37°C and, immediately following treatment, homogenized in RIPA containing 1% SDS. Lysates were separated by SDS-PAGE and immunoblotted with the antibodies listed. **E**, Representative immunoblot images of lysates from PF-719-treated iPSC-derived human cortical neurons. **F**–**I**, Quantification of **E**. PF-719 treatment significantly inhibited Pyk2 activity (pPyk2 Y402 normalized to total Pyk2) (**F**), while no changes in GSK3β activity (pGSK3β Y216 normalized to total GSK3β) were observed at any concentration of PF-719 (**G**). Pyk2 inhibition resulted in increased levels of Tau phosphorylation at S396/S404 (PHF-1) normalized to total Tau (HT7) (**H**) and S202/T205 (AT8) normalized to total Tau (HT7) (**I**) at every concentration of PF-719 administered. Data are graphed as mean ± SEM, one-way ANOVA with Dunnett's multiple comparisons test, *p<0.05, **p<0.01, ***p<0.001, ****p<0.0001, n = 6.

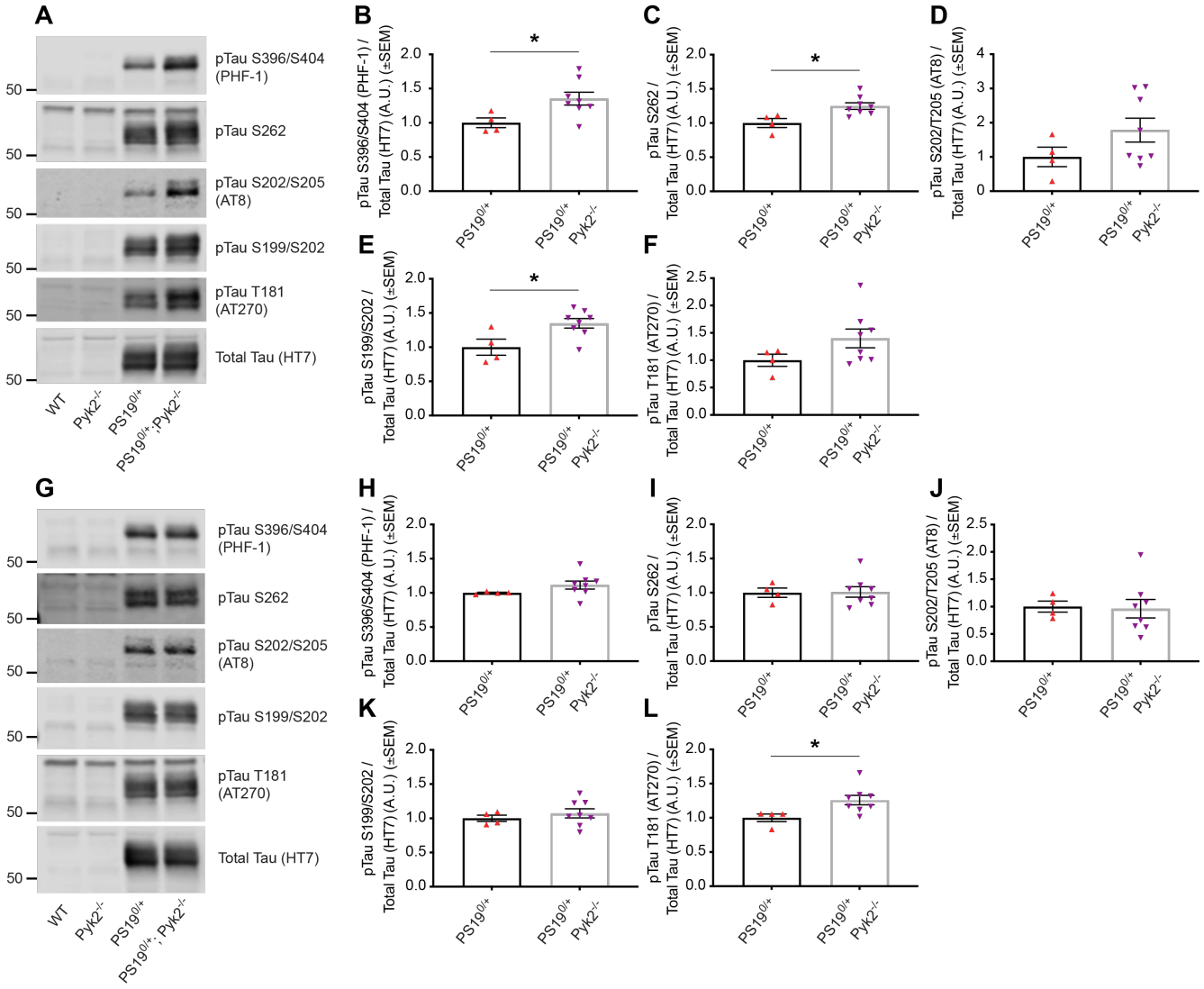

Figure 3. Pyk2 expression suppresses Tau phosphorylation in a PS19$^{0/+}$ animal model of tauopathy. **A**–**L**, TBS-insoluble, SDS-soluble hippocampal (**A**–**F**) and cortical (**G**–**L**) lysates from 9.5–10.5-month-old WT, Pyk2$^{-/-}$, PS19$^{0/+}$ and PS19$^{0/+}$;Pyk2$^{-/-}$ animals were separated by SDS-PAGE and immunoblotted with antibodies against multiple pathophysiologically-relevant phospho-Tau residues as well as total Tau. **A**, Representative immunoblot images of TBS-insoluble, SDS-soluble hippocampal Tau. **B**–**F**, Quantification of protein levels by densitometric analysis reveals significantly greater phosphorylation of hippocampal Tau in lysates from PS19$^{0/+}$;Pyk2$^{-/-}$ animals at pTau S396/S404 (PHF-1) (**B**), pTau S262 (**C**) and pTau S199/S202 (**E**) compared to lysates from PS19$^{0/+}$ animals. All data are normalized total

(HT7) levels of hippocampal Tau. Data are graphed as mean ± SEM, unpaired two-tailed *t*-test, **p*<0.05, *n* = 4–8 mice. **G**, Representative immunoblot images of TBS-insoluble, SDS-soluble cortical Tau. **H**–**L**, Quantification of protein levels by densitometric analysis reveals significantly greater phosphorylation of cortical Tau in lysates from $PS19^{0/+}$;$Pyk2^{-/-}$ animals at pTau S262 (**L**) compared to those from $PS19^{0/+}$ animals. All data are normalized to total (HT7) levels cortical Tau. Data are graphed as mean ± SEM, unpaired two-tailed *t*-test, **p*<0.05, *n* = 4–8 mice.

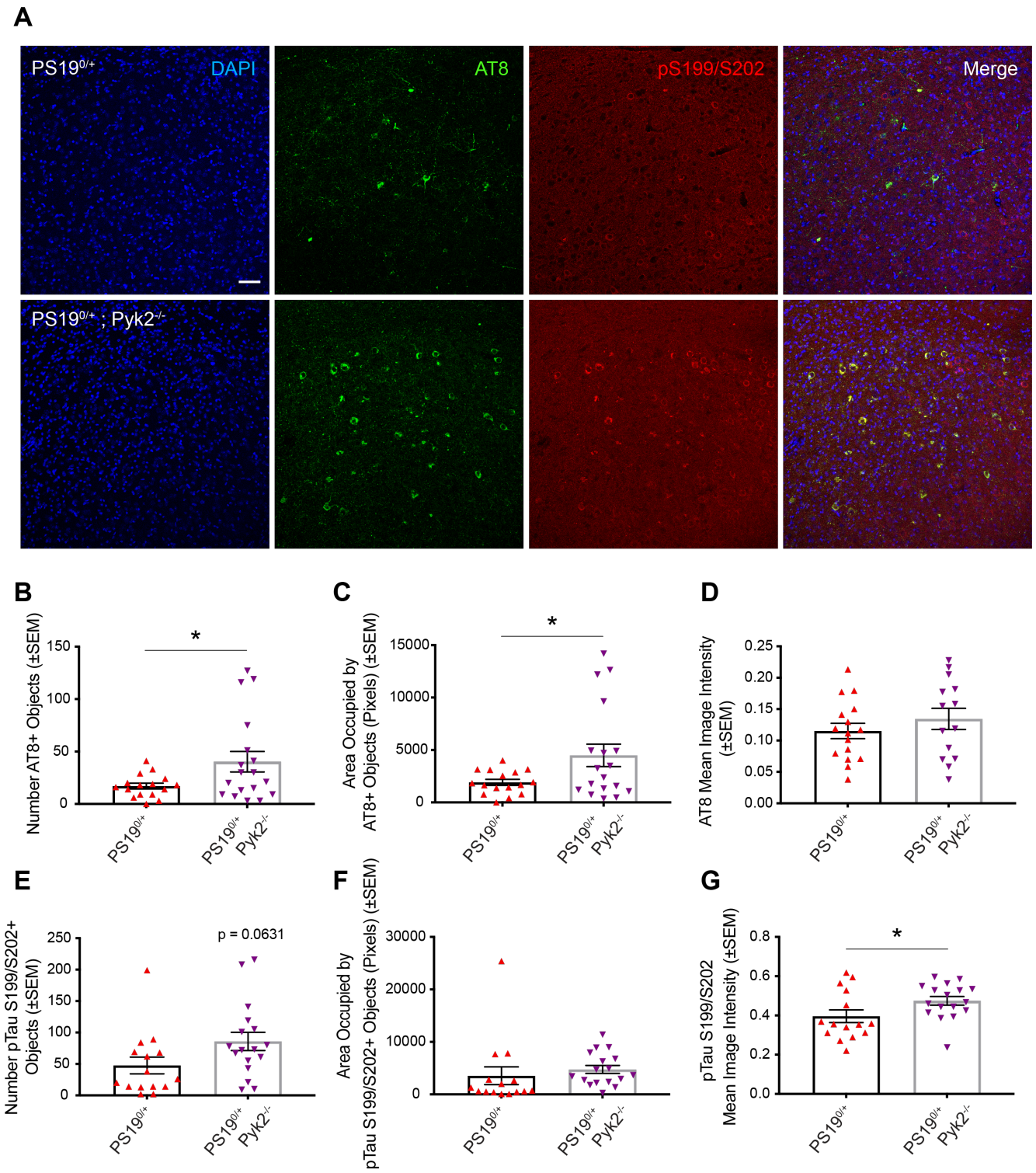

Figure 4. Pyk2 expression is protective against Tau pathology in PS19$^{0/+}$ mice. **A**, Representative immunofluorescent images of DAPI, pTau S202/T205 (AT8) and pTau S199/S202 immunoreactivity in amygdala of 9.5–10.5-month-old WT, Pyk2$^{-/-}$, PS19$^{0/+}$ and

PS19$^{0/+}$;Pyk2$^{-/-}$ animals. Scale bar, 50 μm. **B**–**D**, Quantification of amygdalar pTau S202/T205 (AT8) immunoreactivity reveals significant increases in the number of AT8-positive cell-bodies (objects) (**B**) as well as in the area occupied by those objects (**C**) in PS19$^{0/+}$;Pyk2$^{-/-}$ compared to PS19$^{0/+}$ animals. Data are graphed as mean ± SEM, unpaired two-tailed *t*-test, **p*<0.05, *n* = 14–16 mice. **E**–**G**, Quantification of amygdalar pTau S199/S202 immunoreactivity reveals a significant increase in pTau S199/S202 mean image intensity (**G**) in PS19$^{0/+}$;Pyk2$^{-/-}$ compared to PS19$^{0/+}$ animals. Data are graphed as mean ± SEM, unpaired two-tailed *t*-test, **p*<0.05, *n* = 15–18 mice.

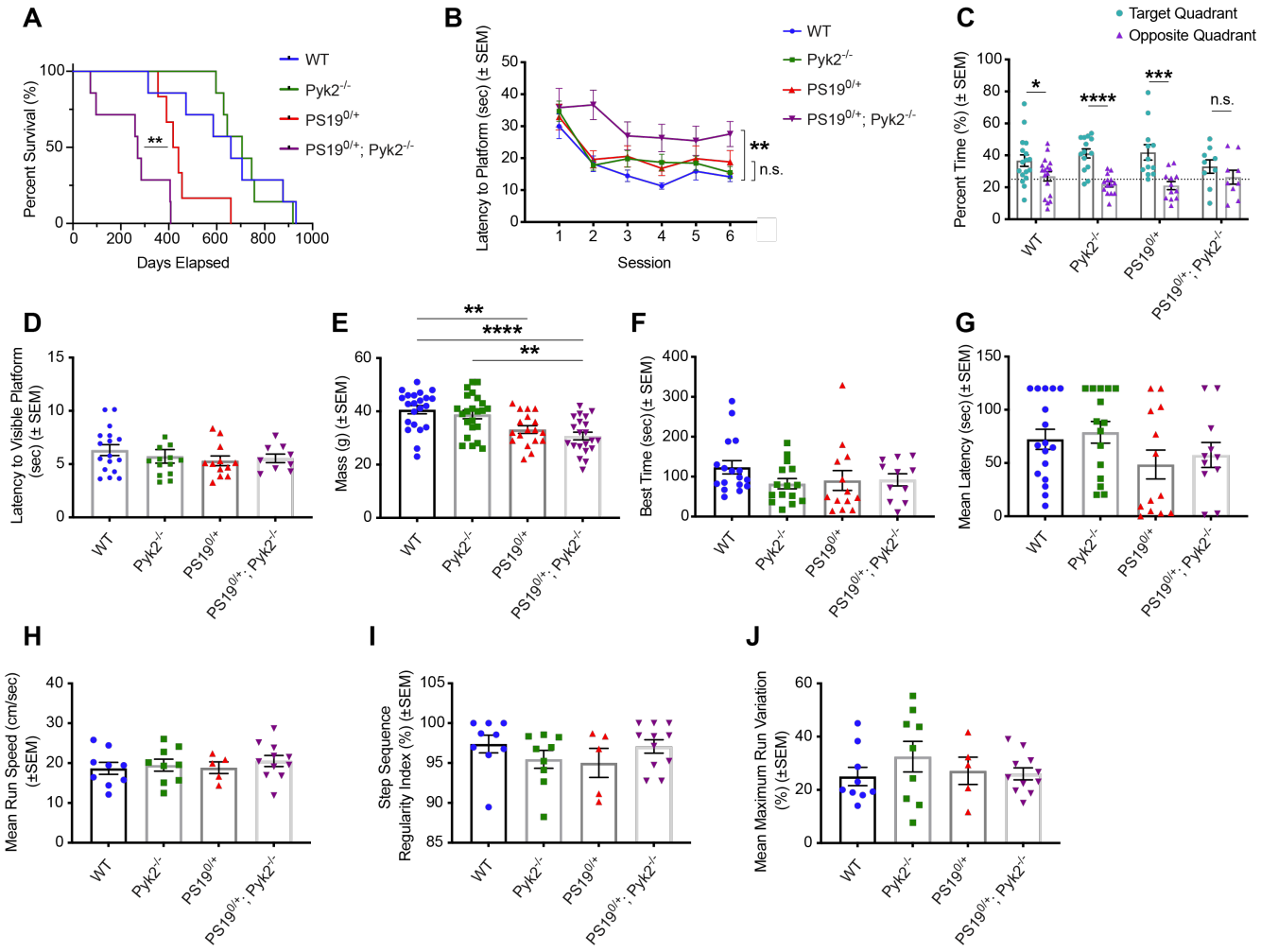

Figure 5. Pyk2 expression is protective against Tau-mediated early death and spatial memory impairment in PS19$^{0/+}$ animals. **A**, Kaplan-Meier survival curve of WT, Pyk2$^{-/-}$, PS19$^{0/+}$ and PS19$^{0/+}$;Pyk2$^{-/-}$ animals. Survivorship of PS19$^{0/+}$;Pyk2$^{-/-}$ mice (median survival, 270 days) is significantly reduced compared to PS19$^{0/+}$ animals (median survival, 429.5 days). Log-rank (Mantel-Cox) test, $^{**}p = 0.0085$, $n = 6–7$ mice. **B**–**D**, Spatial memory of 9–10-month-old mice was assessed using the MWM test. **B**, Latency is defined as the time required to reach a hidden platform across 6 acquisition sessions of 4 trials each. Across the final 4 acquisition sessions, PS19$^{0/+}$;Pyk2$^{-/-}$ animals took significantly longer to reach the platform compared to WT mice. Data are graphed as mean ± SEM, repeated measures ANOVA with Tukey HSD multiple comparisons test, $^{**}p = 0.002$, n.s. = not significant (p =

0.343), *n* = 9–17 mice. **C**, A 60-sec probe trial was performed 24 hr after the final acquisition session with the hidden platform removed. WT, Pyk2$^{-/-}$ and PS19$^{0/+}$ mice spent significantly greater time in the target quadrant compared to the opposite quadrant, while the difference in time spent between the target and opposite quadrants failed to reach significance for PS19$^{0/+}$;Pyk2$^{-/-}$ animals. Data are graphed as mean ± SEM, unpaired two-tailed *t*-test, **p*<0.05, ****p*<0.001, *****p*<0.0001, n.s. = not significant (*p* = 0.2885), *n* = 9–17 mice. Dashed line, 25%. **D**, To rule out visual impairment, latency for animals to find a platform marked with a visual cue was assessed following the probe trial. 4 animals (2 Pyk2$^{-/-}$, 1 PS19$^{0/+}$ and 1 PS19$^{0/+}$;Pyk2$^{-/-}$) were unable to locate the visible platform after 15 trials and were excluded from all MWM analyses. When excluding these animals, there were no significant differences in the time required to reach the visible platform across genotypes. Data are graphed as mean ± SEM, one-way ANOVA with Tukey's multiple comparisons test, *n* = 9–17 mice. **E**, Animal body weights of 9–10-month-old mice across genotypes. PS19$^{0/+}$ weighed significantly less than WT animals while PS19$^{0/+}$;Pyk2$^{-/-}$ animals weighed significantly less than both WT and Pyk2$^{-/-}$ mice. Data are graphed as mean ± SEM, one-way ANOVA with Tukey's multiple comparisons test, ***p*<0.01, *****p*<0.0001, *n* = 18–23 mice. **F**, A rotarod test was performed to assess motor coordination. Latency to fall off the accelerating drum (acceleration: 0.1 rotations/min/sec; top speed: 4 rotations/min) over 5 consecutive trials was assessed and the best time (longest latency) for each animal compared. There were no significant differences in longest latency to fall across genotypes. Data are graphed as mean ± SEM, one-way ANOVA with Tukey's multiple comparisons test, *n* = 11–17 mice. **G**, A wire hang test was conducted to assess grip strength. Animals were placed in the center of a wire grid (1cm by 1cm) and the latency to fall from the inverted grid was determined across 2 120-sec trials. Mean latencies to fall across the 2 trials are plotted in **G.** There were no significant

differences in mean latency to fall across genotypes. Data are graphed as mean ± SEM, one-way ANOVA with Tukey's multiple comparisons test, *n* = 11–17 mice. **H**–**J**, Gait assessment was conducted using a Noldus CatWalk XT system. **H**, There were no significant differences in mean run speed across genotypes. Data are graphed as mean ± SEM, one-way ANOVA with Tukey's multiple comparisons test, *n* = 5–11 mice. **I**, There were no significant differences in step sequence regularity index across genotypes. Data are graphed as mean ± SEM, one-way ANOVA with Tukey's multiple comparisons test, *n* = 5–11 mice. **J**, There were no significant differences in mean maximum run variation across genotypes. Data are graphed as mean ± SEM, one-way ANOVA with Tukey's multiple comparisons test, *n* = 5–11 mice.

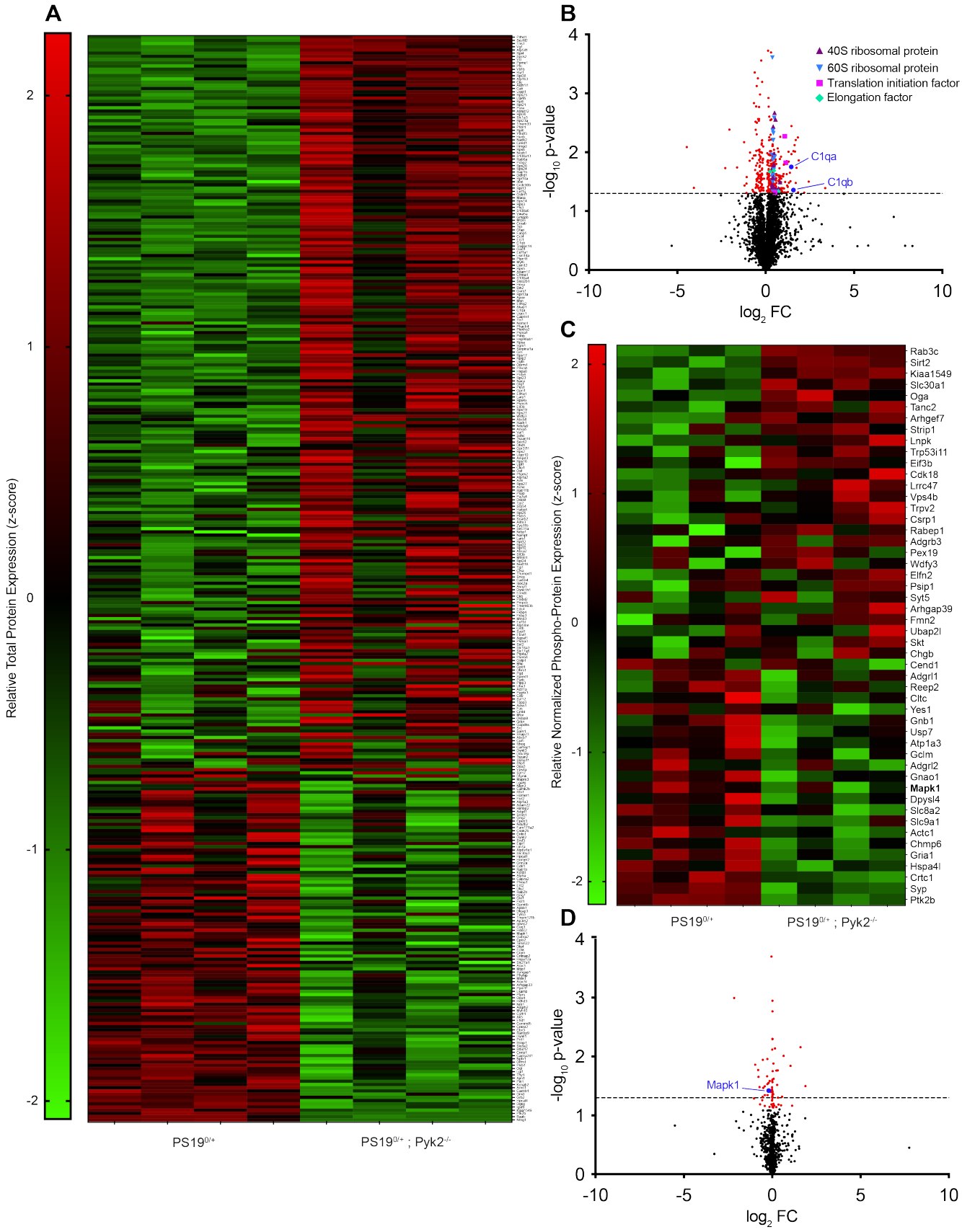
A
Relative Total Protein Expression (z-score)
2
1
0
-1
-2
PS19$^{0/+}$
PS19$^{0/+}$; Pyk2$^{-/-}$
B
-log$_{10}$ p-value
log$_2$ FC
40S ribosomal protein
60S ribosomal protein
Translation initiation factor
Elongation factor
C1qa
C1qb
C
Relative Normalized Phospho-Protein Expression (z-score)
Rab3c
Sirt2
Kiaa1549
Slc30a1
Oga
Tanc2
Arhgef7
Strip1
Lnpk
Trp53i11
Eif3b
Cdk18
Lrrc47
Vps4b
Trpv2
Csrp1
Rabep1
Adgrb3
Pex19
Wdfy3
Elfn2
Psip1
Syt5
Arhgap39
Fmn2
Ubap2l
Skt
Chgb
Cend1
Adgrl1
Reep2
Cltc
Yes1
Gnb1
Usp7
Atp1a3
Gclm
Adgrl2
Gnao1
Mapk1
Dpysl4
Slc8a2
Slc9a1
Actc1
Chmp6
Gria1
Hspa4l
Crtc1
Syp
Ptk2b
D
Mapk1

Figure 6. Proteomic analysis reveals signs of disrupted protein translational, increased synaptic C1q expression and decreased MAPK1 activity in $PS19^{0/+}$;$Pyk2^{-/-}$ animals. **A**–**D**, Synaptosomal fractions were prepared from hippocampi of 9.5–10.5-month-old $PS19^{0/+}$ and $PS19^{0/+}$;$Pyk2^{-/-}$ mice and run through LC-MS/MS to identify significantly differentially regulated proteins between $PS19^{0/+}$ and $PS19^{0/+}$;$Pyk2^{-/-}$ animals. **A**, Heat map showing relative abundance of significantly differentially regulated (p<0.05) synaptic proteins between $PS19^{0/+}$ and $PS19^{0/+}$;$Pyk2^{-/-}$ animals. **B**, Volcano plot of all total synaptic proteins identified via LC-MS/MS. Positive values for Log_2FC represent increased synaptic protein expression in $PS19^{0/+}$;$Pyk2^{-/-}$ compared to $PS19^{0/+}$ mice. Dashed line represents p=0.05. Significantly differentially regulated synaptic proteins shown in red. **C**, Heat map showing relative abundance of significantly differentially regulated (p<0.05), phospho-enriched, synaptic proteins (normalized to total protein abundance) between $PS19^{0/+}$ and $PS19^{0/+}$;$Pyk2^{-/-}$ animals. **D**, Volcano plot of all normalized, phospho-enriched, synaptic proteins identified via LC-MS/MS. Positive values for Log_2FC represent protein upregulation in $Pyk2^{-/-}$ compared to WT. Dashed line represents p=0.05.

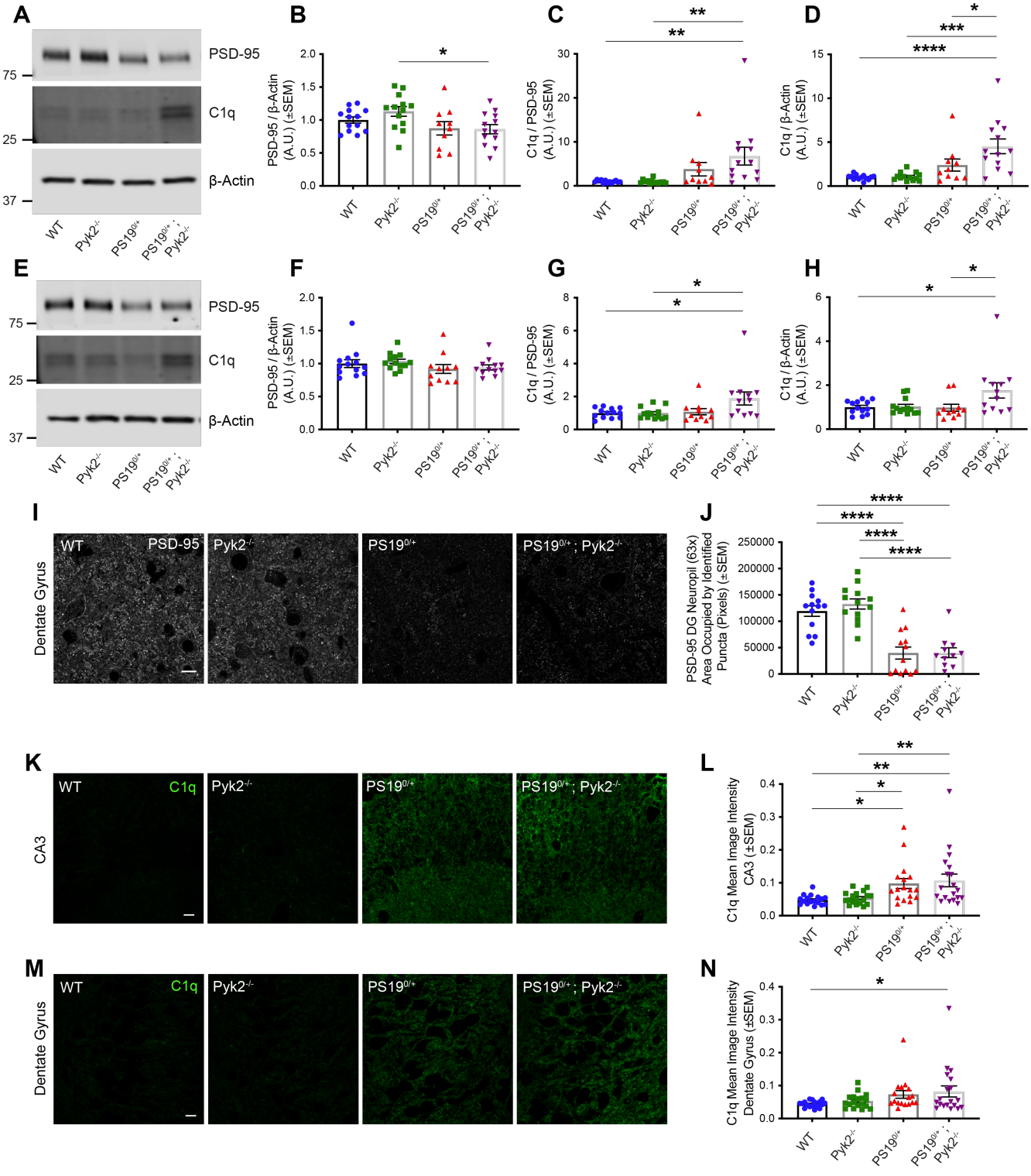

Figure 7. Pyk2 expression protects against Tau-mediated C1q deposition. **A**–**D**, Crude hippocampal, synaptosomal fractions were obtained from 9.5–10.5-month-old WT, Pyk2$^{-/-}$, PS19$^{0/+}$ and PS19$^{0/+}$;Pyk2$^{-/-}$ animals. Lysates were separated by SDS-PAGE and

immunoblotted with the antibodies indicated. **A**, Representative immunoblot images of hippocampal, synaptosomal fractions. **B**–**D**, Quantification of **A**. A significant decrease in synaptic PSD-95 expression (normalized to β-Actin) was observed in synaptosomal fractions from $PS19^{0/+}$;$Pyk2^{-/-}$ hippocampi compared to those from $Pyk2^{-/-}$ animals (**B**). When normalized to PSD-95, a significant increase in synaptic C1q expression was observed in $PS19^{0/+}$;$Pyk2^{-/-}$ hippocampi compared to those from WT and $Pyk2^{-/-}$ animals (**C**). When normalized to β-Actin, an increase in synaptic C1q expression in $PS19^{0/+}$;$Pyk2^{-/-}$ hippocampi was significant compared to those from WT, $Pyk2^{-/-}$ and $PS19^{0/+}$ animals (**D**). Data are graphed as mean ± SEM, one-way ANOVA with Tukey's multiple comparisons test, **p*<0.05, ***p*<0.01, ****p*<0.001, *****p*<0.0001, *n* = 10–13 mice. **E**–**H**, Crude cortical, synaptosomal lysates were obtained from 9.5–10.5-month-old WT, $Pyk2^{-/-}$, $PS19^{0/+}$ and $PS19^{0/+}$;$Pyk2^{-/-}$ animals and immunoblots prepared as described above. **E**, Representative immunoblot images of cortical, synaptosomal fractions. **F**–**H**, Quantification of **E**. No significant changes in cortical, synaptic PSD-95 (normalized to β-Actin) were observed in synaptosomal fractions across genotypes (**F**). When normalized to β-Actin, synaptic PSD-95 expression was significantly higher in $Pyk2^{-/-}$, $PS19^{0/+}$ cortices compared to those from WT and $Pyk2^{-/-}$ animals (**G**). When normalized to β-Actin, $PS19^{0/+}$;$Pyk2^{-/-}$ cortices demonstrated significantly higher synaptic C1q expression compared to cortices from WT and $PS19^{0/+}$ animals (**H**). Data are graphed as mean ± SEM, one-way ANOVA with Tukey's multiple comparisons test, **p*<0.05, *n* = 10–13 mice. **I**, Representative immunofluorescent images of PSD-95 immunoreactivity in dentate gyrus of 9.5–10.5-month-old WT, $Pyk2^{-/-}$, $PS19^{0/+}$ and $PS19^{0/+}$;$Pyk2^{-/-}$ animals. Scale bar, 10 μm. **J**, Quantification of **I**. In the dentate gyrus, both $PS19^{0/+}$ and $PS19^{0/+}$;$Pyk2^{-/-}$ animals demonstrated significant reductions in the area occupied by PSD-95-positive puncta compare to WT and $Pyk2^{-/-}$ animals (**I**). Data are graphed as

mean ± SEM, one-way ANOVA with Tukey's multiple comparisons test, ****p<0.0001, n = 11–13 mice. **K**, Representative immunofluorescent images of C1q immunoreactivity in CA3 of 9.5–10.5-month-old WT, Pyk2$^{-/-}$, PS19$^{0/+}$ and PS19$^{0/+}$;Pyk2$^{-/-}$ animals. Scale bar, 10 μm. **L**, Quantification of **K**. PS19$^{0/+}$ and PS19$^{0/+}$;Pyk2$^{-/-}$ animals showed significantly higher C1q immunoreactivity (mean image intensity) in the CA3 region of the hippocampus compared WT and Pyk2$^{-/-}$ animals (**L**). Data are graphed as mean ± SEM, one-way ANOVA with Tukey's multiple comparisons test, *p<0.05, **p<0.01, n = 17–19 mice. **M**, Representative immunofluorescent images of C1q immunoreactivity in the dentate gyrus of 9.5–10.5-month-old WT, Pyk2$^{-/-}$, PS19$^{0/+}$ and PS19$^{0/+}$;Pyk2$^{-/-}$ animals. Scale bar, 10 μm. **N**, Quantification of **M**. Only PS19$^{0/+}$;Pyk2$^{-/-}$ animals showed significantly higher C1q immunoreactivity in the dentate gyrus compared to WT animals. Data are graphed as mean ± SEM, one-way ANOVA with Tukey's multiple comparisons test, *p<0.05, n = 17–19 mice.

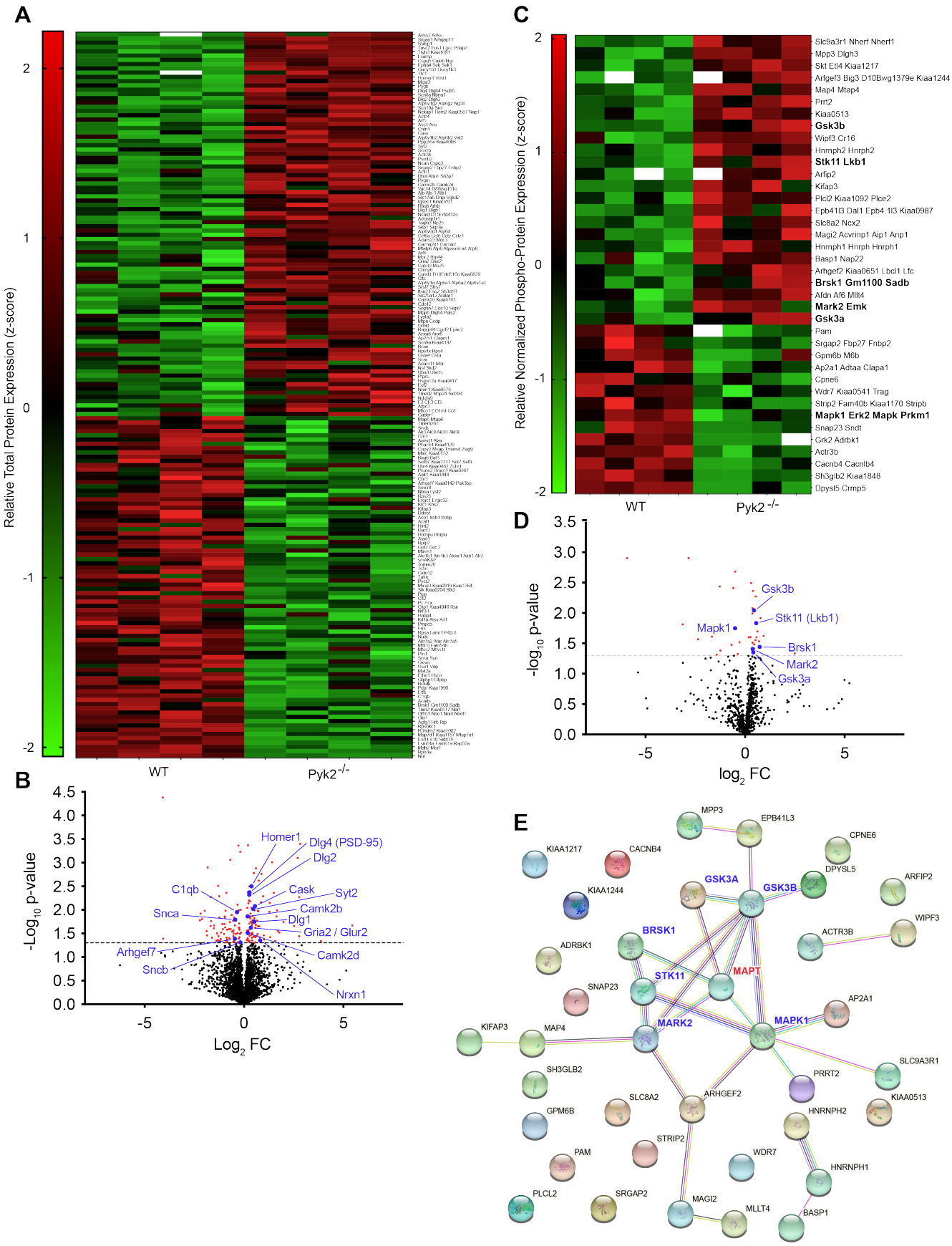
A
Relative Total Protein Expression (z-score)
2
1
0
-1
-2
WT
Pyk2 -/-
C
Relative Normalized Phospho-Protein Expression (z-score)
Slc9a3r1 Nherf Nherf1
Mpp3 Dlgh3
Skt Etl4 Kiaa1217
Arfgef3 Big3 D10Bwg1379e Kiaa1244
Map4 Mtap4
Prrt2
Kiaa0513
Gsk3b
Wipf3 Cr16
Hnrnph2 Hnrph2
Stk11 Lkb1
Arfip2
Kifap3
Plcl2 Kiaa1092 Plce2
Epb41l3 Dal1 Epb4 1l3 Kiaa0987
Slc8a2 Ncx2
Magi2 Acvrinp1 Aip1 Arip1
Hnrnph1 Hnrph Hnrph1
Basp1 Nap22
Arhgef2 Kiaa0651 Lbcl1 Lfc
Brsk1 Gm1100 Sadb
Afdn Af6 Mllt4
Mark2 Emk
Gsk3a
Pam
Srgap2 Fbp27 Fnbp2
Gpm6b M6b
Ap2a1 Adtaa Clapa1
Cpne6
Wdr7 Kiaa0541 Trag
Strip2 Fam40b Kiaa1170 Stripb
Mapk1 Erk2 Mapk Prkm1
Snap23 Sndt
Grk2 Adrbk1
Actr3b
Cacnb4 Cacnlb4
Sh3glb2 Kiaa1848
Dpysl5 Crmp5
WT
Pyk2 -/-
B
-Log10 p-value
Log2 FC
Homer1
Dlg4 (PSD-95)
Dlg2
C1qb
Cask
Syt2
Snca
Camk2b
Dlg1
Gria2 / Glur2
Arhgef7
Camk2d
Sncb
Nrxn1
D
-log10 p-value
log2 FC
Gsk3b
Stk11 (Lkb1)
Mapk1
Brsk1
Mark2
Gsk3a
E
MPP3
EPB41L3
CPNE6
KIAA1217
CACNB4
DPYSL5
GSK3A
GSK3B
ARFIP2
KIAA1244
BRSK1
WIPF3
ACTR3B
ADRBK1
STK11
MAPT
SNAP23
AP2A1
KIFAP3
MAP4
MARK2
MAPK1
SLC9A3R1
SH3GLB2
PRRT2
ARHGEF2
SLC8A2
KIAA0513
GPM6B
HNRNPH2
STRIP2
WDR7
PAM
HNRNPH1
PLCL2
SRGAP2
MAGI2
MLLT4
BASP1

Figure 8. Proteomic analysis reveals potential regulators of Tau phosphorylation modulated by Pyk2. **A**–**D**, Synaptosomal fractions were prepared from hippocampi of 12-month-old WT and Pyk2$^{-/-}$ animals and run through LC-MS/MS to identify proteins that are significantly differentially regulated by Pyk2 expression. **A**, Heat map showing relative abundance of significantly differentially regulated (p<0.05) synaptic proteins between WT and Pyk2$^{-/-}$ animals. **B**, Volcano plot of all total synaptic proteins identified via LC-MS/MS. Positive values for Log_2FC represent protein upregulation in Pyk2$^{-/-}$ compared to WT. Dashed line represents p=0.05. Significantly differentially regulated synaptic proteins shown in red. **C**, Heat map showing relative abundance of significantly differentially regulated (p<0.05), phospho-enriched, synaptic proteins (normalized to total protein abundance) between WT and Pyk2$^{-/-}$ animals. **D**, Volcano plot of all normalized, phospho-enriched, synaptic proteins identified via LC-MS/MS. Positive values for Log_2FC represent protein upregulation in Pyk2$^{-/-}$ compared to WT. Dashed line represents p=0.05. Significantly differentially regulated, synaptic phospho-proteins shown in red. Proximate regulators of Tau shown in blue. **E**, STRING protein-protein interaction network of all significantly differentially regulated, normalized, phospho-enriched, synaptic proteins. The interaction network was supplemented with MAPT (in red) to identify regulators of Tau. Proximate regulators of Tau (in blue) were defined as kinases or phosphatases positioned one or two degrees from MAPT. 6 kinases (and 0 phosphatases) were identified as proximate regulators of Tau modulated by Pyk2.

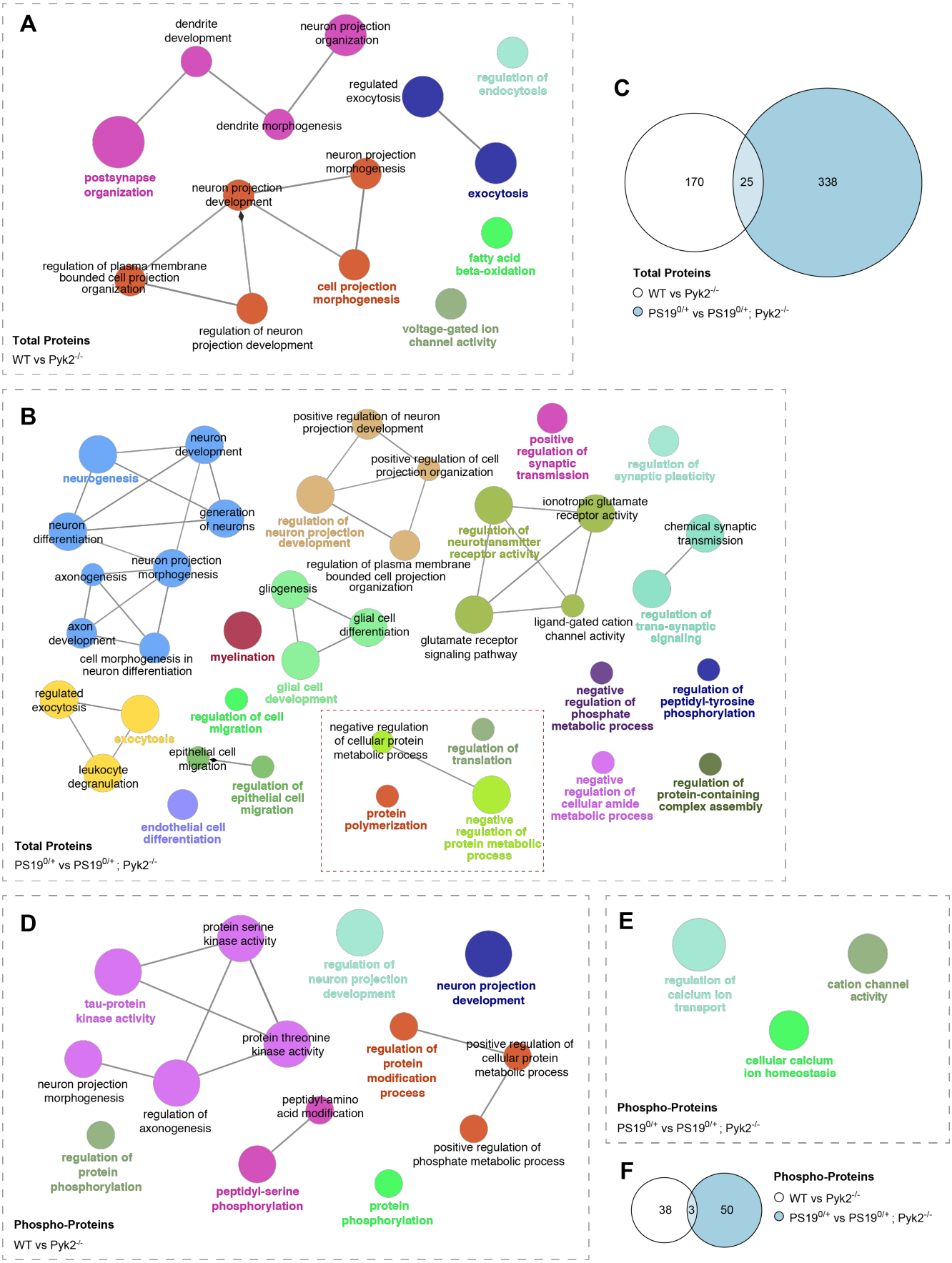
A
dendrite development
neuron projection organization
regulation of endocytosis
regulated exocytosis
dendrite morphogenesis
postsynapse organization
neuron projection morphogenesis
exocytosis
neuron projection development
fatty acid beta-oxidation
regulation of plasma membrane bounded cell projection organization
cell projection morphogenesis
regulation of neuron projection development
voltage-gated ion channel activity
Total Proteins
WT vs Pyk2-/-
C
170
25
338
Total Proteins
WT vs Pyk2-/-
PS190/+ vs PS190/+; Pyk2-/-
B
positive regulation of neuron projection development
positive regulation of synaptic transmission
regulation of synaptic plasticity
neuron development
neurogenesis
positive regulation of cell projection organization
ionotropic glutamate receptor activity
generation of neurons
neuron differentiation
regulation of neuron projection development
regulation of neurotransmitter receptor activity
chemical synaptic transmission
neuron projection morphogenesis
axonogenesis
regulation of plasma membrane bounded cell projection organization
gliogenesis
glial cell differentiation
axon development
myelination
ligand-gated cation channel activity
regulation of trans-synaptic signaling
cell morphogenesis in neuron differentiation
glutamate receptor signaling pathway
glial cell development
negative regulation of phosphate metabolic process
regulation of peptidyl-tyrosine phosphorylation
regulated exocytosis
regulation of cell migration
exocytosis
negative regulation of cellular protein metabolic process
regulation of translation
epithelial cell migration
leukocyte degranulation
regulation of epithelial cell migration
protein polymerization
negative regulation of cellular amide metabolic process
regulation of protein-containing complex assembly
endothelial cell differentiation
negative regulation of protein metabolic process
Total Proteins
PS190/+ vs PS190/+ ; Pyk2-/-
D
protein serine kinase activity
regulation of neuron projection development
neuron projection development
tau-protein kinase activity
protein threonine kinase activity
regulation of protein modification process
positive regulation of cellular protein metabolic process
neuron projection morphogenesis
regulation of axonogenesis
peptidyl-amino acid modification
regulation of protein phosphorylation
positive regulation of phosphate metabolic process
peptidyl-serine phosphorylation
protein phosphorylation
Phospho-Proteins
WT vs Pyk2-/-
E
regulation of calcium ion transport
cation channel activity
cellular calcium ion homeostasis
Phospho-Proteins
PS190/+ vs PS190/+ ; Pyk2-/-
F
38
3
50
Phospho-Proteins
WT vs Pyk2-/-
PS190/+ vs PS190/+ ; Pyk2-/-

Figure 9. Pathway enrichment of proteins with Pyk2-regulated expression. **A**–**B**, Functional networks of identified proteomic hits (total protein fraction) from WT vs Pyk2$^{-/-}$ (**A**) and PS19$^{0/+}$ vs PS19$^{0/+}$;Pyk2$^{-/-}$ (**B**) analyses generated in ClueGO. Pathways involved in protein translation are boxed in red. **C**, Venn Diagram showing overlap of significant total protein hits between analyses. **D**–**E**, Functional networks of phospho-proteomic hits (normalized phospho-enriched fraction) from WT vs Pyk2$^{-/-}$ (**D**) and PS19$^{0/+}$ vs PS19$^{0/+}$;Pyk2$^{-/-}$ (**E**) analyses. **F**, Venn Diagram showing overlap of significant normalized phospho-enriched protein hits between analyses.

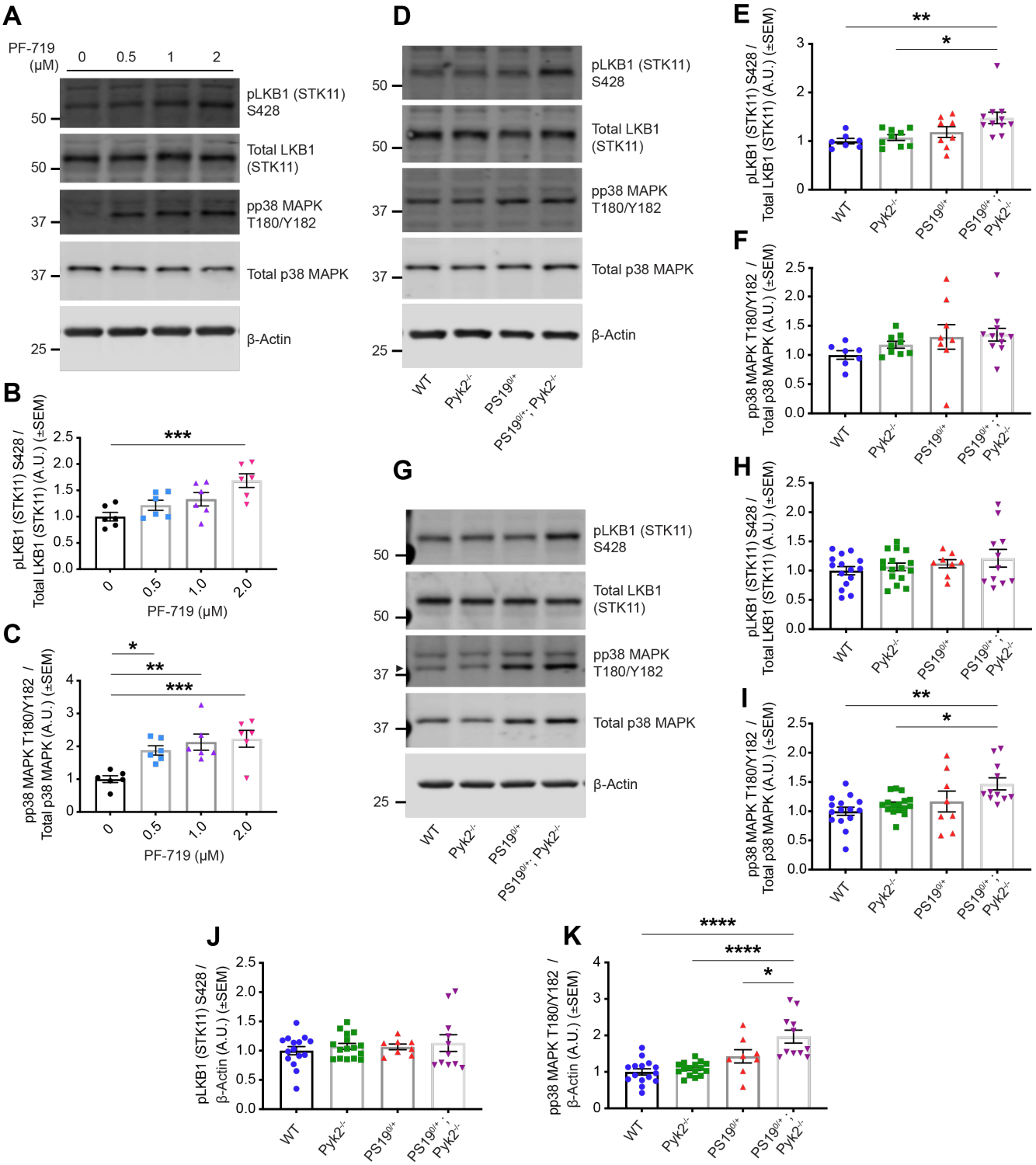

Figure 10. Pyk2 inhibits LKB1 and p38 MAPK activity. **A**–**C**, iPSC-derived human cortical neurons (90–100 days post terminal differentiation) (same as shown in Figure 2e–i) were treated with PF-719 at indicated concentrations for 2 hr at 37°C and, immediately following

treatment, homogenized in RIPA containing 1% SDS. Lysates were separated by SDS-PAGE and immunoblotted with the LKB1 and p38 MAPK antibodies indicated. **A**, Representative immunoblot images of lysates from PF-719-treated iPSC-derived human cortical neurons. **B** and **C**, Quantification of **A**. Pyk2 inhibition significantly increased LKB1 activity (pLKB1 S428 normalized to total LKB1) at 2.0 μM PF-719 (**B**) and significantly increased p38 MAPK activity (pp38 MAPK T180/Y182 normalized to total p38 MAPK) at every concentration of PF-719 (**C**). Data are graphed as mean ± SEM, one-way ANOVA with Dunnett's multiple comparisons test, *p<0.05, **p<0.01, ***p<0.001, n = 6. **D**–**F**, TBS-soluble lysates from hippocampi of 9.5–10.5-month-old WT, Pyk2$^{-/-}$, PS19$^{0/+}$ and PS19$^{0/+}$;Pyk2$^{-/-}$ animals were separated by SDS-PAGE and immunoblotted with the LKB1 and p38 MAPK antibodies listed. **D**, Representative immunoblot images of TBS-soluble hippocampal lysates. **E** and **F**, Quantification of **D**. A significant increase in TBS-soluble LKB1 activity (pLKB1 S428 normalized to total LKB1) is observed in PS19$^{0/+}$;Pyk2$^{-/-}$ animals compared to WT and Pyk2$^{-/-}$ animals (**E**), while there were no significant differences in TBS-soluble MAPK activity (pp38 MAPK T180/Y182 normalized to total p38 MAPK) observed across genotypes (**F**). Data are graphed as mean ± SEM, one-way ANOVA with Tukey's multiple comparisons test, *p<0.05, **p<0.01, n = 7–11 mice. **G**–**K**, TBS-insoluble, SDS-soluble lysates from hippocampi of 9.5–10.5-month-old WT, Pyk2$^{-/-}$, PS19$^{0/+}$ and PS19$^{0/+}$;Pyk2$^{-/-}$ animals were separated by SDS-PAGE and immunoblotted with the antibodies indicated. **G**, Representative immunoblot images of TBS-insoluble, SDS-soluble hippocampal lysates. Arrowhead indicates pp38 MAPK T180/Y182. **H**–**K**, Quantification of **G**. While no significant differences in TBS-insoluble, SDS-soluble LKB1 activity (pLKB1 S428 normalized to total LKB1) were observed across genotypes (**H**), PS19$^{0/+}$;Pyk2$^{-/-}$ animals demonstrated a significant increase in TBS-insoluble, SDS-soluble p38 MAPK activity (pp38 MAPK T180/Y182 normalized to total p38

MAPK) compared to WT and Pyk2$^{-/-}$ animals (**I**). No differences were observed in absolute levels of TBS-insoluble, SDS-soluble phospho-LKB1 (pLKB1 S428 normalized to β-Actin) across genotypes (**J**), however PS19$^{0/+}$;Pyk2$^{-/-}$ exhibited a significant increase in absolute levels of TBS-insoluble, SDS-soluble phosho-p38 MAPK (pp38 MAPK T180/Y182 normalized to β-Actin) compared to WT, Pyk2$^{-/-}$ and PS19$^{0/+}$ animals (**K**). Data are graphed as mean ± SEM, one-way ANOVA with Tukey's multiple comparisons test, *p<0.05, **p<0.01, ****p<0.0001, n = 8–16 mice.

TABLES

Fraction	Analysis	% Associated Genes	Associated Genes Found	Number of Genes	Pathway Term	GO ID	Term P-Value	Term P-Value Corrected with Bonferroni Step Down
Total Protein	WT vs Pyk2$^{-/-}$	6.10	[ABCD2, ACADS, ACAT1, CNR1, ETFB]	5	fatty acid beta-oxidation	GO:0006635	7.55E-05	0.007321993
		6.06	[ABCD2, CDC42, DBNL, DLG4, EPHA4, KIF1A]	6	neuron projection organization	GO:0106027	1.45E-05	0.001450712
		4.92	[ACTN1, ARF6, CDC42, DBNL, DLG1, DLG4, EPHA4, KIF1A, PTPRS]	9	postsynapse organization	GO:0099173	5.68E-05	5.68E-05
		3.90	[CDC42, DBNL, DLG4, EPHA4, KIF1A, MAP6]	6	dendrite morphogenesis	GO:0048813	1.72E-04	0.015991856
		3.10	[AAK1, AP2M1, ARF6, ATAD1, CDC42, DLG4, TF]	7	regulation of endocytosis	GO:0030100	2.03E-04	0.018696253
		3.02	[ARF6, CDC42, DBNL, DLG4, EPHA4, KIF1A, MAP6, PTPRS]	8	dendrite development	GO:0016358	8.42E-05	0.008083191
		2.75	[CNR1, DLG1, DLG2, DLG4, GRIA2, SCN1B, SCN8A, SCN9A]	8	voltage-gated ion channel activity	GO:0005244	1.61E-04	0.015097501
		2.12	[ARF6, BRSK1, CNR1, CNTN1, DBNL, EPHA4, KIF1A, MAP6, PTPRS, SCN1B]	10	**regulation of neuron projection development**	GO:0010975	2.05E-04	0.018639542
		1.79	[BRSK1, CDC42, CSPG5, DBNL, DLG4, EPHA4, ITSN2, KIF1A, MAP6, OLFM1, PTPRS, SCN1B, SYT2]	13	cell projection morphogenesis	GO:0048858	1.22E-04	0.011542529
		1.73	[ACTN1, ACTN4, CAB39, CAND1, CNR1, CSPG5, DBNL, DDOST, EEF2, HABP4, MLEC, PYGB, SYT2, TF, UBR4]	15	**regulated exocytosis**	GO:0045055	4.99E-05	0.004892033
		1.73	[ACTN1, ACTN4, CAB39, CAND1, CHMP6, CNR1, CSPG5, DBNL, DDOST, EEF2, HABP4, MLEC, NSF, PYGB, SYT2, TF, UBR4]	17	**exocytosis**	GO:0006887	1.48E-05	0.001465131
		1.72	[ARF6, BRSK1, CDC42, CNR1, CNTN1, DBNL, EPHA4, KIF1A, MAP6, PTPRS, SCN1B, SEPTIN7]	12	**regulation of plasma membrane bounded cell projection organization**	GO:0120035	3.24E-04	0.029116126
		1.69	[BRSK1, CDC42, DBNL, DLG4, EPHA4, ITSN2, KIF1A, MAP6, OLFM1, PTPRS, SCN1B, SYT2]	12	**neuron projection morphogenesis**	GO:0048812	3.68E-04	0.032738513
		1.40	[ARF6, BRSK1, CDC42, CNR1, CNTN1, DBNL, DLG4, EPHA4, ITSN2, KIF1A, MAP6, OLFM1, PTPRS, SCN1B, SYT2]	15	neuron projection development	GO:0031175	5.08E-04	0.044721907
	PS19$^{0/+}$ vs PS19$^{0/+}$;Pyk2$^{-/-}$	10.34	[DLG2, DLG4, MINK1, NLGN3, NPTX1, OPRM1, PRRT1, PTK2B, SRC]	9	regulation of neurotransmitter receptor activity	GO:0099601	8.49E-08	2.16E-05
		9.88	[DLG2, DLG4, GRIK4, MINK1, NLGN3, OPRM1, PRRT1, PTK2B]	8	ionotropic glutamate receptor activity	GO:0004970	6.51E-07	1.62E-04
		8.26	[ABCA2, C1QA, CD9, DMD, GFAP, GRN, GSTP1, PRDX6, SIRT2, TSPAN2]	10	glial cell development	GO:0021782	1.38E-07	3.48E-05
		7.76	[DLG2, DLG4, GRIK4, MINK1, NLGN3, OPRM1, PLCB1, PRRT1, PTK2B]	9	glutamate receptor signaling pathway	GO:0007215	1.01E-06	2.51E-04
		7.09	[ABCA2, CD9, HEXB, MTOR, PRDX6, PTN, SCN2A, SIRT2, TSPAN2, UGT8]	10	myelination	GO:0042552	5.76E-07	1.44E-04
		6.67	[DMD, PLCB1, PTN, PTPRS, RAB1B, RAP1B, RAP2B, TJP2]	8	endothelial cell differentiation	GO:0045446	1.27E-05	0.003012572
		5.88	[APOE, DLG4, FLOT1, GFAP, LGI1, NLGN3, PRRT1, PTK2B, PTN, SYT12]	10	positive regulation of synaptic transmission	GO:0050806	3.17E-06	7.63E-04
		5.75	[APBB1, APOE, CNTN1, DMD, EHD1, GRN, MTOR, OPA1, PTK2B, PTN]	10	positive regulation of neuron projection development	GO:0010976	3.90E-06	9.36E-04
		5.34	[APOE, CPEB3, CPLX2, DLG4, ERC2, GFAP, PRRT1, PTK2B, PTN, SYT12, VGF]	11	regulation of synaptic plasticity	GO:0048167	2.59E-06	6.30E-04
		5.06	[ABCA2, C1QA, CD9, DMD, GFAP, GRN, GSTP1, MTOR, PRDX6, PTN, SIRT2, TSPAN2]	12	glial cell differentiation	GO:0010001	1.57E-06	3.84E-04
		5.02	[APOE, CPEB3, CPLX2, DLG4, ERC2, FABP5, FLOT1, GFAP, GRIK4, LGI1, MTOR, NLGN3, NPTX1, NTNG1, PLCB1, PRRT1, PTK2B, PTN, PTPRS, RAP1B, SRC, SYT12, VGF]	23	regulation of trans-synaptic signaling	GO:0099177	2.19E-11	5.74E-09
		4.63	[DLG2, DLG4, DMD, GRIK4, MINK1, NLGN3, OPRM1, PRRT1, PTK2B, RYR1]	10	ligand-gated cation channel activity	GO:0099094	2.59E-05	0.006110782
		4.48	[APOE, CALR, CPEB3, EDC4, LARP1, PIN1, PURA, RACK1, RTN1, UPF1]	10	negative regulation of cellular amide metabolic process	GO:0034249	3.40E-05	0.007919981
		4.42	[ABCA2, C1QA, CD9, DMD, GFAP, GRN, GSTP1, HEXB, MTOR, PRDX6, PTK2B, PTN, SIRT2, TSPAN2]	14	gliogenesis	GO:0042063	1.06E-06	2.62E-04
		4.20	[APOE, CALR, CSNK2B, GRN, MTOR, PLPP3, PPM1F, PTK2B, PTN, SRC]	10	regulation of epithelial cell migration	GO:0010632	5.89E-05	0.013542207
		3.60	[APBB1, APOE, CNTN1, DGKG, DMD, EHD1, FKBP4, GFAP, GRN, MTOR, NTNG1, OPA1, PKN1, PTK2B, PTN, PTPRS, THY1]	17	**regulation of neuron projection development**	GO:0010975	1.23E-06	3.02E-04
		3.59	[APOE, CPEB3, CPLX2, DLG2, DLG4, ERC2, FLOT1, GFAP, GRIK4, LGI1, LIN7A, MINK1, MTOR, NLGN3, NPTX1, NTNG1, OPRM1, PLCB1, PRRT1, PTK2B, PTN, PTPRS, RAP1B, SLC18A3, SRC, SYPL1, SYT12, VGF]	28	chemical synaptic transmission	GO:0007268	3.09E-10	8.07E-08
		3.58	[CADM4, CD81, CNTN1, DLG4, MTOR, PTK2B, RACK1, RAP2B, SRC, THY1]	10	regulation of peptidyl-tyrosine phosphorylation	GO:0050730	2.17E-04	0.048624534
		3.54	[APOE, CALR, CSNK2B, GRN, MTOR, PKN1, PLPP3, PPM1F, PTK2B, PTN, SRC]	11	epithelial cell migration	GO:0010631	1.18E-04	0.026898848
		3.45	[APBB1, APOE, CNTN1, DLG4, DMD, EHD1, GRN, MTOR, OPA1, PKN1, PTK2B, PTN, SRC]	13	positive regulation of cell projection organization	GO:0031346	3.66E-05	0.008487912
		3.37	[ARL6, ARPC5, CLIP1, FKBP4, GRB2, MTOR, OPA1, PIN1, PKN1, PTK2B, TPPP3]	11	protein polymerization	GO:0051258	1.78E-04	0.040236304
		3.22	[APBB1, APOE, FLOT1, GRB2, GRN, LGI1, NLGN3, NPTX1, NTNG1, OLFM1, PKN1, PTN, PTPRS, RHOG, S100A6, SRC, THY1, TSPAN2]	18	axon development	GO:0061564	2.88E-06	6.96E-04
		3.19	[AMPD3, ARPC5, BIN2, CPLX2, CSNK2B, CTSA, DDOST, FABP5, GRN, GSTP1, HEXB, PA2G4, PRDX6, PTGES2, RAB6A, RAP1B, RAP2B, RHOG, VAT1]	19	leukocyte degranulation	GO:0043299	1.73E-06	4.23E-04
		3.16	[AMPD3, ANXA5, ARPC5, ATP9A, BIN2, CD9, CPLX2, CSNK2B, CTSA, DDOST, ERC2, FABP5, GRN, GSTP1, HABP4, HEXB, LIN7A, PA2G4, PKN1, PRDX6, PTGES2, RAB6A, RAP1B, RAP2B, RHOG, SYT12, SYT17, TLN1, VAT1, VPS4A, VTI1B]	31	**exocytosis**	GO:0006887	7.34E-10	1.90E-07
		3.12	[APOE, ARPC5, CLIP1, CRYAB, FKBP4, GFAP, GRB2, IRGM, MTOR, PKN1, PTK2B, RACK1, RAP1B, SRC, TPPP3]	15	regulation of protein-containing complex assembly	GO:0043254	2.93E-05	0.006858316
		3.12	[AMPD3, ANXA5, ARPC5, BIN2, CD9, CPLX2, CSNK2B, CTSA, DDOST, ERC2, FABP5, GRN, GSTP1, HABP4, HEXB, PA2G4, PRDX6, PTGES2, RAB6A, RAP1B, RAP2B, RHOG, SYT12, SYT17, TLN1, VAT1, VTI1B]	27	**regulated exocytosis**	GO:0045055	1.41E-08	3.61E-06
		3.11	[APBB1, APOE, DLG4, DMD, FLOT1, GRB2, LGI1, MINK1, NLGN3, NPTX1, NTNG1, OLFM1, OPA1, PKN1, PTN, PTPRS, RHOG, S100A6, SRC, SYT17, THY1, UGT8]	22	**neuron projection morphogenesis**	GO:0048812	3.78E-07	9.50E-05
		2.97	[APBB1, APOE, DLG4, FLOT1, GRB2, LGI1, MINK1, NLGN3, NPTX1, NTNG1, OLFM1, OPA1, PKN1, PTN, PTPRS, RHOG, S100A6, SRC, THY1]	19	cell morphogenesis involved in neuron differentiation	GO:0048667	4.88E-06	0.001166078
		2.95	[CALR, CPEB3, EDC4, EEF1D, EEF1G, EIF3B, HABP4, LARP1, MTOR, PA2G4, PTK2B, PURA, RACK1, UPF1]	14	regulation of translation	GO:0006417	9.95E-05	0.022778961
		2.94	[APBB1, APOE, FLOT1, GRB2, LGI1, NLGN3, NPTX1, NTNG1, OLFM1, PKN1, PTPRS, RHOG, S100A6, SRC, THY1]	15	axonogenesis	GO:0007409	5.71E-05	0.013191499
		2.79	[APBB1, APOE, C1QA, CNTN1, CPEB3, DGKG, DLG4, DMD, EHD1, FKBP4, FLOT1, GFAP, GPM6B, GRB2, GRN, LGI1, MINK1, MTOR, NLGN3, NPTX1, NTNG1, OLFM1, OPA1, PKN1, PTK2B, PTN, PTPRS, RHOG, S100A6, SRC, SYT17, THY1, TSPAN2, UGT8]	34	neuron development	GO:0048666	2.33E-09	6.02E-07
		2.78	[ABCA2, APOE, CADM4, DMD, GSTP1, MTOR, PKN1, PLPP3, PPM1F, PPME1, PTN, RACK1, SIRT2, THY1]	14	negative regulation of phosphate metabolic process	GO:0045936	1.84E-04	0.041490973
		2.72	[APBB1, APOE, CNTN1, DGKG, DMD, EHD1, FKBP4, GFAP, GRN, MTOR, NTNG1, OPA1, PKN1, PTK2B, PTN, PTPRS, RHOG, SRC, THY1]	19	**regulation of plasma membrane bounded cell projection organization**	GO:0120035	1.66E-05	0.003934112
		2.58	[APCS, APOE, CADM4, CALR, CNTN1, CPEB3, CRYAB, CTSA, DMD, EDC4, ERC2, FLOT2, GSTP1, LARP1, MTOR, OGT, PFDN1, PIN1, PKN1, PLPP3, PPM1F, PPME1, PTN, PURA, RACK1, RTN1, SIRT2, SRC, THY1, UPF1]	30	negative regulation of protein metabolic process	GO:0051248	1.41E-07	3.55E-05
		2.46	[ABCA2, APBB1, APOE, C1QA, CALR, CD9, CNTN1, CPEB3, DGKG, DLG4, DMD, EHD1, FKBP4, FLOT1, GFAP, GPM6B, GRB2, GRN, GSTP1, HEXB, LGI1, MINK1, MTOR, NLGN3, NPTX1, NTNG1, OLFM1, OPA1, OPRM1, PIN1, PKN1, PRDX6, PTK2B, PTN, PTPRS, RHOG, S100A6, SIRT2, SRC, SYT17, THY1, TSPAN2, UGT8]	43	neurogenesis	GO:0022008	5.77E-10	1.50E-07
		2.43	[APBB1, APOE, C1QA, CALR, CNTN1, CPEB3, DGKG, DLG4, DMD, EHD1, FKBP4, FLOT1, GFAP, GPM6B, GRB2, GRN, LGI1, MINK1, MTOR, NLGN3, NPTX1, NTNG1, OLFM1, OPA1, PIN1, PKN1, PTK2B, PTN, PTPRS, RHOG, S100A6, SRC, SYT17, THY1, TSPAN2, UGT8]	36	neuron differentiation	GO:0030182	2.77E-08	7.09E-06
		2.37	[APOE, CALR, CD81, CD9, CNTN1, CSNK2B, GRN, GSTP1, MINK1, MTOR, NTNG1, PKN1, PLCB1, PLPP3, PPM1F, PTK2B, PTN, RACK1, RAP2B, RHOG, SRC, THY1]	22	regulation of cell migration	GO:0030334	2.87E-05	0.006756045
		2.33	[APBB1, APOE, C1QA, CALR, CNTN1, CPEB3, DGKG, DLG4, DMD, EHD1, FKBP4, FLOT1, GFAP, GPM6B, GRB2, GRN, LGI1, MINK1, MTOR, NLGN3, NPTX1, NTNG1, OLFM1, OPA1, OPRM1, PIN1, PKN1, PTK2B, PTN, PTPRS, RHOG, S100A6, SIRT2, SRC, SYT17, THY1, TSPAN2, UGT8]	38	generation of neurons	GO:0048699	3.20E-08	8.16E-06
		2.11	[APOE, CADM4, CALR, CPEB3, CRYAB, DMD, EDC4, ERC2, GSTP1, LARP1, MTOR, OGT, PKN1, PLPP3, PPM1F, PPME1, PTN, PURA, RACK1, SIRT2, SRC, THY1, UPF1]	23	negative regulation of cellular protein metabolic process	GO:0032269	1.53E-04	0.034655683

Table 1. Identified Gene Ontology (GO) enrichment pathways of total protein hits across proteomic analyses. Identified pathways (nodes) are sorted by analysis (WT vs Pyk2$^{-/-}$ and PS19$^{0/+}$ vs PS19$^{0/+}$;Pyk2$^{-/-}$) and by percent associated genes. Common pathways between analyses are bolded.

Fraction	Analysis	% Associated Genes	Associated Genes Found	Number of Genes	Pathway Term	GO ID	Term P-Value	Term P-Value Corrected with Bonferroni Step Down
Normalized Phospho-Enriched Protein	WT vs Pyk2$^{-/-}$	11.43	[BRSK1, GSK3A, GSK3B, MARK2]	4	tau-protein kinase activity	GO:0050321	4.49E-08	5.39E-07
		2.33	[BRSK1, GSK3B, MARK2, STK11]	4	regulation of axonogenesis	GO:0050770	2.76E-05	2.76E-04
		1.48	[AP2A1, BRSK1, GSK3A, GSK3B, MAGI2, MARK2, STK11]	7	regulation of neuron projection development	GO:0010975	3.06E-07	3.37E-06
		1.31	[BRSK1, GSK3A, GSK3B, MARK2, STK11]	5	protein serine kinase activity	GO:0106310	3.71E-05	3.34E-04
		1.31	[BRSK1, GSK3A, GSK3B, MARK2, STK11]	5	protein threonine kinase activity	GO:0106311	3.71E-05	3.34E-04
		1.19	[GSK3A, GSK3B, MARK2, PLCL2]	4	peptidyl-serine phosphorylation	GO:0018105	3.62E-04	0.002893702
		0.93	[AP2A1, BRSK1, CPNE6, GPM6B, GSK3A, GSK3B, MAGI2, MAP4, MARK2, STK11]	10	neuron projection development	GO:0031175	2.92E-08	3.79E-07
		0.71	[BRSK1, CPNE6, GSK3B, MARK2, STK11]	5	neuron projection morphogenesis	GO:0048812	6.72E-04	0.004700896
		0.47	[GSK3A, MAGI2, MARK2, MPP3, STK11]	5	positive regulation of phosphate metabolic process	GO:0045937	0.004069528	0.012208583
		0.41	[BRSK1, GSK3A, GSK3B, MARK2, MPP3, PLCL2, STK11]	7	protein phosphorylation	GO:0006468	0.001289881	0.007739284
		0.41	[GSK3A, GSK3B, MAGI2, MARK2, MPP3, PLCL2, STK11]	7	regulation of protein modification process	GO:0031399	0.001294324	0.006471619
		0.39	[GSK3A, MARK2, MPP3, PLCL2, STK11]	5	regulation of protein phosphorylation	GO:0001932	0.008870538	0.017741077
		0.39	[GSK3A, GSK3B, MAGI2, MARK2, MPP3, STK11]	6	positive regulation of cellular protein metabolic process	GO:0032270	0.00389758	0.015590322
		0.36	[GSK3A, GSK3B, MARK2, MPP3, PLCL2]	5	peptidyl-amino acid modification	GO:0018193	0.011955289	0.011955289
	PS19$^{0/+}$ vs PS19$^{0/+}$;Pyk2$^{-/-}$	1.54	[GNAO1, PTK2B, SLC30A1, TRPV2]	4	regulation of calcium ion transport	GO:0051924	4.89E-04	0.003424011
		0.89	[GRIA1, PTK2B, SCN2A, SLC30A1, TRPV2]	5	cation channel activity	GO:0005261	0.001096794	0.006580766
		0.85	[GRIA1, PTK2B, SLC30A1, TRPV2]	4	cellular calcium ion homeostasis	GO:0006874	0.004364709	0.021823543

Table 2. Identified Gene Ontology (GO) enrichment pathways of normalized phospho-enriched protein hits across phospho-proteomic analyses. Identified pathways (nodes) are sorted by analysis (WT vs Pyk2$^{-/-}$ and PS19$^{0/+}$ vs PS19$^{0/+}$;Pyk2$^{-/-}$) and by percent associated genes.

ADDITIONAL INFORMATION

Supplemental Figures 1-7 and Supplemental Table 1.

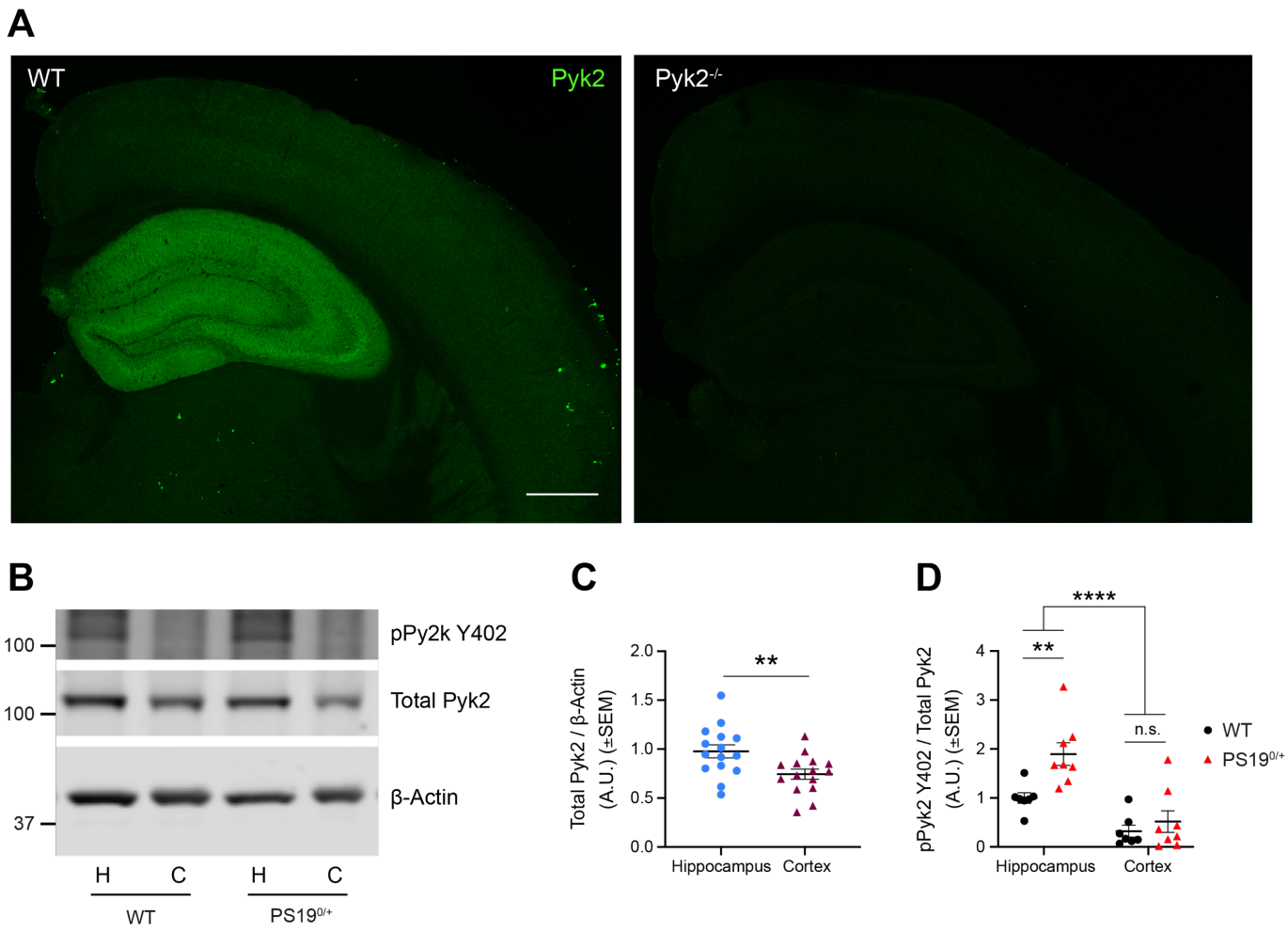

Supplemental Figure 1. Pyk2 expression is predominantly enriched in hippocampus compared to cortex, while PS19-driven Pyk2 activity is confined to hippocampus. **A**, Tiled, immunofluorescent images of Pyk2 immunoreactivity in hippocampus, cortex and thalamus of 9.5–10.5-month-old WT and Pyk2$^{-/-}$ mice. Scale bar, 500 µm. **B**, Representative immunoblot images of TBS-insoluble, SDS-soluble Pyk2 from hippocampus and cortex of 9.5–10.5-month WT and PS19$^{0/+}$ animals. **C** and **D**, Quantification of **B**. **C**, Pyk2 expression is significantly reduced in cortex compared to hippocampus of WT and PS19$^{0/+}$ mice. Data are graphed as mean ± SEM, unpaired two-tailed *t*-test, ***p*<0.01, *n* = 15 mice. **D**, Overall Pyk2 activation

(pPyk2 Y402 normalized to total Pyk2) is significantly reduced in cortex compared to hippocampus of WT and PS19$^{0/+}$ mice, while significant Tau-induced Pyk2 activation (pPyk2 Y402 normalized to total Pyk2) in PS19$^{0/+}$ compared to WT mice is restricted to hippocampus. Data are graphed as mean ± SEM, two-way ANOVA, $^{**}p<0.01$; unpaired two-tailed t-test, $^{**}p<0.01$, n.s. = not significant ($p = 0.4657$), $n = 7–8$ mice.

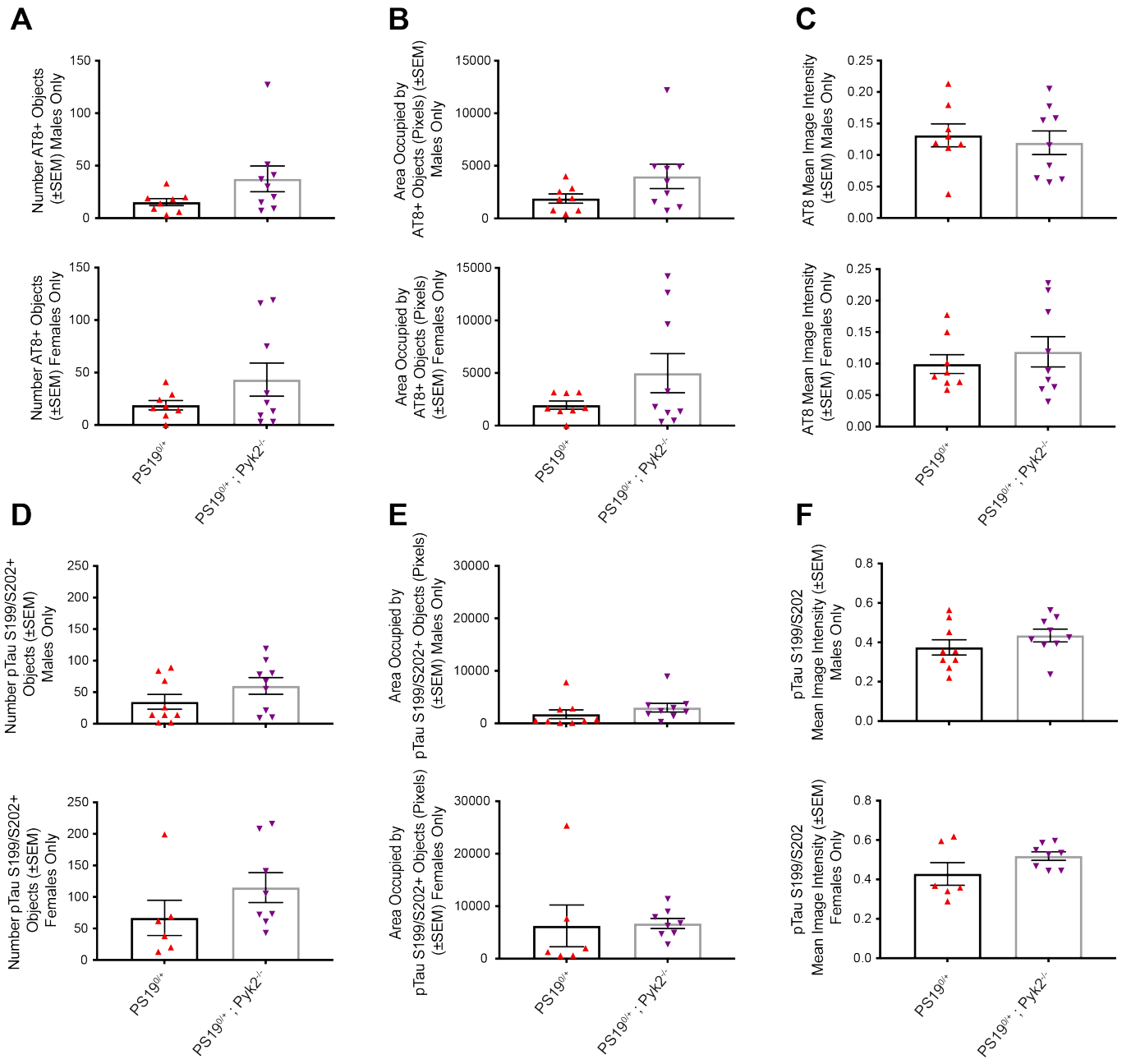

Supplemental Figure 2. Augmented Tau pathology in amygdala of PS19$^{0/+}$;Pyk2$^{-/-}$ compared to PS19$^{0/+}$ mice is driven neither by males nor females alone. **A**–**C**, Quantification of amygdalar AT8 immunoreactivity in 9.5–10.5-month-old PS19$^{0/+}$ and PS19$^{0/+}$;Pyk2$^{-/-}$ animals segregated by sex. No significant differences in the number of AT8-positive cell bodies (objects) (**A**), the area occupied by AT8-postive cell bodies (**B**) or AT8 mean image intensity (**C**) in either male or female PS19$^{0/+}$ and PS19$^{0/+}$;Pyk2$^{-/-}$ animals when segregated by sex.

Data are graphed as mean ± SEM, unpaired two-tailed *t*-test, *n* = 8–9 mice. **D**–**F**, Quantification of amygdalar pTau S199/S202 immunoreactivity in 9.5–10.5-month-old $PS19^{0/+}$ and $PS19^{0/+}$;$Pyk2^{-/-}$ animals segregated by sex. No significant differences in number of pTau S199/S202-positive cell bodies (objects) (**D**), area occupied by pTau S199/S202-postive cell bodies (**E**) or pTau S199/S202 mean image intensity (**F**) in male or female $PS19^{0/+}$ and $PS19^{0/+}$;$Pyk2^{-/-}$ animals when segregated by sex. Data are graphed as mean ± SEM, unpaired two-tailed *t*-test, *n* = 6–9 mice.

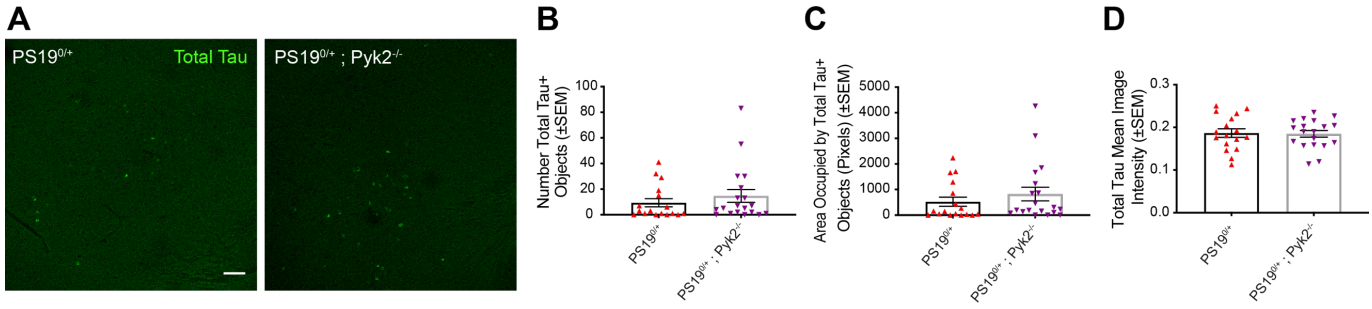

Supplemental Figure 3. Pyk2 deletion fails to result in detectable changes in total Tau immunofluorescence histologically. **A**, Representative immunofluorescent images of total Tau immunoreactivity in amygdala of 9.5–10.5-month-old WT, Pyk2$^{-/-}$, PS19$^{0/+}$ and PS19$^{0/+}$;Pyk2$^{-/-}$ animals. Scale bar, 100 µm. **B**–**D**, Quantification of **A**. Quantification of amygdalar total Tau immunoreactivity reveals no significant changes in the number of total Tau-positive cell bodies (objects) (**B**), the area occupied by those objects (**C**) or in mean image intensity (**D**) between PS19$^{0/+}$ and PS19$^{0/+}$;Pyk2$^{-/-}$ animals. Data are graphed as mean ± SEM, unpaired two-tailed *t*-test, *n* = 17–19 mice.

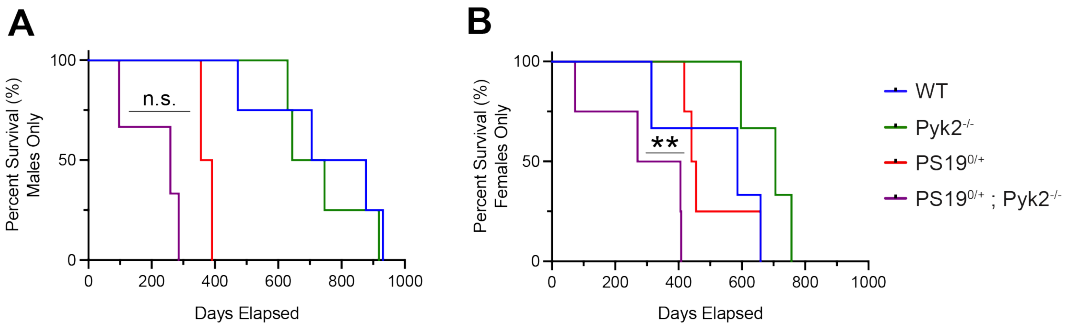

Supplemental Figure 4. Reduced survivorship in PS19$^{0/+}$;Pyk2$^{-/-}$ compared to PS19$^{0/+}$ mice is primarily driven by female animals. **A** and **B**, Kaplan-Meier survival curves of WT, Pyk2$^{-/-}$, PS19$^{0/+}$ and PS19$^{0/+}$;Pyk2$^{-/-}$ animals segregated by sex. Survivorship of male PS19$^{0/+}$;Pyk2$^{-/-}$ mice (median survival, 259 days) is not significantly reduced compared to male PS19$^{0/+}$ animals (median survival, 373 days). Log-rank (Mantel-Cox) test, n.s. = not significant (p = 0.0634), n = 2–3 mice (**A**). Survivorship of female PS19$^{0/+}$;Pyk2$^{-/-}$ mice (median survival, 338 days) is significantly less than that of female PS19$^{0/+}$ animals (median survival, 448 days). Log-rank (Mantel-Cox) test, **p = 0.0067, n = 4 mice (**B**).

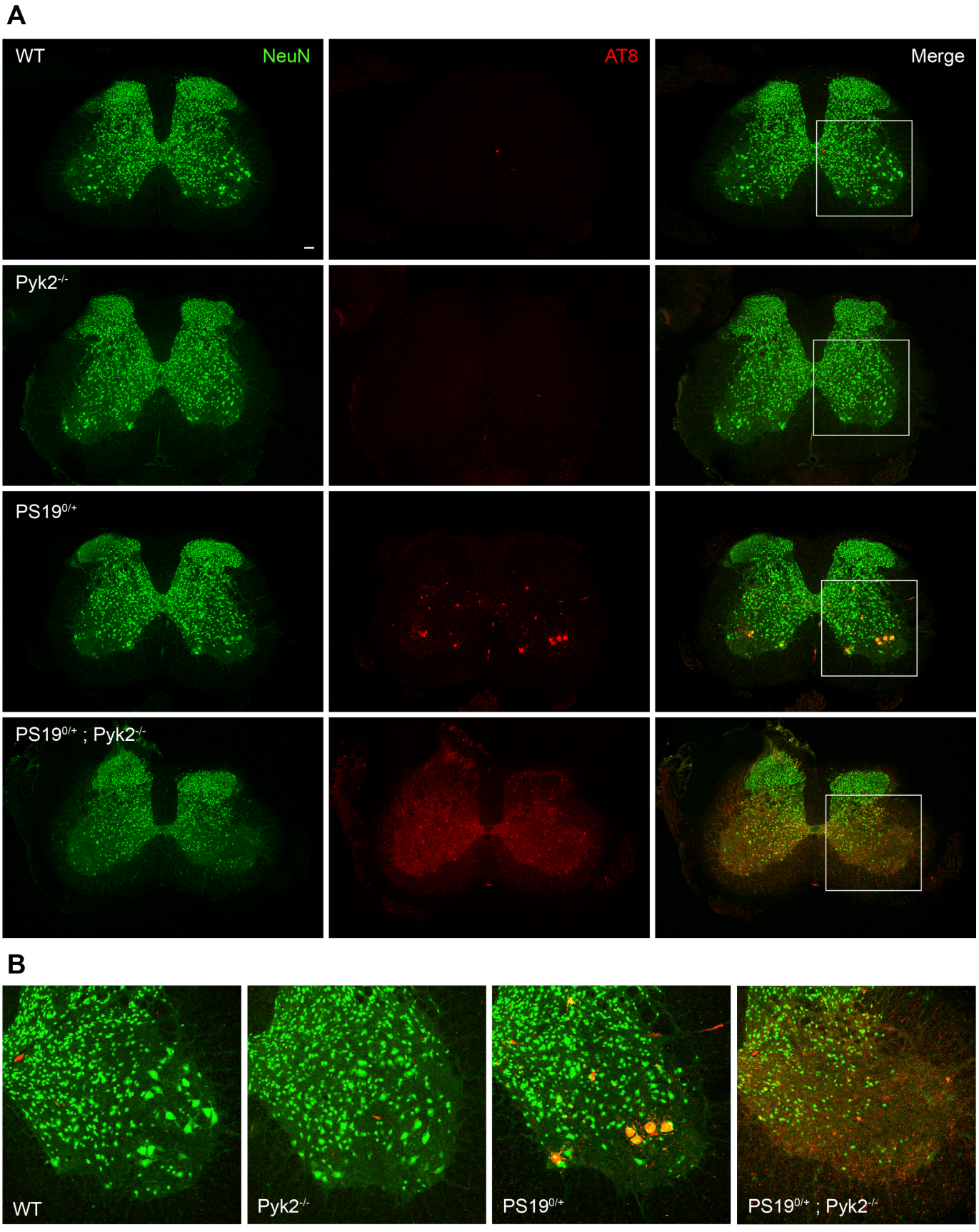
A
WT
NeuN
AT8
Merge
Pyk2-/-
PS190/+
PS190/+ ; Pyk2-/-
B
WT
Pyk2-/-
PS190/+
PS190/+ ; Pyk2-/-

Supplemental Figure 5. PS19-driven Tau pathology is present in spinal cord lumbar enlargement of PS19$^{0/+}$ and PS19$^{0/+}$;Pyk2$^{-/-}$ animals. **A** and **B**, Immunofluorescent images of lumbar spinal cord from 9.5–10.5-month-old WT, Pyk2$^{-/-}$, PS19$^{0/+}$ and PS19$^{0/+}$;Pyk2$^{-/-}$ animals labeled with NeuN (green) and pTau S202/T205 (AT8) (red). Scale bar, 100 μm. **B**, Enlargement of ventral horn shown in **A** (white box) demonstrating colocalization of NeuN and AT8 immunofluorescence in PS19$^{0/+}$ spinal cord and loss of NeuN-positive neuronal cell bodies in PS19$^{0/+}$;Pyk2$^{-/-}$ spinal cord.

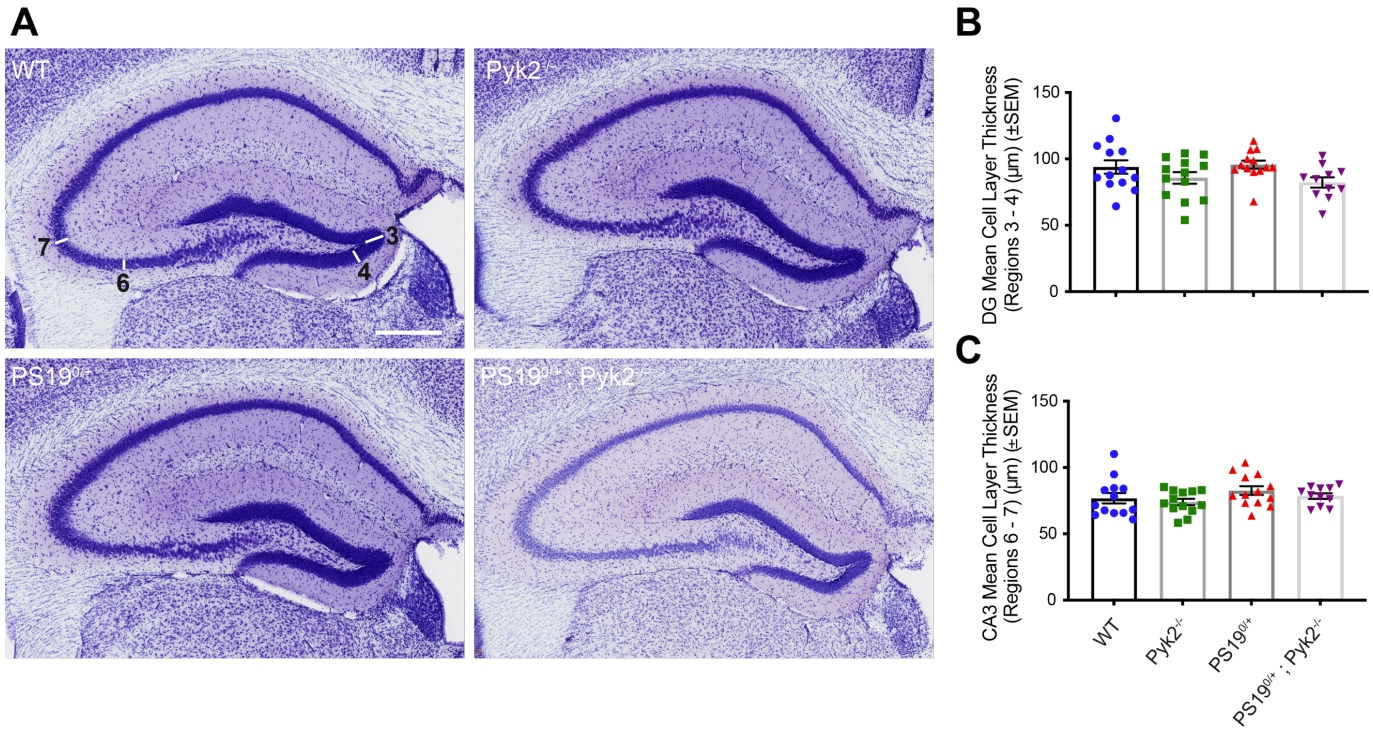

Supplemental Figure 6. No evidence of Tau-induced hippocampal neurodegeneration in PS19$^{0/+}$ or PS19$^{0/+}$;Pyk2$^{-/-}$ animals. **A**, Representative images of cresyl violet-stained sections from 9.5–10.5-month-old WT, Pyk2$^{-/-}$, PS19$^{0/+}$ and PS19$^{0/+}$;Pyk2$^{-/-}$ animals. Scale bar, 400 µm. **B** and **C**, Quantification of hippocampal cell layer thickness in the dentate gyrus (regions 3 and 4) and CA3 (regions 6 and 7) labeled in **A**. There were no significant differences in mean cell layer thickness of the dentate gyrus (**B**) or CA3 (**C**) across genotypes. Data are graphed as mean ± SEM, one-way ANOVA with Tukey's multiple comparisons test, *n* = 11–13 mice.

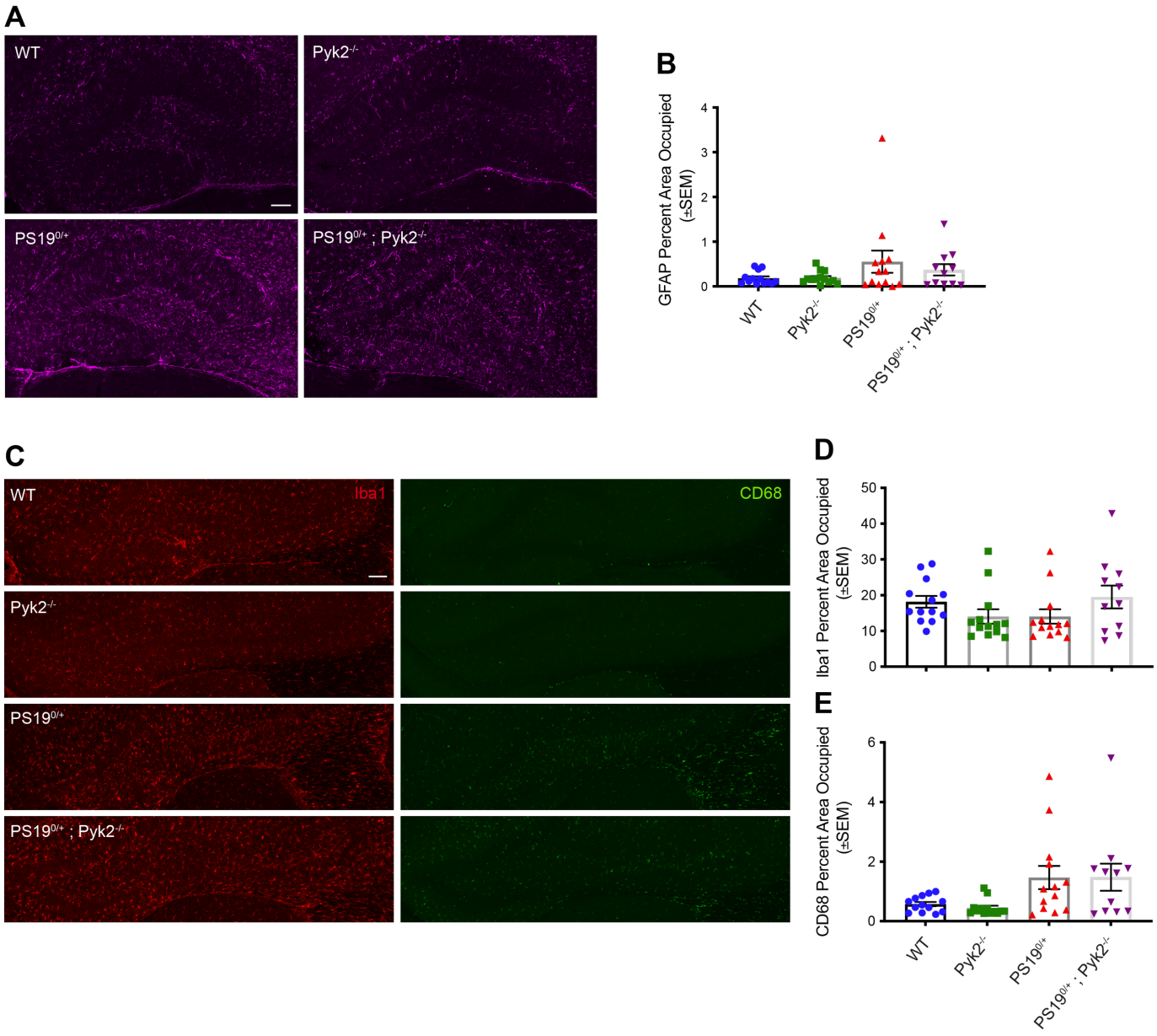

Supplemental Figure 7. Pyk2 deletion fails to result in detectable modulation of Tau-induced gliosis. **A**, Representative tiled, immunofluorescent images of GFAP immunoreactivity in dentate gyrus of 9.5–10.5-month-old WT, Pyk2$^{-/-}$, PS19$^{0/+}$ and PS19$^{0/+}$;Pyk2$^{-/-}$ animals. Scale bar, 100 µm. **B**, Quantification of **A**. There were no significant differences in astrogliosis (GFAP percent area occupied) across genotypes (**B**). Data are graphed as mean ± SEM, one-way ANOVA with Tukey's multiple comparisons test, *n* = 11–13 mice. **C**, Representative tiled, immunofluorescent images of Iba1 (red) and CD68 (green) immunoreactivity in

hippocampus of 9.5–10.5-month-old WT, Pyk2$^{-/-}$, PS19$^{0/+}$ and PS19$^{0/+}$;Pyk2$^{-/-}$ animals. Scale bar, 100 μm. **D** and **E**, Quantification of **C**. There were no significant differences in total hippocampal microglia (Iba1 percent area occupied) (**D**) nor activated hippocampal microglia (CD68 percent area occupied) (**E**) across genotypes. Data are graphed as mean ± SEM, one-way ANOVA with Tukey's multiple comparisons test, *n* = 11–13 mice.

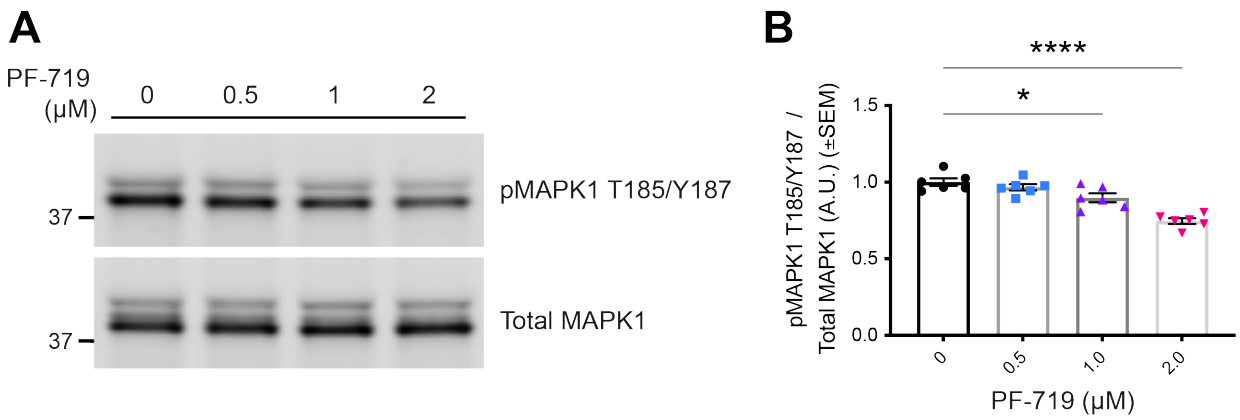

Supplemental Figure 8. Pyk2 activates MAPK1. **A** and **B**, Pyk2 was pharmacologically inhibited in iPSC-derived human cortical neurons (90–100 days post terminal differentiation) (same as shown in Figure 2E–I) using PF-719 at the concentrations indicated. **A**, Representative immunoblot images of lysates from PF-719-treated iPSC-derived human cortical neurons. **B**, Quantification of **A**. Pyk2 inhibition significantly decreased MAPK1 activity (pMAPK1 T185/Y187 normalized to total MAPK1) at 1.0 and 2.0 μM PF-719 (**B**). Data are graphed as mean ± SEM, one-way ANOVA with Dunnett's multiple comparisons test, **p*<0.05, *****p*<0.0001, *n* = 6.

Fraction	Analysis	% Associated Genes	Associated Genes Found	Number of Genes	Pathway Term	KEGG ID	Term P-Value	Term P-Value Corrected with Bonferroni Step Down
Total Protein	WT vs $Pyk2^{-/-}$	NA	NA	NA	NA	NA	NA	NA
	$PS19^{0/+}$ vs $PS19^{0/+}$;$Pyk2^{-/-}$	1.89	[CSNK2B, CYTB, DLG4, FUS, MTOR, PLCB1, PLCB3, RYR1, UQCR10]	9	Pathways of neurodegeneration	KEGG:05022	0.187479957	0.187479957

Supplemental Table 1. Kyoto Encyclopedia of Genes and Genomes (KEGG) enrichment for total protein hits across proteomic analyses. Only one node, “pathways of neurodegeneration,” was identified from hits generated from the $PS19^{0/+}$ vs $PS19^{0/+}$;$Pyk2^{-/-}$ analysis, while no pathways were identified for the WT vs $Pyk2^{-/-}$ analysis.

ABBREVIATIONS

Aβ – amyloid beta

Aβo – oligomeric amyloid beta

AU – airy unit

A.U. – arbitrary units

ACN – acetonitrile

aCSF – artificial cerebrospinal fluid

AD – Alzheimer's disease

ANOVA – analysis of variance

APP – amyloid precursor protein

APP/PS1 – APPswe/PS1ΔE9

BCA – bicinchoninic acid

BDNF – brain-derived neurotrophic factor

BSA – bovine serum albumin

CD68 – cluster of differentiation 68

CNS – central nervous system

DAPI – 4′,6-diamidino-2-phenylindole

DEP – differentially expressed protein

DMEM – Dulbecco's Modified Eagle's Medium

DMSO – dimethyl sulfoxide

DTT – dithiothreitol

EDTA – ethylenediaminetetraacetic acid

EN – enriched

FDR – false discovery rate

FT – flow through

FTD – frontotemporal dementia

GFAP – glial fibrillary acidic protein

GSK3β – glycogen synthase kinase 3 beta

GWAS – genome wide association study

Hek293T – human embryonic kidney 293 with SV40 large T antigen

hiPSC – human induced pluripotent stem cell

IACUC – institutional animal care and use committee

IAM – iodoacetamide

JAX – The Jackson Laboratory

JNK – c-Jun N-terminal kinase

LC-MS/MS – liquid chromatography with tandem mass spectrometry

LKB1 (STK11) – liver kinase B1 (serine/threonine kinase 11)

LOAD – late-onset Alzheimer's disease

LSM – laser scanning microscope

MAPK1 – mitogen-activated protein kinase 1

MAPT – microtubule-associated protein Tau

MEM – Eagle′s minimum essential medium

mGluR5 – metabotropic glutamate receptor 5

MWM – Morris water maze

P2' – second (crude synaptosomal) pellet

p38 MAPK – p38 mitogen-activated protein kinase

PBS – phosphate-buffered saline

PFA – paraformaldehyde

PrP^{C} – cellular prion protein

PS1 – presenilin 1

PSD-95 – post-synaptic density protein 95

PTK2B – protein tyrosine kinase 2 beta

RIPA – radioimmunoprecipitation assay buffer

SDS – sodium dodecyl sulfate

SDS-PAGE – sodium dodecyl sulfate-polyacrylamide gel electrophoresis

SEM – standard error of the mean

SMAD – SMA (small worm phenotype) / MAD (mothers against decapentaplegic)

SPE – solid-phase extraction

TBS – tris-buffered saline

TBST – tris-buffered saline with Tween 20

TFA – trifluoroacetic acid

UPLC – ultra performance liquid chromatography

WT – wild type

DECLARATIONS

Ethics approval and consent to participate. Not applicable.

Consent for publication. Not applicable.

Availability of data and materials. The proteomic datasets analyzed during the current study are available from the corresponding author on reasonable request.

Competing interests. None.

Funding. A.H.B. was supported by the NIH NIA fellowship award F31AG066483 and the NIH NINDS training grants T32NS007224 and T32NS041228. S.H.N. received a PhD fellowship from Boehringer Ingelheim Fonds. This work was supported by grants from the NIA and the Falk Medical Research Trust to S.M.S. Additional support came from NIH Yale/NIDA Neuroproteomics Centre (DA018343). The Orbitrap Fusion mass spectrometer and the UPLC utilized were supported in part by NIH SIG grants 1S10ODOD018034 & 1S10OD019967, respectively, and Yale School of Medicine.

Authors' contributions. Conceptualization, A.H.B. and S.M.S.; Methodology, A.H.B., S.H.N., F.G., L.M.S., B.H., S.A.S., T.T.L., and S.M.S.; Investigation, A.H.B., S.H.N., F.G., L.M.S., B.H., S.A.S. and T.T.L.; Writing – Original Draft, A.H.B. and S.M.S.; Writing – Review & Editing, all; Funding Acquisition, S.M.S.; Resources, A.H.B. and S.M.S; Supervision, S.M.S. All authors read and approved the final manuscript.

Acknowledgments. We thank Kristin DeLuca and Stefano Sodi for excellent technical assistance. We thank Katherine Wilczak, Jean Kanyo and Edward Z. Voss for assistance with proteomics sample, data collection and initial analysis.

DISCLOSURE

Chapter 3 was accepted for publication in *Molecular Neurodegeneration* on March 2nd, 2022.

Experiments presented in Figure 1 were conducted by Fulin Guan.

AUTHORS

A. Harrison Brody[1], Sarah Helena Nies[1,2], Fulin Guan[1], Levi M. Smith[1], Bandhan Mukherjee[1], Santiago A. Salazar[1], Suho Lee[1], TuKiet T. Lam[3,4], Stephen M. Strittmatter[1,*]

[1]Cellular Neuroscience, Neurodegeneration and Repair Program, Departments of Neurology and Neuroscience, Yale School of Medicine, New Haven, CT, USA

[2]Graduate School of Cellular and Molecular Neuroscience, University of Tübingen, D-72074 Tübingen, Germany

[3]Department of Molecular Biophysics and Biochemistry, Yale School of Medicine, New Haven, CT, USA.

[4]Keck MS & Proteomics Resource, Yale School of Medicine, New Haven, CT, USA.

*Correspondence to: Stephen M. Strittmatter, Department of Neuroscience, Yale School of Medicine New Haven, CT, USA; e-mail: stephen.strittmatter@yale.edu

A. Harrison Brody: harrison.brody@yale.edu

Sarah Helena Nies: s.nies@yale.edu

Fulin Guan: fulinguancn@outlook.com

Levi M. Smith: levimerlinsmith@gmail.com

Bandhan Mukherjee: bandhan.mukherjee@yale.edu

Santiago A. Salazar: santiago.v.salazar@gmail.com

Suho Lee: lake1980@gmail.com

TuKiet T. Lam: tukiet.lam@yale.edu

CHAPTER 4

Future Directions

As the global population continues to age, and as deaths due to heart disease and cancer continue to decline, current projections suggest that rising cases of Alzheimer's disease (AD) may overwhelm existing global health care infrastructure in the 21st century. In order to develop safe and effective disease-modifying therapeutics for the successful treatment of AD, a more complete understanding of AD pathophysiology is critical. A growing list of genetic AD risk factors identified through a number of recent genome wide association studies (GWAS) provides unique insight into the molecular mechanisms that influence AD susceptibility [132, 133, 181, 183, 184]. Most optimistically, elucidating how these thirty or so genes modulate AD risk may reveal novel therapeutic targets for the treatment of AD.

While our group has previously reported that the genetic AD risk factor Pyk2 is necessary for Aβo-induced spine loss *in vitro* and for a number of Aβ-associated phenotypes in APP/PS1 animals (including synapse loss, memory impairment and astrogliosis) *in vivo*, the results presented here suggest a protective role for Pyk2 with respect to the pathological processing of Tau [186, 187]. Inhibition of Pyk2 pharmacologically in both PS19 hippocampal brain slices and in iPSC-derived human neurons increases the phosphorylation of Tau at a number of pathophysiologically-relevant residues, and genetic deletion of Pyk2 from PS19 animals significantly exacerbates Tau phosphorylation as well as Tau-associated early death, memory impairment and synaptic C1q deposition. Phosphoproteomic analysis reveals a number of proximate regulators of Tau modulated by Pyk2 expression, and the activity of at least one hit, LKB1, is suppressed by basal levels of Pyk2 activity. While LKB1 has not been shown to phosphorylate Tau directly, the activity of p38 MAPK, a direct substrate of LKB1

known to directly phosphorylate Tau, is also suppressed by Pyk2 [203-207, 234]. Furthermore, the activities of both proteins are significantly increased in $PS19^{0/+};Pyk2^{-/-}$ animals, suggesting that these proteins may at least partially explain the exacerbated Tau-associated phenotypes observed in $PS19^{0/+};Pyk2^{-/-}$ mice.

Though these results suggest that the mechanism by which Pyk2 suppresses Tau phosphorylation may involve Pyk2's ability to inhibit LKB1 and p38 MAPK activity, whether Pyk2 suppresses LKB1 activity directly or indirectly is still unknown. Direct tyrosine kinase-mediated regulation of LKB1 activity has been previously reported; Fyn has been shown to directly phosphorylate LKB1 at Y261 and Y365, leading to changes in LKB1 cellular distribution and activity [252]. In experiments presented here, LKB1 activity was assessed through the phosphorylation of S428, which is required for the nuclear export of LKB1 into the cytoplasm as well as LKB1's ability to bind to and phosphorylate substrates including AMPK [237-239]. Future experiments are required to determine whether Pyk2 may also phosphorylate tyrosine resides of LKB1 or whether Pyk2 modulates intermediate factors that regulate S428 phosphorylation. Whether Pyk2 modulates p38 MAPK activity exclusively through LKB1 is also unknown. Further investigation is needed to rule out the contribution of other kinases that may mediate Pyk2's ability to regulate the phosphorylation of p38 MAPK at T180/Y182, though direct phosphorylation of Y182 by Pyk2 is possible. In addition, although we report the validation of just two Pyk2-modulated regulator of Tau phosphorylation identified via phosphoproteomics (LKB1 and MAPK1), additional hits (such as MARK2 and Brsk1) may also represent potentially exciting avenues for further investigation.

Combined with results previously reported by our group that Pyk2 contributes to Aβ toxicity, the results reported here, suggesting a protective role for Pyk2 in suppressing Tau

phosphorylation and toxicity, evince divergent roles for Pyk2 in the pathophysiology of AD. Since AD is defined both by toxic Aβ signaling and Tau dysregulation, developing a unified understand of Pyk2's role in regulating the toxicity of both proteins is crucial. Our group has previously reported that Pyk2 expression is necessary for both Aβo-induced synapse loss in mouse primary hippocampal neurons and for Aβo-induced impairments in synaptic plasticity (LTP) in hippocampal slices [186, 187], and there is reason to suggest that Pyk2 may also contribute to Tau-mediated synapse loss.

Results presented in Chapter 3 show a significant reduction in synapse density within the dentate gyrus of $PS19^{0/+}$ and $PS19^{0/+}$;$Pyk2^{-/-}$ animals, with no significant difference in PSD-95-positive immunoreactivity between these two genotypes. However, immunohistology of PSD-95-postive synaptic puncta in the amygdala and the CA3 region of the hippocampus reveal a significant reduction in synapse density only in $PS19^{0/+}$ animals, with no such reduction in $PS19^{0/+}$;$Pyk2^{-/-}$ mice (data not shown), suggesting that Pyk2 may be playing a role that contributes to Tau-mediated synapse loss in these regions. If confirmed, these results would indicate a generalized role of Pyk2 in synaptic dysfunction and loss with respect to both Aβ and Tau. Our group has previously shown that Pyk2 over-expression is sufficient to induce synapse loss in the absence of either Pyk2 and Tau, providing further evidence that aberrant Pyk2 expression, activation or localization can destabilize synaptic integrity [187]. Our group has also reported that Aβ-signaling causes a shift in the subcellular distribution of Pyk2, leading to the mislocalization of Pyk2 into dendritic spines [187]. These observations support a theoretical mechanism that may explain how the divergent roles of Pyk2, with respect to Aβ and Tau, might contribute to the pathogenesis of AD. If Aβ-signaling drives Pyk2 localization away from cellular compartments (where it is able to suppresses Tau phosphorylation) towards dendritic spines (where it can contribute to synapse loss), Aβ-

induced changes to Pyk2 subcellular localization may partly explain how this single AD risk factor drives AD progression. Experiments designed to probe whether Aβ-induced changes in Pyk2 subcellular localization, per se, lead to increased levels of Tau phosphorylation have yet to be conducted.

These results, which suggest a protective role of Pyk2 in suppressing Tau phosphorylation, must be reconciled with previous findings revealing the necessity of Pyk2 for Aβ-induced synaptotoxicity. Unfortunately, these diverging roles for Pyk2 with respect to Aβ toxicity and Tau dysfunction preclude Pyk2 as a potential therapeutic target using conventional pharmacological strategies. Inhibition of Pyk2 may spare Aβ toxicity at the expense of increased Tau phosphorylation, while activation of Pyk2 would likely yield the opposite effect. However, considering these results, and contingent on the validation of the mechanistic framework proposed here, future innovative strategies capable of regulating the subcellular distribution of proteins such as Pyk2 may one day prove useful in the fight against AD.

REFERENCES

1. Association As: **Alzheimer's disease facts and figures.** *Alzheimer's and Dementia* 2017, **13:**325-373.
2. Association As: **Alzheimer's disease facts and figures.** *Alzheimer's and Dementia* 2016, **12:**495-509.
3. Hurd MD, Martorell P, Delavande A, Mullen KJ, Langa KM: **Monetary costs of dementia in the United States.** *The New England journal of medicine* 2013, **368:**1326-1334.
4. Grundke-Iqbal I, Iqbal K, Tung YC, Quinlan M, Wisniewski HM, Binder LI: **Abnormal phosphorylation of the microtubule-associated protein tau (tau) in Alzheimer cytoskeletal pathology.** *Proceedings of the National Academy of Sciences* 1986, **83:**4913-4917.
5. Alzheimer A: **Über eine eigenartige Erkrankung der Hirnrinde.** *Allgemeine Zeitschrift fur Psychiatrie und Psychisch-gerichtliche Medizin* 1907, **64:**146-148.
6. Haass C, Selkoe DJ: **Soluble protein oligomers in neurodegeneration: lessons from the Alzheimer's amyloid beta-peptide.** *Nature reviews Molecular cell biology* 2007, **8:**101-112.
7. Serrano-Pozo A, Frosch MP, Masliah E, Hyman BT: **Neuropathological alterations in Alzheimer disease.** *Cold Spring Harb Perspect Med* 2011, **1:**a006189.
8. Holtzman DM, Morris JC, Goate AM: **Alzheimer's disease: the challenge of the second century.** *Sci Transl Med* 2011, **3:**77sr71.
9. Murphy C, Gilmore M, Seery C, Salmon D, Lasker B: **Olfactory thresholds are associated with degree of dementia in Alzheimer's disease.** *Neurobiol Aging* 1990, **11:**465-469.
10. Hardy JA, Higgins GA: **Alzheimer's disease: the amyloid cascade hypothesis.** *Science* 1992, **256:**184-185.
11. Bertram L, Lill CM, Tanzi RE: **The genetics of Alzheimer disease: back to the future.** *Neuron* 2010, **68:**270-281.
12. Levy E, Carman M, Fernandez-Madrid I, Power M, Lieberburg I, van Duinen S, Bots G, Luyendijk W, Frangione B: **Mutation of the Alzheimer's disease amyloid gene in hereditary cerebral hemorrhage, Dutch type.** *Science* 1990, **248:**1124-1126.
13. Bitan G, Kirkitadze MD, Lomakin A, Vollers SS, Benedek GB, Teplow DB: **Amyloid beta -protein (Abeta) assembly: Abeta 40 and Abeta 42 oligomerize through distinct pathways.** *Proc Natl Acad Sci U S A* 2003, **100:**330-335.
14. Jack CR, Jr., Knopman DS, Jagust WJ, Petersen RC, Weiner MW, Aisen PS, Shaw LM, Vemuri P, Wiste HJ, Weigand SD, et al: **Tracking pathophysiological processes in Alzheimer's disease: an updated hypothetical model of dynamic biomarkers.** *Lancet Neurol* 2013, **12:**207-216.
15. Fagan AM, Mintun MA, Mach RH, Lee SY, Dence CS, Shah AR, LaRossa GN, Spinner ML, Klunk WE, Mathis CA, et al: **Inverse relation between in vivo amyloid imaging load and cerebrospinal fluid Abeta42 in humans.** *Ann Neurol* 2006, **59:**512-519.
16. Shaw LM, Vanderstichele H, Knapik-Czajka M, Clark CM, Aisen PS, Petersen RC, Blennow K, Soares H, Simon A, Lewczuk P, et al: **Cerebrospinal fluid biomarker signature in Alzheimer's disease neuroimaging initiative subjects.** *Ann Neurol* 2009, **65:**403-413.
17. Fagan AM, Mintun MA, Shah AR, Aldea P, Roe CM, Mach RH, Marcus D, Morris JC, Holtzman DM: **Cerebrospinal fluid tau and ptau(181) increase with cortical**

amyloid deposition in cognitively normal individuals: implications for future clinical trials of Alzheimer's disease. *Embo Mol Med* 2009, **1:**371-380.
18. McKhann GM, Knopman DS, Chertkow H, Hyman BT, Jack CR, Jr., Kawas CH, Klunk WE, Koroshetz WJ, Manly JJ, Mayeux R, et al: **The diagnosis of dementia due to Alzheimer's disease: recommendations from the National Institute on Aging-Alzheimer's Association workgroups on diagnostic guidelines for Alzheimer's disease.** *Alzheimers Dement* 2011, **7:**263-269.
19. Sperling RA, Aisen PS, Beckett LA, Bennett DA, Craft S, Fagan AM, Iwatsubo T, Jack CR, Jr., Kaye J, Montine TJ, et al: **Toward defining the preclinical stages of Alzheimer's disease: recommendations from the National Institute on Aging-Alzheimer's Association workgroups on diagnostic guidelines for Alzheimer's disease.** *Alzheimers Dement* 2011, **7:**280-292.
20. Karran E, Mercken M, De Strooper B: **The amyloid cascade hypothesis for Alzheimer's disease: an appraisal for the development of therapeutics.** *Nat Rev Drug Discov* 2011, **10:**698-712.
21. Games D, Adams D, Alessandrini R, Barbour R, Berthelette P, Blackwell C, Carr T, Clemens J, Donaldson T, Gillespie F, et al.: **Alzheimer-type neuropathology in transgenic mice overexpressing V717F beta-amyloid precursor protein.** *Nature* 1995, **373:**523-527.
22. Citron M, Westaway D, Xia W, Carlson G, Diehl T, Levesque G, Johnson-wood K, Lee M, Seubert P, Davis A, et al: **Mutant presenilins of Alzheimer's disease increase production of 42-residue amyloid β-protein in both transfected cells and transgenic mice.** *Nat Med* 1997, **3:**67-72.
23. Puolivali J, Wang J, Heikkinen T, Heikkila M, Tapiola T, van Groen T, Tanila H: **Hippocampal A beta 42 levels correlate with spatial memory deficit in APP and PS1 double transgenic mice.** *Neurobiol Dis* 2002, **9:**339-347.
24. Oddo S, Caccamo A, Kitazawa M, Tseng BP, LaFerla FM: **Amyloid deposition precedes tangle formation in a triple transgenic model of Alzheimer's disease.** *Neurobiol Aging* 2003, **24:**1063-1070.
25. Oddo S, Caccamo A, Shepherd JD, Murphy MP, Golde TE, Kayed R, Metherate R, Mattson MP, Akbari Y, LaFerla FM: **Triple-Transgenic Model of Alzheimer's Disease with Plaques and Tangles.** *Neuron* 2003, **39:**409-421.
26. Oakley H, Cole SL, Logan S, Maus E, Shao P, Craft J, Guillozet-Bongaarts A, Ohno M, Disterhoft J, Van Eldik L, et al: **Intraneuronal beta-amyloid aggregates, neurodegeneration, and neuron loss in transgenic mice with five familial Alzheimer's disease mutations: potential factors in amyloid plaque formation.** *J Neurosci* 2006, **26:**10129-10140.
27. Ingelsson M, Fukumoto H, Newell KL, Growdon JH, Hedley-Whyte ET, Frosch MP, Albert MS, Hyman BT, Irizarry MC: **Early A beta accumulation and progressive synaptic loss, gliosis, and tangle formation in AD brain.** *Neurology* 2004, **62:**925-931.
28. Shankar GM, Li S, Mehta TH, Garcia-Munoz A, Shepardson NE, Smith I, Brett FM, Farrell MA, Rowan MJ, Lemere CA, et al: **Amyloid-beta protein dimers isolated directly from Alzheimer's brains impair synaptic plasticity and memory.** *Nat Med* 2008, **14:**837-842.
29. Perez-Nievas BG, Stein TD, Tai HC, Dols-Icardo O, Scotton TC, Barroeta-Espar I, Fernandez-Carballo L, de Munain EL, Perez J, Marquie M, et al: **Dissecting phenotypic traits linked to human resilience to Alzheimer's pathology.** *Brain* 2013, **136:**2510-2526.

30. Holmes C, Boche D, Wilkinson D, Yadegarfar G, Hopkins V, Bayer A, Jones RW, Bullock R, Love S, Neal JW, et al: **Long-term effects of Aβ42 immunisation in Alzheimer's disease: follow-up of a randomised, placebo-controlled phase I trial.** *The Lancet* 2008, **372:**216-223.
31. Doody RS, Raman R, Farlow M, Iwatsubo T, Vellas B, Joffe S, Kieburtz K, He F, Sun X, Thomas RG, et al: **A phase 3 trial of semagacestat for treatment of Alzheimer's disease.** *N Engl J Med* 2013, **369:**341-350.
32. Doody RS, Thomas RG, Farlow M, Iwatsubo T, Vellas B, Joffe S, Kieburtz K, Raman R, Sun X, Aisen PS, et al: **Phase 3 trials of solanezumab for mild-to-moderate Alzheimer's disease.** *N Engl J Med* 2014, **370:**311-321.
33. Salloway S, Sperling R, Fox NC, Blennow K, Klunk W, Raskind M, Sabbagh M, Honig LS, Porsteinsson AP, Ferris S, et al: **Two phase 3 trials of bapineuzumab in mild-to-moderate Alzheimer's disease.** *N Engl J Med* 2014, **370:**322-333.
34. Spires-Jones TL, Hyman BT: **The intersection of amyloid beta and tau at synapses in Alzheimer's disease.** *Neuron* 2014, **82:**756-771.
35. Hsia AY, Masliah E, McConlogue L, Yu GQ, Tatsuno G, Hu K, Kholodenko D, Malenka RC, Nicoll RA, Mucke L: **Plaque-independent disruption of neural circuits in Alzheimer's disease mouse models.** *Proc Natl Acad Sci U S A* 1999, **96:**3228-3233.
36. Lambert MP, Barlow AK, Chromy BA, Edwards C, Freed R, Liosatos M, Morgan TE, Rozovsky I, Trommer B, Viola KL, et al: **Diffusible, nonfibrillar ligands derived from A 1-42 are potent central nervous system neurotoxins.** *Proceedings of the National Academy of Sciences* 1998, **95:**6448-6453.
37. Kayed R, Head E, Thompson JL, McIntire TM, Milton SC, Cotman CW, Glabe CG: **Common structure of soluble amyloid oligomers implies common mechanism of pathogenesis.** *Science* 2003, **300:**486-489.
38. Gong Y, Chang L, Viola KL, Lacor PN, Lambert MP, Finch CE, Krafft GA, Klein WL: **Alzheimer's disease-affected brain: presence of oligomeric A beta ligands (ADDLs) suggests a molecular basis for reversible memory loss.** *Proc Natl Acad Sci U S A* 2003, **100:**10417-10422.
39. Lue LF, Kuo YM, Roher AE, Brachova L, Shen Y, Sue L, Beach T, Kurth JH, Rydel RE, Rogers J: **Soluble amyloid beta peptide concentration as a predictor of synaptic change in Alzheimer's disease.** *Am J Pathol* 1999, **155:**853-862.
40. McLean CA, Cherny RA, Fraser FW, Fuller SJ, Smith MJ, Beyreuther K, Bush AI, Masters CL: **Soluble pool of Abeta amyloid as a determinant of severity of neurodegeneration in Alzheimer's disease.** *Ann Neurol* 1999, **46:**860-866.
41. DaRocha-Souto B, Scotton TC, Coma M, Serrano-Pozo A, Hashimoto T, Sereno L, Rodriguez M, Sanchez B, Hyman BT, Gomez-Isla T: **Brain oligomeric beta-amyloid but not total amyloid plaque burden correlates with neuronal loss and astrocyte inflammatory response in amyloid precursor protein/tau transgenic mice.** *J Neuropathol Exp Neurol* 2011, **70:**360-376.
42. Kostylev MA, Kaufman AC, Nygaard HB, Patel P, Haas LT, Gunther EC, Vortmeyer A, Strittmatter SM: **Prion-Protein-interacting Amyloid-beta Oligomers of High Molecular Weight Are Tightly Correlated with Memory Impairment in Multiple Alzheimer Mouse Models.** *The Journal of biological chemistry* 2015, **290:**17415-17438.
43. Reiman EM, Chen K, Liu X, Bandy D, Yu M, Lee W, Ayutyanont N, Keppler J, Reeder SA, Langbaum JB, et al: **Fibrillar amyloid-beta burden in cognitively normal people at 3 levels of genetic risk for Alzheimer's disease.** *Proc Natl Acad Sci U S A* 2009, **106:**6820-6825.

44. Koffie RM, Meyer-Luehmann M, Hashimoto T, Adams KW, Mielke ML, Garcia-Alloza M, Micheva KD, Smith SJ, Kim ML, Lee VM, et al: **Oligomeric amyloid beta associates with postsynaptic densities and correlates with excitatory synapse loss near senile plaques.** *Proc Natl Acad Sci U S A* 2009, **106:**4012-4017.
45. Esparza TJ, Zhao H, Cirrito JR, Cairns NJ, Bateman RJ, Holtzman DM, Brody DL: **Amyloid-beta oligomerization in Alzheimer dementia versus high-pathology controls.** *Ann Neurol* 2013, **73:**104-119.
46. Savage MJ, Kalinina J, Wolfe A, Tugusheva K, Korn R, Cash-Mason T, Maxwell JW, Hatcher NG, Haugabook SJ, Wu G, et al: **A sensitive abeta oligomer assay discriminates Alzheimer's and aged control cerebrospinal fluid.** *J Neurosci* 2014, **34:**2884-2897.
47. Yang T, Hong S, O'Malley T, Sperling RA, Walsh DM, Selkoe DJ: **New ELISAs with high specificity for soluble oligomers of amyloid beta-protein detect natural Abeta oligomers in human brain but not CSF.** *Alzheimers Dement* 2013, **9:**99-112.
48. Benilova I, Karran E, De Strooper B: **The toxic Abeta oligomer and Alzheimer's disease: an emperor in need of clothes.** *Nat Neurosci* 2012, **15:**349-357.
49. Lansbury PT: **Evolution of amyloid: What normal protein folding may tell us about fibrillogenesis and disease.** *Proceedings of the National Academy of Sciences* 1999, **96:**3342-3344.
50. Scheff SW, Price DA, Schmitt FA, DeKosky ST, Mufson EJ: **Synaptic alterations in CA1 in mild Alzheimer disease and mild cognitive impairment.** *Neurology* 2007, **68:**1501-1508.
51. Lanz TA, Carter DB, Merchant KM: **Dendritic spine loss in the hippocampus of young PDAPP and Tg2576 mice and its prevention by the ApoE2 genotype.** *Neurobiol Dis* 2003, **13:**246-253.
52. Heiss JK, Barrett J, Yu Z, Haas LT, Kostylev MA, Strittmatter SM: **Early Activation of Experience-Independent Dendritic Spine Turnover in a Mouse Model of Alzheimer's Disease.** *Cereb Cortex* 2016.
53. Almeida CG, Tampellini D, Takahashi RH, Greengard P, Lin MT, Snyder EM, Gouras GK: **Beta-amyloid accumulation in APP mutant neurons reduces PSD-95 and GluR1 in synapses.** *Neurobiol Dis* 2005, **20:**187-198.
54. Roselli F, Tirard M, Lu J, Hutzler P, Lamberti P, Livrea P, Morabito M, Almeida OF: **Soluble beta-amyloid1-40 induces NMDA-dependent degradation of postsynaptic density-95 at glutamatergic synapses.** *J Neurosci* 2005, **25:**11061-11070.
55. Jurgensen S, Ferreira ST: **Nicotinic receptors, amyloid-beta, and synaptic failure in Alzheimer's disease.** *J Mol Neurosci* 2010, **40:**221-229.
56. Hong S, Beja-Glasser VF, Nfonoyim BM, Frouin A, Li S, Ramakrishnan S, Merry KM, Shi Q, Rosenthal A, Barres BA, et al: **Complement and microglia mediate early synapse loss in Alzheimer mouse models.** *Science* 2016, **352:**712-716.
57. Kolodkin AL, Levengood DV, Rowe EG, Tai YT, Giger RJ, Ginty DD: **Neuropilin is a semaphorin III receptor.** *Cell* 1997, **90:**753-762.
58. Takahashi T, Fournier A, Nakamura F, Wang LH, Murakami Y, Kalb RG, Fujisawa H, Strittmatter SM: **Plexin-neuropilin-1 complexes form functional semaphorin-3A receptors.** *Cell* 1999, **99:**59-69.
59. Nakamura F, Tanaka M, Takahashi T, Kalb RG, Strittmatter SM: **Neuropilin-1 extracellular domains mediate semaphorin D/III-induced growth cone collapse.** *Neuron* 1998, **21:**1093-1100.

60. Takahashi T, Nakamura F, Strittmatter SM: **Neuronal and non-neuronal collapsin-1 binding sites in developing chick are distinct from other semaphorin binding sites.** *J Neurosci* 1997, **17:**9183-9193.
61. Fournier AE, GrandPre T, Strittmatter SM: **Identification of a receptor mediating Nogo-66 inhibition of axonal regeneration.** *Nature* 2001, **409:**341-346.
62. Liu BP, Fournier A, GrandPre T, Strittmatter SM: **Myelin-associated glycoprotein as a functional ligand for the Nogo-66 receptor.** *Science* 2002, **297:**1190-1193.
63. Owuor K, Harel NY, Englot DJ, Hisama F, Blumenfeld H, Strittmatter SM: **LGI1-associated epilepsy through altered ADAM23-dependent neuronal morphology.** *Mol Cell Neurosci* 2009, **42:**448-457.
64. Rajagopalan S, Deitinghoff L, Davis D, Conrad S, Skutella T, Chedotal A, Mueller BK, Strittmatter SM: **Neogenin mediates the action of repulsive guidance molecule.** *Nat Cell Biol* 2004, **6:**756-762.
65. Hu F, Padukkavidana T, Vaegter CB, Brady OA, Zheng Y, Mackenzie IR, Feldman HH, Nykjaer A, Strittmatter SM: **Sortilin-mediated endocytosis determines levels of the frontotemporal dementia protein, progranulin.** *Neuron* 2010, **68:**654-667.
66. Lauren J, Gimbel DA, Nygaard HB, Gilbert JW, Strittmatter SM: **Cellular prion protein mediates impairment of synaptic plasticity by amyloid-beta oligomers.** *Nature* 2009, **457:**1128-1132.
67. Chen S, Yadav SP, Surewicz WK: **Interaction between human prion protein and amyloid-beta (Abeta) oligomers: role OF N-terminal residues.** *J Biol Chem* 2010, **285:**26377-26383.
68. Calella AM, Farinelli M, Nuvolone M, Mirante O, Moos R, Falsig J, Mansuy IM, Aguzzi A: **Prion protein and Abeta-related synaptic toxicity impairment.** *Embo Mol Med* 2010, **2:**306-314.
69. Balducci C, Beeg M, Stravalaci M, Bastone A, Sclip A, Biasini E, Tapella L, Colombo L, Manzoni C, Borsello T, et al: **Synthetic amyloid-beta oligomers impair long-term memory independently of cellular prion protein.** *Proc Natl Acad Sci U S A* 2010, **107:**2295-2300.
70. Rushworth JV, Griffiths HH, Watt NT, Hooper NM: **Prion protein-mediated toxicity of amyloid-beta oligomers requires lipid rafts and the transmembrane LRP1.** *J Biol Chem* 2013, **288:**8935-8951.
71. Kessels HW, Nguyen LN, Nabavi S, Malinow R: **The prion protein as a receptor for amyloid-beta.** *Nature* 2010, **466:**E3-4; discussion E4-5.
72. Zhang D, Qi Y, Klyubin I, Ondrejcak T, Sarell CJ, Cuello AC, Collinge J, Rowan MJ: **Targeting glutamatergic and cellular prion protein mechanisms of amyloid beta-mediated persistent synaptic plasticity disruption: Longitudinal studies.** *Neuropharmacology* 2017, **121:**231-246.
73. Scott-McKean JJ, Surewicz K, Choi JK, Ruffin VA, Salameh AI, Nieznanski K, Costa AC, Surewicz WK: **Soluble prion protein and its N-terminal fragment prevent impairment of synaptic plasticity by Abeta oligomers: Implications for novel therapeutic strategy in Alzheimer's disease.** *Neurobiol Dis* 2016, **91:**124-131.
74. Hu NW, Nicoll AJ, Zhang D, Mably AJ, O'Malley T, Purro SA, Terry C, Collinge J, Walsh DM, Rowan MJ: **mGlu5 receptors and cellular prion protein mediate amyloid-beta-facilitated synaptic long-term depression in vivo.** *Nat Commun* 2014, **5:**3374.
75. Nicoll AJ, Panico S, Freir DB, Wright D, Terry C, Risse E, Herron CE, O'Malley T, Wadsworth JD, Farrow MA, et al: **Amyloid-beta nanotubes are associated with prion protein-dependent synaptotoxicity.** *Nat Commun* 2013, **4:**2416.

76. Barry AE, Klyubin I, Mc Donald JM, Mably AJ, Farrell MA, Scott M, Walsh DM, Rowan MJ: **Alzheimer's disease brain-derived amyloid-beta-mediated inhibition of LTP in vivo is prevented by immunotargeting cellular prion protein.** *J Neurosci* 2011, **31:**7259-7263.
77. Haas LT, Salazar SV, Kostylev MA, Um JW, Kaufman AC, Strittmatter SM: **Metabotropic glutamate receptor 5 couples cellular prion protein to intracellular signalling in Alzheimer's disease.** *Brain* 2016, **139:**526-546.
78. Bate C, Williams A: **Amyloid-beta-induced synapse damage is mediated via cross-linkage of cellular prion proteins.** *J Biol Chem* 2011, **286:**37955-37963.
79. Kudo W, Lee HP, Zou WQ, Wang X, Perry G, Zhu X, Smith MA, Petersen RB, Lee HG: **Cellular prion protein is essential for oligomeric amyloid-beta-induced neuronal cell death.** *Hum Mol Genet* 2012, **21:**1138-1144.
80. Ostapchenko VG, Beraldo FH, Mohammad AH, Xie YF, Hirata PH, Magalhaes AC, Lamour G, Li H, Maciejewski A, Belrose JC, et al: **The prion protein ligand, stress-inducible phosphoprotein 1, regulates amyloid-beta oligomer toxicity.** *J Neurosci* 2013, **33:**16552-16564.
81. Chung E, Ji Y, Sun Y, Kascsak RJ, Kascsak RB, Mehta PD, Strittmatter SM, Wisniewski T: **Anti-PrPC monoclonal antibody infusion as a novel treatment for cognitive deficits in an Alzheimer's disease model mouse.** *Bmc Neurosci* 2010, **11:**130.
82. Gimbel DA, Nygaard HB, Coffey EE, Gunther EC, Lauren J, Gimbel ZA, Strittmatter SM: **Memory impairment in transgenic Alzheimer mice requires cellular prion protein.** *J Neurosci* 2010, **30:**6367-6374.
83. Dohler F, Sepulveda-Falla D, Krasemann S, Altmeppen H, Schluter H, Hildebrand D, Zerr I, Matschke J, Glatzel M: **High molecular mass assemblies of amyloid-beta oligomers bind prion protein in patients with Alzheimer's disease.** *Brain* 2014, **137:**873-886.
84. Um JW, Nygaard HB, Heiss JK, Kostylev MA, Stagi M, Vortmeyer A, Wisniewski T, Gunther EC, Strittmatter SM: **Alzheimer amyloid-beta oligomer bound to postsynaptic prion protein activates Fyn to impair neurons.** *Nat Neurosci* 2012, **15:**1227-1235.
85. Creese I, Burt DR, Snyder SH: **Dopamine receptor binding predicts clinical and pharmacological potencies of antischizophrenic drugs.** *Science* 1976, **192:**481-483.
86. Freir DB, Nicoll AJ, Klyubin I, Panico S, Mc Donald JM, Risse E, Asante EA, Farrow MA, Sessions RB, Saibil HR, et al: **Interaction between prion protein and toxic amyloid beta assemblies can be therapeutically targeted at multiple sites.** *Nat Commun* 2011, **2:**336.
87. Resenberger UK, Harmeier A, Woerner AC, Goodman JL, Muller V, Krishnan R, Vabulas RM, Kretzschmar HA, Lindquist S, Hartl FU, et al: **The cellular prion protein mediates neurotoxic signalling of beta-sheet-rich conformers independent of prion replication.** *Embo J* 2011, **30:**2057-2070.
88. Fluharty BR, Biasini E, Stravalaci M, Sclip A, Diomede L, Balducci C, La Vitola P, Messa M, Colombo L, Forloni G, et al: **An N-terminal fragment of the prion protein binds to amyloid-beta oligomers and inhibits their neurotoxicity in vivo.** *J Biol Chem* 2013, **288:**7857-7866.
89. Cisse M, Halabisky B, Harris J, Devidze N, Dubal DB, Sun B, Orr A, Lotz G, Kim DH, Hamto P, et al: **Reversing EphB2 depletion rescues cognitive functions in Alzheimer model.** *Nature* 2011, **469:**47-52.

90. Smith LM, Strittmatter SM: **Binding Sites for Amyloid-beta Oligomers and Synaptic Toxicity.** *Cold Spring Harb Perspect Med* 2017, **7**.
91. Larson M, Sherman MA, Amar F, Nuvolone M, Schneider JA, Bennett DA, Aguzzi A, Lesne SE: **The complex PrP(c)-Fyn couples human oligomeric Abeta with pathological tau changes in Alzheimer's disease.** *J Neurosci* 2012, **32:**16857-16871a.
92. Collins MO, Husi H, Yu L, Brandon JM, Anderson CN, Blackstock WP, Choudhary JS, Grant SG: **Molecular characterization and comparison of the components and multiprotein complexes in the postsynaptic proteome.** *J Neurochem* 2006, **97 Suppl 1:**16-23.
93. Um JW, Kaufman AC, Kostylev M, Heiss JK, Stagi M, Takahashi H, Kerrisk ME, Vortmeyer A, Wisniewski T, Koleske AJ, et al: **Metabotropic glutamate receptor 5 is a coreceptor for Alzheimer abeta oligomer bound to cellular prion protein.** *Neuron* 2013, **79:**887-902.
94. Kaufman AC, Salazar SV, Haas LT, Yang J, Kostylev MA, Jeng AT, Robinson SA, Gunther EC, van Dyck CH, Nygaard HB, Strittmatter SM: **Fyn inhibition rescues established memory and synapse loss in Alzheimer mice.** *Ann Neurol* 2015, **77:**953-971.
95. Haas LT, Strittmatter SM: **Oligomers of Amyloid beta Prevent Physiological Activation of the Cellular Prion Protein-Metabotropic Glutamate Receptor 5 Complex by Glutamate in Alzheimer Disease.** *J Biol Chem* 2016, **291:**17112-17121.
96. Haas LT, Salazar SV, Smith LM, Zhao HR, Cox TO, Herber CS, Degnan AP, Balakrishnan A, Macor JE, Albright CF, Strittmatter SM: **Silent Allosteric Modulation of mGluR5 Maintains Glutamate Signaling while Rescuing Alzheimer's Mouse Phenotypes.** *Cell Reports* 2017, **in press**.
97. Ronesi JA, Huber KM: **Homer interactions are necessary for metabotropic glutamate receptor-induced long-term depression and translational activation.** *J Neurosci* 2008, **28:**543-547.
98. Jin M, Shepardson N, Yang T, Chen G, Walsh D, Selkoe DJ: **Soluble amyloid beta-protein dimers isolated from Alzheimer cortex directly induce Tau hyperphosphorylation and neuritic degeneration.** *Proc Natl Acad Sci U S A* 2011, **108:**5819-5824.
99. Wang Q, Walsh DM, Rowan MJ, Selkoe DJ, Anwyl R: **Block of long-term potentiation by naturally secreted and synthetic amyloid beta-peptide in hippocampal slices is mediated via activation of the kinases c-Jun N-terminal kinase, cyclin-dependent kinase 5, and p38 mitogen-activated protein kinase as well as metabotropic glutamate receptor type 5.** *J Neurosci* 2004, **24:**3370-3378.
100. Renner M, Lacor PN, Velasco PT, Xu J, Contractor A, Klein WL, Triller A: **Deleterious effects of amyloid beta oligomers acting as an extracellular scaffold for mGluR5.** *Neuron* 2010, **66:**739-754.
101. Hamilton A, Esseltine JL, DeVries RA, Cregan SP, Ferguson SS: **Metabotropic glutamate receptor 5 knockout reduces cognitive impairment and pathogenesis in a mouse model of Alzheimer's disease.** *Mol Brain* 2014, **7:**40.
102. Overk CR, Cartier A, Shaked G, Rockenstein E, Ubhi K, Spencer B, Price DL, Patrick C, Desplats P, Masliah E: **Hippocampal neuronal cells that accumulate alpha-synuclein fragments are more vulnerable to Abeta oligomer toxicity via mGluR5--implications for dementia with Lewy bodies.** *Mol Neurodegener* 2014, **9:**18.
103. Raka F, Di Sebastiano AR, Kulhawy SC, Ribeiro FM, Godin CM, Caetano FA, Angers S, Ferguson SS: **Ca(2+)/calmodulin-dependent protein kinase II interacts with**

group I metabotropic glutamate and facilitates receptor endocytosis and ERK1/2 signaling: role of beta-amyloid. *Mol Brain* 2015, **8:**21.
104. Zhang H, Wu L, Pchitskaya E, Zakharova O, Saito T, Saido T, Bezprozvanny I: **Neuronal Store-Operated Calcium Entry and Mushroom Spine Loss in Amyloid Precursor Protein Knock-In Mouse Model of Alzheimer's Disease.** *J Neurosci* 2015, **35:**13275-13286.
105. Beraldo FH, Ostapchenko VG, Caetano FA, Guimaraes AL, Ferretti GD, Daude N, Bertram L, Nogueira KO, Silva JL, Westaway D, et al: **Regulation of Amyloid beta Oligomer Binding to Neurons and Neurotoxicity by the Prion Protein-mGluR5 Complex.** *J Biol Chem* 2016, **291:**21945-21955.
106. Lu YM, Jia ZP, Janus C, Henderson JT, Gerlai R, Wojtowicz JM, Roder JC: **Mice lacking metabotropic glutamate receptor 5 show impaired learning and reduced CA1 long-term potentiation (LTP) but normal CA3 LTP.** *Journal of Neuroscience* 1997, **17:**5196-5205.
107. Campbell UC, Lalwani K, Hernandez L, Kinney GG, Conn PJ, Bristow LJ: **The mGluR5 antagonist 2-methyl-6-(phenylethynyl)-pyridine (MPEP) potentiates PCP-induced cognitive deficits in rats.** *Psychopharmacology (Berl)* 2004, **175:**310-318.
108. Porter RH, Jaeschke G, Spooren W, Ballard TM, Buttelmann B, Kolczewski S, Peters JU, Prinssen E, Wichmann J, Vieira E, et al: **Fenobam: a clinically validated nonbenzodiazepine anxiolytic is a potent, selective, and noncompetitive mGlu5 receptor antagonist with inverse agonist activity.** *J Pharmacol Exp Ther* 2005, **315:**711-721.
109. Xu J, Zhu Y, Contractor A, Heinemann SF: **mGluR5 has a critical role in inhibitory learning.** *J Neurosci* 2009, **29:**3676-3684.
110. Rodriguez AL, Grier MD, Jones CK, Herman EJ, Kane AS, Smith RL, Williams R, Zhou Y, Marlo JE, Days EL, et al: **Discovery of novel allosteric modulators of metabotropic glutamate receptor subtype 5 reveals chemical and functional diversity and in vivo activity in rat behavioral models of anxiolytic and antipsychotic activity.** *Mol Pharmacol* 2010, **78:**1105-1123.
111. Abou Farha K, Bruggeman R, Balje-Volkers C: **Metabotropic glutamate receptor 5 negative modulation in phase I clinical trial: potential impact of circadian rhythm on the neuropsychiatric adverse reactions-do hallucinations matter?** *ISRN Psychiatry* 2014, **2014:**652750.
112. Bochner DN, Sapp RW, Adelson JD, Zhang S, Lee H, Djurisic M, Syken J, Dan Y, Shatz CJ: **Blocking PirB up-regulates spines and functional synapses to unlock visual cortical plasticity and facilitate recovery from amblyopia.** *Sci Transl Med* 2014, **6:**258ra140.
113. Atwal JK, Pinkston-Gosse J, Syken J, Stawicki S, Wu Y, Shatz C, Tessier-Lavigne M: **PirB is a functional receptor for myelin inhibitors of axonal regeneration.** *Science* 2008, **322:**967-970.
114. Syken J, Grandpre T, Kanold PO, Shatz CJ: **PirB restricts ocular-dominance plasticity in visual cortex.** *Science* 2006, **313:**1795-1800.
115. Kim T, Vidal GS, Djurisic M, William CM, Birnbaum ME, Garcia KC, Hyman BT, Shatz CJ: **Human LilrB2 is a beta-amyloid receptor and its murine homolog PirB regulates synaptic plasticity in an Alzheimer's model.** *Science* 2013, **341:**1399-1404.

116. Wang H-Y, Lee DHS, D'Andrea MR, Peterson PA, Shank RP, Reitz AB: **β-Amyloid1–42Binds to α7 Nicotinic Acetylcholine Receptor with High Affinity.** *J Biol Chem* 2000, **275:**5626-5632.
117. Hogg RC, Raggenbass M, Bertrand D: **Nicotinic acetylcholine receptors: from structure to brain function.** *Rev Physiol Biochem Pharmacol* 2003, **147:**1-46.
118. Dineley KT, Westerman M, Bui D, Bell K, Ashe KH, Sweatt JD: **beta-amyloid activates the mitogen-activated protein kinase cascade via hippocampal alpha 7 nicotinic acetylcholine receptors: In vitro and in vivo mechanisms related to Alzheimer's disease.** *Journal of Neuroscience* 2001, **21:**4125-4133.
119. Snyder EM, Nong Y, Almeida CG, Paul S, Moran T, Choi EY, Nairn AC, Salter MW, Lombroso PJ, Gouras GK, Greengard P: **Regulation of NMDA receptor trafficking by amyloid-beta.** *Nat Neurosci* 2005, **8:**1051-1058.
120. Mulkey RM, Endo S, Shenolikar S, Malenka RC: **Involvement of a calcineurin/inhibitor-1 phosphatase cascade in hippocampal long-term depression.** *Nature* 1994, **369:**486-488.
121. Koffie RM, Hyman BT, Spires-Jones TL: **Alzheimer's disease: synapses gone cold.** *Mol Neurodegener* 2011, **6:**63.
122. Zhang Y, Venkitaramani DV, Gladding CM, Zhang Y, Kurup P, Molnar E, Collingridge GL, Lombroso PJ: **The tyrosine phosphatase STEP mediates AMPA receptor endocytosis after metabotropic glutamate receptor stimulation.** *J Neurosci* 2008, **28:**10561-10566.
123. Lee G, Thangavel R, Sharma VM, Litersky JM, Bhaskar K, Fang SM, Do LH, Andreadis A, Van Hoesen G, Ksiezak-Reding H: **Phosphorylation of tau by fyn: implications for Alzheimer's disease.** *J Neurosci* 2004, **24:**2304-2312.
124. Bhaskar K, Hobbs GA, Yen SH, Lee G: **Tyrosine phosphorylation of tau accompanies disease progression in transgenic mouse models of tauopathy.** *Neuropathol Appl Neurobiol* 2010, **36:**462-477.
125. Vergara C, Ordonez-Gutierrez L, Wandosell F, Ferrer I, del Rio JA, Gavin R: **Role of PrP(C) Expression in Tau Protein Levels and Phosphorylation in Alzheimer's Disease Evolution.** *Mol Neurobiol* 2015, **51:**1206-1220.
126. Zempel H, Thies E, Mandelkow E, Mandelkow EM: **Abeta oligomers cause localized Ca(2+) elevation, missorting of endogenous Tau into dendrites, Tau phosphorylation, and destruction of microtubules and spines.** *J Neurosci* 2010, **30:**11938-11950.
127. Roberson ED, Scearce-Levie K, Palop JJ, Yan F, Cheng IH, Wu T, Gerstein H, Yu GQ, Mucke L: **Reducing endogenous tau ameliorates amyloid beta-induced deficits in an Alzheimer's disease mouse model.** *Science* 2007, **316:**750-754.
128. Ittner LM, Ke YD, Delerue F, Bi M, Gladbach A, van Eersel J, Wolfing H, Chieng BC, Christie MJ, Napier IA, et al: **Dendritic function of tau mediates amyloid-beta toxicity in Alzheimer's disease mouse models.** *Cell* 2010, **142:**387-397.
129. Mondragon-Rodriguez S, Trillaud-Doppia E, Dudilot A, Bourgeois C, Lauzon M, Leclerc N, Boehm J: **Interaction of endogenous tau protein with synaptic proteins is regulated by N-methyl-D-aspartate receptor-dependent tau phosphorylation.** *J Biol Chem* 2012, **287:**32040-32053.
130. Roche KW, Standley S, McCallum J, Dune Ly C, Ehlers MD, Wenthold RJ: **Molecular determinants of NMDA receptor internalization.** *Nat Neurosci* 2001, **4:**794-802.
131. Nygaard HB, Wagner AF, Bowen GS, Good SP, MacAvoy MG, Strittmatter KA, Kaufman AC, Rosenberg BJ, Sekine-Konno T, Varma P, et al: **A phase Ib multiple ascending dose study of the safety, tolerability, and central nervous system**

availability of AZD0530 (saracatinib) in Alzheimer's disease. *Alzheimers Res Ther* 2015, **7:**35.
132. Lambert JC, Ibrahim-Verbaas CA, Harold D, Naj AC, Sims R, Bellenguez C, DeStafano AL, Bis JC, Beecham GW, Grenier-Boley B, et al: **Meta-analysis of 74,046 individuals identifies 11 new susceptibility loci for Alzheimer's disease.** *Nat Genet* 2013, **45:**1452-1458.
133. Beecham GW, Hamilton K, Naj AC, Martin ER, Huentelman M, Myers AJ, Corneveaux JJ, Hardy J, Vonsattel JP, Younkin SG, et al: **Genome-wide association meta-analysis of neuropathologic features of Alzheimer's disease and related dementias.** *PLoS genetics* 2014, **10:**e1004606.
134. van Dyck CH, Nygaard HB, Chen K, Donohue MC, Raman R, Rissman RA, Brewer JB, Koeppe RA, Chow TW, Rafii MS, et al: **Effect of AZD0530 on Cerebral Metabolic Decline in Alzheimer Disease: A Randomized Clinical Trial.** *JAMA Neurol* 2019, **76:**1219-1229.
135. Rhinn H, Fujita R, Qiang L, Cheng R, Lee JH, Abeliovich A: **Integrative genomics identifies APOE epsilon4 effectors in Alzheimer's disease.** *Nature* 2013, **500:**45-50.
136. Huang Y-Q, Lu W-Y, Ali DW, Pelkey KA, Pitcher GM, Lu YM, Aoto H, Roder JC, Sasaki T, Salter MW, MacDonald JF: **CAKβ/Pyk2 Kinase Is a Signaling Link for Induction of Long-Term Potentiation in CA1 Hippocampus.** *Neuron* 2001, **29:**485-496.
137. Heidinger V, Manzerra P, Wang XQ, Strasser U, Yu SP, Choi DW, Behrens MM: **Metabotropic glutamate receptor 1-induced upregulation of NMDA receptor current: Mediation through the Pyk2/Src-family kinase pathway in cortical neurons.** *Journal of Neuroscience* 2002, **22:**5452-5461.
138. Seabold GK, Burette A, Lim IA, Weinberg RJ, Hell JW: **Interaction of the tyrosine kinase Pyk2 with the N-methyl-D-aspartate receptor complex via the Src homology 3 domains of PSD-95 and SAP102.** *J Biol Chem* 2003, **278:**15040-15048.
139. Park SY, Avraham HK, Avraham S: **RAFTK/Pyk2 activation is mediated by trans-acting autophosphorylation in a Src-independent manner.** *J Biol Chem* 2004, **279:**33315-33322.
140. Bartos JA, Ulrich JD, Li H, Beazely MA, Chen Y, Macdonald JF, Hell JW: **Postsynaptic clustering and activation of Pyk2 by PSD-95.** *J Neurosci* 2010, **30:**449-463.
141. Giralt A, Brito V, Chevy Q, Simonnet C, Otsu Y, Cifuentes-Diaz C, de Pins B, Coura R, Alberch J, Gines S, et al: **Pyk2 modulates hippocampal excitatory synapses and contributes to cognitive deficits in a Huntington's disease model.** *Nat Commun* 2017, **8:**15592.
142. Hsin H, Kim MJ, Wang CF, Sheng M: **Proline-rich tyrosine kinase 2 regulates hippocampal long-term depression.** *J Neurosci* 2010, **30:**11983-11993.
143. Collins M, Bartelt RR, Houtman JC: **T cell receptor activation leads to two distinct phases of Pyk2 activation and actin cytoskeletal rearrangement in human T cells.** *Mol Immunol* 2010, **47:**1665-1674.
144. Collins M, Tremblay M, Chapman N, Curtiss M, Rothman PB, Houtman JC: **The T cell receptor-mediated phosphorylation of Pyk2 tyrosines 402 and 580 occurs via a distinct mechanism than other receptor systems.** *J Leukoc Biol* 2010, **87:**691-701.
145. Hartigan JA, Xiong WC, Johnson GV: **Glycogen synthase kinase 3beta is tyrosine phosphorylated by PYK2.** *Biochem Biophys Res Commun* 2001, **284:**485-489.

146. Sayas CL, Ariaens A, Ponsioen B, Moolenaar WH: **GSK-3 is activated by the tyrosine kinase Pyk2 during LPA1-mediated neurite retraction.** *Mol Biol Cell* 2006, **17:**1834-1844.
147. Hooper C, Killick R, Lovestone S: **The GSK3 hypothesis of Alzheimer's disease.** *J Neurochem* 2008, **104:**1433-1439.
148. Nguyen TH, Liu J, Lombroso PJ: **Striatal enriched phosphatase 61 dephosphorylates Fyn at phosphotyrosine 420.** *J Biol Chem* 2002, **277:**24274-24279.
149. Ferreira IL, Bajouco LM, Mota SI, Auberson YP, Oliveira CR, Rego AC: **Amyloid beta peptide 1-42 disturbs intracellular calcium homeostasis through activation of GluN2B-containing N-methyl-d-aspartate receptors in cortical cultures.** *Cell Calcium* 2012, **51:**95-106.
150. Reisberg B, Doody R, Mobius HJ: **Memantine in moderate-to-severe Alzheimer's disease - Reply.** *New Engl J Med* 2003, **349:**610-610.
151. Mota SI, Ferreira IL, Rego AC: **Dysfunctional synapse in Alzheimer's disease - A focus on NMDA receptors.** *Neuropharmacology* 2014, **76 Pt A:**16-26.
152. Yan SD, Chen X, Fu J, Chen M, Zhu H, Roher A, Slattery T, Zhao L, Nagashima M, Morser J, et al: **RAGE and amyloid-beta peptide neurotoxicity in Alzheimer's disease.** *Nature* 1996, **382:**685-691.
153. Yaar M, Zhai S, Pilch PF, Doyle SM, Eisenhauer PB, Fine RE, Gilchrest BA: **Binding of beta-amyloid to the p75 neurotrophin receptor induces apoptosis. A possible mechanism for Alzheimer's disease.** *J Clin Invest* 1997, **100:**2333-2340.
154. Kuner P, Schubenel R, Hertel C: **?-amyloid binds to p75NTRand activates NF?B in human neuroblastoma cells.** *J Neurosci Res* 1998, **54:**798-804.
155. Park JH, Gimbel DA, GrandPre T, Lee JK, Kim JE, Li W, Lee DH, Strittmatter SM: **Alzheimer precursor protein interaction with the Nogo-66 receptor reduces amyloid-beta plaque deposition.** *J Neurosci* 2006, **26:**1386-1395.
156. Fu AK, Hung KW, Huang H, Gu S, Shen Y, Cheng EY, Ip FC, Huang X, Fu WY, Ip NY: **Blockade of EphA4 signaling ameliorates hippocampal synaptic dysfunctions in mouse models of Alzheimer's disease.** *Proc Natl Acad Sci U S A* 2014, **111:**9959-9964.
157. Kam TI, Song S, Gwon Y, Park H, Yan JJ, Im I, Choi JW, Choi TY, Kim J, Song DK, et al: **FcgammaRIIb mediates amyloid-beta neurotoxicity and memory impairment in Alzheimer's disease.** *J Clin Invest* 2013, **123:**2791-2802.
158. Carlo AS, Gustafsen C, Mastrobuoni G, Nielsen MS, Burgert T, Hartl D, Rohe M, Nykjaer A, Herz J, Heeren J, et al: **The pro-neurotrophin receptor sortilin is a major neuronal apolipoprotein E receptor for catabolism of amyloid-beta peptide in the brain.** *J Neurosci* 2013, **33:**358-370.
159. Xie L, Helmerhorst E, Taddei K, Plewright B, Van Bronswijk W, Martins R: **Alzheimer's beta-amyloid peptides compete for insulin binding to the insulin receptor.** *J Neurosci* 2002, **22:**RC221.
160. Wang L, Chiang HC, Wu W, Liang B, Xie Z, Yao X, Ma W, Du S, Zhong Y: **Epidermal growth factor receptor is a preferred target for treating amyloid-beta-induced memory loss.** *Proc Natl Acad Sci U S A* 2012, **109:**16743-16748.
161. Izzo NJ, Staniszewski A, To L, Fa M, Teich AF, Saeed F, Wostein H, Walko T, 3rd, Vaswani A, Wardius M, et al: **Alzheimer's therapeutics targeting amyloid beta 1-42 oligomers I: Abeta 42 oligomer binding to specific neuronal receptors is displaced by drug candidates that improve cognitive deficits.** *Plos One* 2014, **9:**e111898.

162. Izzo NJ, Xu J, Zeng C, Kirk MJ, Mozzoni K, Silky C, Rehak C, Yurko R, Look G, Rishton G, et al: **Alzheimer's therapeutics targeting amyloid beta 1-42 oligomers II: Sigma-2/PGRMC1 receptors mediate Abeta 42 oligomer binding and synaptotoxicity.** *Plos One* 2014, **9:**e111899.
163. Takahashi K, Yamanaka S: **Induction of pluripotent stem cells from mouse embryonic and adult fibroblast cultures by defined factors.** *Cell* 2006, **126:**663-676.
164. Rowe RG, Daley GQ: **Induced pluripotent stem cells in disease modelling and drug discovery.** *Nat Rev Genet* 2019, **20:**377-388.
165. Arber C, Alatza A, Leckey CA, Paterson RW, Zetterberg H, Wray S: **Mass spectrometry analysis of tau and amyloid-beta in iPSC-derived models of Alzheimer's disease and dementia.** *J Neurochem* 2021, **159:**305-317.
166. Nehme R, Zuccaro E, Ghosh SD, Li C, Sherwood JL, Pietilainen O, Barrett LE, Limone F, Worringer KA, Kommineni S, et al: **Combining NGN2 Programming with Developmental Patterning Generates Human Excitatory Neurons with NMDAR-Mediated Synaptic Transmission.** *Cell Rep* 2018, **23:**2509-2523.
167. Treutlein B, Lee QY, Camp JG, Mall M, Koh W, Shariati SA, Sim S, Neff NF, Skotheim JM, Wernig M, Quake SR: **Dissecting direct reprogramming from fibroblast to neuron using single-cell RNA-seq.** *Nature* 2016, **534:**391-395.
168. Chambers SM, Fasano CA, Papapetrou EP, Tomishima M, Sadelain M, Studer L: **Highly efficient neural conversion of human ES and iPS cells by dual inhibition of SMAD signaling.** *Nat Biotechnol* 2009, **27:**275-280.
169. Maroof AM, Keros S, Tyson JA, Ying SW, Ganat YM, Merkle FT, Liu B, Goulburn A, Stanley EG, Elefanty AG, et al: **Directed differentiation and functional maturation of cortical interneurons from human embryonic stem cells.** *Cell Stem Cell* 2013, **12:**559-572.
170. Shi Y, Kirwan P, Smith J, Robinson HP, Livesey FJ: **Human cerebral cortex development from pluripotent stem cells to functional excitatory synapses.** *Nat Neurosci* 2012, **15:**477-486, S471.
171. Shi Y, Kirwan P, Livesey FJ: **Directed differentiation of human pluripotent stem cells to cerebral cortex neurons and neural networks.** *Nat Protoc* 2012, **7:**1836-1846.
172. Duan D, Fu Y, Paxinos G, Watson C: **Spatiotemporal expression patterns of Pax6 in the brain of embryonic, newborn, and adult mice.** *Brain Struct Funct* 2013, **218:**353-372.
173. Chuang HC, Huang TN, Hsueh YP: **Neuronal excitation upregulates Tbr1, a high-confidence risk gene of autism, mediating Grin2b expression in the adult brain.** *Front Cell Neurosci* 2014, **8:**280.
174. Huang Y, Song NN, Lan W, Hu L, Su CJ, Ding YQ, Zhang L: **Expression of transcription factor Satb2 in adult mouse brain.** *Anat Rec (Hoboken)* 2013, **296:**452-461.
175. Noctor SC, Flint AC, Weissman TA, Wong WS, Clinton BK, Kriegstein AR: **Dividing precursor cells of the embryonic cortical ventricular zone have morphological and molecular characteristics of radial glia.** *J Neurosci* 2002, **22:**3161-3173.
176. Chavali VRM, Haider N, Rathi S, Vrathasha V, Alapati T, He J, Gill K, Nikonov R, Duong TT, McDougald DS, et al: **Dual SMAD inhibition and Wnt inhibition enable efficient and reproducible differentiations of induced pluripotent stem cells into retinal ganglion cells.** *Sci Rep* 2020, **10:**11828.

177. Chung WS, Allen NJ, Eroglu C: **Astrocytes Control Synapse Formation, Function, and Elimination.** *Cold Spring Harb Perspect Biol* 2015, **7:**a020370.
178. De Felice FG, Wu D, Lambert MP, Fernandez SJ, Velasco PT, Lacor PN, Bigio EH, Jerecic J, Acton PJ, Shughrue PJ, et al: **Alzheimer's disease-type neuronal tau hyperphosphorylation induced by A beta oligomers.** *Neurobiol Aging* 2008, **29:**1334-1347.
179. Tomiyama T, Matsuyama S, Iso H, Umeda T, Takuma H, Ohnishi K, Ishibashi K, Teraoka R, Sakama N, Yamashita T, et al: **A mouse model of amyloid beta oligomers: their contribution to synaptic alteration, abnormal tau phosphorylation, glial activation, and neuronal loss in vivo.** *J Neurosci* 2010, **30:**4845-4856.
180. **2021 Alzheimer's disease facts and figures.** *Alzheimers Dement* 2021, **17:**327-406.
181. Kamboh MI, Demirci FY, Wang X, Minster RL, Carrasquillo MM, Pankratz VS, Younkin SG, Saykin AJ, Alzheimer's Disease Neuroimaging I, Jun G, et al: **Genome-wide association study of Alzheimer's disease.** *Transl Psychiatry* 2012, **2:**e117.
182. Li YQ, Tan MS, Wang HF, Tan CC, Zhang W, Zheng ZJ, Kong LL, Wang ZX, Tan L, Jiang T, et al: **Common variant in PTK2B is associated with late-onset Alzheimer's disease: A replication study and meta-analyses.** *Neurosci Lett* 2016, **621:**83-87.
183. Kunkle BW, Grenier-Boley B, Sims R, Bis JC, Damotte V, Naj AC, Boland A, Vronskaya M, van der Lee SJ, Amlie-Wolf A, et al: **Genetic meta-analysis of diagnosed Alzheimer's disease identifies new risk loci and implicates Abeta, tau, immunity and lipid processing.** *Nat Genet* 2019, **51:**414-430.
184. Jansen IE, Savage JE, Watanabe K, Bryois J, Williams DM, Steinberg S, Sealock J, Karlsson IK, Hagg S, Athanasiu L, et al: **Genome-wide meta-analysis identifies new loci and functional pathways influencing Alzheimer's disease risk.** *Nat Genet* 2019, **51:**404-413.
185. Chan G, White CC, Winn PA, Cimpean M, Replogle JM, Glick LR, Cuerdon NE, Ryan KJ, Johnson KA, Schneider JA, et al: **CD33 modulates TREM2: convergence of Alzheimer loci.** *Nat Neurosci* 2015, **18:**1556-1558.
186. Salazar SV, Cox TO, Lee S, Brody AH, Chyung AS, Haas LT, Strittmatter SM: **Alzheimer's Disease Risk Factor Pyk2 Mediates Amyloid-beta-Induced Synaptic Dysfunction and Loss.** *J Neurosci* 2019, **39:**758-772.
187. Lee S, Salazar SV, Cox TO, Strittmatter SM: **Pyk2 Signaling through Graf1 and RhoA GTPase Is Required for Amyloid-beta Oligomer-Triggered Synapse Loss.** *J Neurosci* 2019, **39:**1910-1929.
188. Tokiwa G, Dikic I, Lev S, Schlessinger J: **Activation of Pyk2 by stress signals and coupling with JNK signaling pathway.** *Science* 1996, **273:**792-794.
189. Murasawa S, Matsubara H, Mori Y, Masaki H, Tsutsumi Y, Shibasaki Y, Kitabayashi I, Tanaka Y, Fujiyama S, Koyama Y, et al: **Angiotensin II initiates tyrosine kinase Pyk2-dependent signalings leading to activation of Rac1-mediated c-Jun NH2-terminal kinase.** *J Biol Chem* 2000, **275:**26856-26863.
190. Frank GD, Eguchi S, Motley ED, Sasaki T, Inagami T: **Unique regulation of c-Jun N-terminal kinase by PYK2/CAK-beta in angiotensin II-stimulated vascular smooth muscle cells.** *Biochem Biophys Res Commun* 2001, **286:**692-696.
191. Kodama H, Fukuda K, Takahashi E, Tahara S, Tomita Y, Ieda M, Kimura K, Owada KM, Vuori K, Ogawa S: **Selective involvement of p130Cas/Crk/Pyk2/c-Src in endothelin-1-induced JNK activation.** *Hypertension* 2003, **41:**1372-1379.

192. Xiong W, Parsons JT: **Induction of apoptosis after expression of PYK2, a tyrosine kinase structurally related to focal adhesion kinase.** *J Cell Biol* 1997, **139:**529-539.
193. Dhanasekaran DN, Reddy EP: **JNK-signaling: A multiplexing hub in programmed cell death.** *Genes Cancer* 2017, **8:**682-694.
194. Lovestone S, Reynolds CH, Latimer D, Davis DR, Anderton BH, Gallo JM, Hanger D, Mulot S, Marquardt B, Stabel S, et al.: **Alzheimer's disease-like phosphorylation of the microtubule-associated protein tau by glycogen synthase kinase-3 in transfected mammalian cells.** *Curr Biol* 1994, **4:**1077-1086.
195. Hong M, Chen DC, Klein PS, Lee VM: **Lithium reduces tau phosphorylation by inhibition of glycogen synthase kinase-3.** *J Biol Chem* 1997, **272:**25326-25332.
196. Munoz-Montano JR, Moreno FJ, Avila J, Diaz-Nido J: **Lithium inhibits Alzheimer's disease-like tau protein phosphorylation in neurons.** *FEBS Lett* 1997, **411:**183-188.
197. Noble W, Planel E, Zehr C, Olm V, Meyerson J, Suleman F, Gaynor K, Wang L, LaFrancois J, Feinstein B, et al: **Inhibition of glycogen synthase kinase-3 by lithium correlates with reduced tauopathy and degeneration in vivo.** *Proc Natl Acad Sci U S A* 2005, **102:**6990-6995.
198. Caccamo A, Oddo S, Tran LX, LaFerla FM: **Lithium reduces tau phosphorylation but not A beta or working memory deficits in a transgenic model with both plaques and tangles.** *Am J Pathol* 2007, **170:**1669-1675.
199. Lucas JJ, Hernandez F, Gomez-Ramos P, Moran MA, Hen R, Avila J: **Decreased nuclear beta-catenin, tau hyperphosphorylation and neurodegeneration in GSK-3beta conditional transgenic mice.** *EMBO J* 2001, **20:**27-39.
200. Narendra Talabattula VA, Morgan P, Frech MJ, Uhrmacher AM, Herchenroder O, Putzer BM, Rolfs A, Luo J: **Non-canonical pathway induced by Wnt3a regulates beta-catenin via Pyk2 in differentiating human neural progenitor cells.** *Biochem Biophys Res Commun* 2017, **491:**40-46.
201. Dourlen P, Fernandez-Gomez FJ, Dupont C, Grenier-Boley B, Bellenguez C, Obriot H, Caillierez R, Sottejeau Y, Chapuis J, Bretteville A, et al: **Functional screening of Alzheimer risk loci identifies PTK2B as an in vivo modulator and early marker of Tau pathology.** *Mol Psychiatry* 2017, **22:**874-883.
202. Li C, Gotz J: **Pyk2 is a Novel Tau Tyrosine Kinase that is Regulated by the Tyrosine Kinase Fyn.** *J Alzheimers Dis* 2018, **64:**205-221.
203. Xu HG, Zhai YX, Chen J, Lu Y, Wang JW, Quan CS, Zhao RX, Xiao X, He Q, Werle KD, et al: **LKB1 reduces ROS-mediated cell damage via activation of p38.** *Oncogene* 2015, **34:**3848-3859.
204. Huang SW, Chyuan IT, Shiue C, Yu MC, Hsu YF, Hsu MJ: **Lovastatin-mediated MCF-7 cancer cell death involves LKB1-AMPK-p38MAPK-p53-survivin signalling cascade.** *J Cell Mol Med* 2020, **24:**1822-1836.
205. Reynolds CH, Nebreda AR, Gibb GM, Utton MA, Anderton BH: **Reactivating kinase/p38 phosphorylates tau protein in vitro.** *J Neurochem* 1997, **69:**191-198.
206. Reynolds CH, Betts JC, Blackstock WP, Nebreda AR, Anderton BH: **Phosphorylation sites on tau identified by nanoelectrospray mass spectrometry: differences in vitro between the mitogen-activated protein kinases ERK2, c-Jun N-terminal kinase and P38, and glycogen synthase kinase-3beta.** *J Neurochem* 2000, **74:**1587-1595.
207. Feijoo C, Campbell DG, Jakes R, Goedert M, Cuenda A: **Evidence that phosphorylation of the microtubule-associated protein Tau by SAPK4/p38delta at Thr50 promotes microtubule assembly.** *J Cell Sci* 2005, **118:**397-408.

208. Lauretti E, Pratico D: **Glucose deprivation increases tau phosphorylation via P38 mitogen-activated protein kinase.** *Aging Cell* 2015, **14:**1067-1074.
209. Maphis N, Jiang S, Xu G, Kokiko-Cochran ON, Roy SM, Van Eldik LJ, Watterson DM, Lamb BT, Bhaskar K: **Selective suppression of the alpha isoform of p38 MAPK rescues late-stage tau pathology.** *Alzheimers Res Ther* 2016, **8:**54.
210. Okigaki M, Davis C, Falasca M, Harroch S, Felsenfeld DP, Sheetz MP, Schlessinger J: **Pyk2 regulates multiple signaling events crucial for macrophage morphology and migration.** *Proc Natl Acad Sci U S A* 2003, **100:**10740-10745.
211. Sousa AMM, Zhu Y, Raghanti MA, Kitchen RR, Onorati M, Tebbenkamp ATN, Stutz B, Meyer KA, Li M, Kawasawa YI, et al: **Molecular and cellular reorganization of neural circuits in the human lineage.** *Science* 2017, **358:**1027-1032.
212. Krishnan N, Lam TT, Fritz A, Rempinski D, O'Loughlin K, Minderman H, Berezney R, Marzluff WF, Thapar R: **The prolyl isomerase Pin1 targets stem-loop binding protein (SLBP) to dissociate the SLBP-histone mRNA complex linking histone mRNA decay with SLBP ubiquitination.** *Mol Cell Biol* 2012, **32:**4306-4322.
213. Kandyliari A, Mallouchos A, Papandroulakis N, Golla JP, Lam TT, Sakellari A, Karavoltsos S, Vasiliou V, Kapsokefalou M: **Nutrient Composition and Fatty Acid and Protein Profiles of Selected Fish By-Products.** *Foods* 2020, **9**.
214. Bindea G, Mlecnik B, Hackl H, Charoentong P, Tosolini M, Kirilovsky A, Fridman WH, Pages F, Trajanoski Z, Galon J: **ClueGO: a Cytoscape plug-in to decipher functionally grouped gene ontology and pathway annotation networks.** *Bioinformatics* 2009, **25:**1091-1093.
215. Szklarczyk D, Gable AL, Nastou KC, Lyon D, Kirsch R, Pyysalo S, Doncheva NT, Legeay M, Fang T, Bork P, et al: **The STRING database in 2021: customizable protein-protein networks, and functional characterization of user-uploaded gene/measurement sets.** *Nucleic Acids Res* 2021, **49:**D605-D612.
216. Qian D, Lev S, van Oers NS, Dikic I, Schlessinger J, Weiss A: **Tyrosine phosphorylation of Pyk2 is selectively regulated by Fyn during TCR signaling.** *J Exp Med* 1997, **185:**1253-1259.
217. Canobbio I, Cipolla L, Guidetti GF, Manganaro D, Visconte C, Kim S, Okigaki M, Falasca M, Kunapuli SP, Torti M: **The focal adhesion kinase Pyk2 links Ca2+ signalling to Src family kinase activation and protein tyrosine phosphorylation in thrombin-stimulated platelets.** *Biochem J* 2015, **469:**199-210.
218. Yoshiyama Y, Higuchi M, Zhang B, Huang SM, Iwata N, Saido TC, Maeda J, Suhara T, Trojanowski JQ, Lee VM: **Synapse loss and microglial activation precede tangles in a P301S tauopathy mouse model.** *Neuron* 2007, **53:**337-351.
219. Takeuchi H, Iba M, Inoue H, Higuchi M, Takao K, Tsukita K, Karatsu Y, Iwamoto Y, Miyakawa T, Suhara T, et al: **P301S mutant human tau transgenic mice manifest early symptoms of human tauopathies with dementia and altered sensorimotor gating.** *PLoS One* 2011, **6:**e21050.
220. Sun Y, Guo Y, Feng X, Jia M, Ai N, Dong Y, Zheng Y, Fu L, Yu B, Zhang H, et al: **The behavioural and neuropathologic sexual dimorphism and absence of MIP-3alpha in tau P301S mouse model of Alzheimer's disease.** *J Neuroinflammation* 2020, **17:**72.
221. Meier S, Bell M, Lyons DN, Rodriguez-Rivera J, Ingram A, Fontaine SN, Mechas E, Chen J, Wolozin B, LeVine H, 3rd, et al: **Pathological Tau Promotes Neuronal Damage by Impairing Ribosomal Function and Decreasing Protein Synthesis.** *J Neurosci* 2016, **36:**1001-1007.

222. Koren SA, Hamm MJ, Meier SE, Weiss BE, Nation GK, Chishti EA, Arango JP, Chen J, Zhu H, Blalock EM, Abisambra JF: **Tau drives translational selectivity by interacting with ribosomal proteins.** *Acta Neuropathol* 2019, **137:**571-583.
223. Mangleburg CG, Wu T, Yalamanchili HK, Guo C, Hsieh YC, Duong DM, Dammer EB, De Jager PL, Seyfried NT, Liu Z, Shulman JM: **Integrated analysis of the aging brain transcriptome and proteome in tauopathy.** *Mol Neurodegener* 2020, **15:**56.
224. Evans HT, Taylor D, Kneynsberg A, Bodea LG, Gotz J: **Altered ribosomal function and protein synthesis caused by tau.** *Acta Neuropathol Commun* 2021, **9:**110.
225. Drewes G, Lichtenberg-Kraag B, Doring F, Mandelkow EM, Biernat J, Goris J, Doree M, Mandelkow E: **Mitogen activated protein (MAP) kinase transforms tau protein into an Alzheimer-like state.** *Embo J* 1992, **11:**2131-2138.
226. Nagaraj S, Want A, Laskowska-Kaszub K, Fesiuk A, Vaz S, Logarinho E, Wojda U: **Candidate Alzheimer's Disease Biomarker miR-483-5p Lowers TAU Phosphorylation by Direct ERK1/2 Repression.** *Int J Mol Sci* 2021, **22**.
227. Schneider A, Biernat J, von Bergen M, Mandelkow E, Mandelkow EM: **Phosphorylation that detaches tau protein from microtubules (Ser262, Ser214) also protects it against aggregation into Alzheimer paired helical filaments.** *Biochemistry* 1999, **38:**3549-3558.
228. Robbins DJ, Zhen E, Owaki H, Vanderbilt CA, Ebert D, Geppert TD, Cobb MH: **Regulation and properties of extracellular signal-regulated protein kinases 1 and 2 in vitro.** *J Biol Chem* 1993, **268:**5097-5106.
229. Robinson MJ, Cheng M, Khokhlatchev A, Ebert D, Ahn N, Guan KL, Stein B, Goldsmith E, Cobb MH: **Contributions of the mitogen-activated protein (MAP) kinase backbone and phosphorylation loop to MEK specificity.** *J Biol Chem* 1996, **271:**29734-29739.
230. Stevens B, Allen NJ, Vazquez LE, Howell GR, Christopherson KS, Nouri N, Micheva KD, Mehalow AK, Huberman AD, Stafford B, et al: **The classical complement cascade mediates CNS synapse elimination.** *Cell* 2007, **131:**1164-1178.
231. Stephan AH, Madison DV, Mateos JM, Fraser DA, Lovelett EA, Coutellier L, Kim L, Tsai HH, Huang EJ, Rowitch DH, et al: **A dramatic increase of C1q protein in the CNS during normal aging.** *J Neurosci* 2013, **33:**13460-13474.
232. Dejanovic B, Huntley MA, De Maziere A, Meilandt WJ, Wu T, Srinivasan K, Jiang Z, Gandham V, Friedman BA, Ngu H, et al: **Changes in the Synaptic Proteome in Tauopathy and Rescue of Tau-Induced Synapse Loss by C1q Antibodies.** *Neuron* 2018, **100:**1322-1336 e1327.
233. Hong S, Beja-Glasser VF, Nfonoyim BM, Frouin A, Li S, Ramakrishnan S, Merry KM, Shi Q, Rosenthal A, Barres BA, et al: **Complement and microglia mediate early synapse loss in Alzheimer mouse models.** *Science* 2016, **352:**712-716.
234. Wang JW, Imai Y, Lu B: **Activation of PAR-1 kinase and stimulation of tau phosphorylation by diverse signals require the tumor suppressor protein LKB1.** *J Neurosci* 2007, **27:**574-581.
235. Park SY, Lee HR, Lee WS, Shin HK, Kim HY, Hong KW, Kim CD: **Cilostazol Modulates Autophagic Degradation of beta-Amyloid Peptide via SIRT1-Coupled LKB1/AMPKalpha Signaling in Neuronal Cells.** *PLoS One* 2016, **11:**e0160620.
236. Wani A, Al Rihani SB, Sharma A, Weadick B, Govindarajan R, Khan SU, Sharma PR, Dogra A, Nandi U, Reddy CN, et al: **Crocetin promotes clearance of amyloid-beta by inducing autophagy via the STK11/LKB1-mediated AMPK pathway.** *Autophagy* 2021**:**1-20.

237. Xie Z, Dong Y, Zhang M, Cui MZ, Cohen RA, Riek U, Neumann D, Schlattner U, Zou MH: **Activation of protein kinase C zeta by peroxynitrite regulates LKB1-dependent AMP-activated protein kinase in cultured endothelial cells.** *J Biol Chem* 2006, **281:**6366-6375.
238. Xie Z, Dong Y, Scholz R, Neumann D, Zou MH: **Phosphorylation of LKB1 at serine 428 by protein kinase C-zeta is required for metformin-enhanced activation of the AMP-activated protein kinase in endothelial cells.** *Circulation* 2008, **117:**952-962.
239. Xie Z, Dong Y, Zhang J, Scholz R, Neumann D, Zou MH: **Identification of the serine 307 of LKB1 as a novel phosphorylation site essential for its nucleocytoplasmic transport and endothelial cell angiogenesis.** *Mol Cell Biol* 2009, **29:**3582-3596.
240. Doza YN, Cuenda A, Thomas GM, Cohen P, Nebreda AR: **Activation of the MAP kinase homologue RK requires the phosphorylation of Thr-180 and Tyr-182 and both residues are phosphorylated in chemically stressed KB cells.** *FEBS Lett* 1995, **364:**223-228.
241. Askari N, Beenstock J, Livnah O, Engelberg D: **p38alpha is active in vitro and in vivo when monophosphorylated at threonine 180.** *Biochemistry* 2009, **48:**2497-2504.
242. Lajevic MD, Suleiman S, Cohen RL, Chambers DA: **Activation of p38 mitogen-activated protein kinase by norepinephrine in T-lineage cells.** *Immunology* 2011, **132:**197-208.
243. Beenstock J, Melamed D, Mooshayef N, Mordechay D, Garfinkel BP, Ahn NG, Admon A, Engelberg D: **p38beta Mitogen-Activated Protein Kinase Modulates Its Own Basal Activity by Autophosphorylation of the Activating Residue Thr180 and the Inhibitory Residues Thr241 and Ser261.** *Mol Cell Biol* 2016, **36:**1540-1554.
244. Stancu IC, Ris L, Vasconcelos B, Marinangeli C, Goeminne L, Laporte V, Haylani LE, Couturier J, Schakman O, Gailly P, et al: **Tauopathy contributes to synaptic and cognitive deficits in a murine model for Alzheimer's disease.** *FASEB J* 2014, **28:**2620-2631.
245. Zhang B, Carroll J, Trojanowski JQ, Yao Y, Iba M, Potuzak JS, Hogan AM, Xie SX, Ballatore C, Smith AB, 3rd, et al: **The microtubule-stabilizing agent, epothilone D, reduces axonal dysfunction, neurotoxicity, cognitive deficits, and Alzheimer-like pathology in an interventional study with aged tau transgenic mice.** *J Neurosci* 2012, **32:**3601-3611.
246. Cavallini A, Brewerton S, Bell A, Sargent S, Glover S, Hardy C, Moore R, Calley J, Ramachandran D, Poidinger M, et al: **An unbiased approach to identifying tau kinases that phosphorylate tau at sites associated with Alzheimer disease.** *J Biol Chem* 2013, **288:**23331-23347.
247. Hyman BT, Elvhage TE, Reiter J: **Extracellular signal regulated kinases. Localization of protein and mRNA in the human hippocampal formation in Alzheimer's disease.** *Am J Pathol* 1994, **144:**565-572.
248. Ferrer I, Blanco R, Carmona M, Puig B: **Phosphorylated mitogen-activated protein kinase (MAPK/ERK-P), protein kinase of 38 kDa (p38-P), stress-activated protein kinase (SAPK/JNK-P), and calcium/calmodulin-dependent kinase II (CaM kinase II) are differentially expressed in tau deposits in neurons and glial cells in tauopathies.** *J Neural Transm (Vienna)* 2001, **108:**1397-1415.
249. Pei JJ, Braak H, An WL, Winblad B, Cowburn RF, Iqbal K, Grundke-Iqbal I: **Up-regulation of mitogen-activated protein kinases ERK1/2 and MEK1/2 is**

associated with the progression of neurofibrillary degeneration in Alzheimer's disease. *Brain Res Mol Brain Res* 2002, **109:**45-55.
250. Gerschutz A, Heinsen H, Grunblatt E, Wagner AK, Bartl J, Meissner C, Fallgatter AJ, Al-Sarraj S, Troakes C, Ferrer I, et al: **Neuron-specific alterations in signal transduction pathways associated with Alzheimer's disease.** *J Alzheimers Dis* 2014, **40:**135-142.
251. Johnson ECB, Carter EK, Dammer EB, Duong DM, Gerasimov ES, Liu Y, Liu J, Betarbet R, Ping L, Yin L, et al: **Large-scale deep multi-layer analysis of Alzheimer's disease brain reveals strong proteomic disease-related changes not observed at the RNA level.** *Nat Neurosci* 2022, **25:**213-225.
252. Yamada E, Pessin JE, Kurland IJ, Schwartz GJ, Bastie CC: **Fyn-dependent regulation of energy expenditure and body weight is mediated by tyrosine phosphorylation of LKB1.** *Cell Metab* 2010, **11:**113-124.